


Predictive model of fermionic dark matter halos with a quantum core and an isothermal atmosphere

Pierre-Henri Chavanis

Laboratoire de Physique Théorique, Université de Toulouse, CNRS, UPS, Toulouse, France

 (Received 6 January 2022; accepted 20 July 2022; published 29 August 2022)

We develop a thermodynamical model of fermionic dark matter halos at finite temperature. Statistical equilibrium states may be justified by a process of violent collisionless relaxation in the sense of Lynden-Bell or from a collisional relaxation of nongravitational origin if the fermions are self-interacting. The most probable state (maximum entropy state) generically has a “core-halo” structure with a quantum core (fermion ball) surrounded by an isothermal atmosphere. The quantum core is equivalent to a polytrope of index $n = 3/2$. The Pauli exclusion principle creates a quantum pressure that prevents gravitational collapse and solves the core-cusp problem of the cold dark matter model. The isothermal atmosphere (which is similar to the Navarro-Frenk-White profile of cold dark matter) accounts for the flat rotation curves of the galaxies at large distances. We numerically solve the equation of hydrostatic equilibrium with the Fermi-Dirac equation of state and determine the density profiles and rotation curves of fermionic dark matter halos. We impose that the surface density of the dark matter halos has the universal value $\Sigma_0 = \rho_0 r_h = 141 M_\odot/\text{pc}^2$ obtained from the observations. For a fermion mass $m = 165 \text{ eV}/c^2$, the “minimum halo” has a mass $(M_h)_{\min} = 10^8 M_\odot$ and a radius $(r_h)_{\min} = 597 \text{ pc}$ similar to dwarf spheroidals like Fornax. This ultracompact halo corresponds to a completely degenerate fermion ball at $T = 0$. This is the ground state of the self-gravitating Fermi gas. For ultracompact dark matter halos with a mass $(M_h)_{\min} < M_h < (M_h)_{\text{CCP}} = 6.73 \times 10^8 M_\odot$ (canonical critical point), the quantum core is surrounded by a tenuous classical isothermal atmosphere. Dark matter halos with a mass $M_h > (M_h)_{\text{CCP}}$ are dominated by the classical isothermal atmosphere. They may be purely gaseous (similar to the Burkert profile) or harbor a fermion ball. The gaseous solution is stable in all statistical ensembles. The core-halo solution is canonically unstable (having a negative specific heat) but, for small dark matter halos with a mass $(M_h)_{\text{CCP}} < M_h < (M_h)_{\text{MCP}} = 1.08 \times 10^{10} M_\odot$ (microcanonical critical point), it is microcanonically stable. By maximizing the entropy at fixed mass and energy we find that the mass of the quantum core scales with the halo mass as $M_c/(M_h)_{\min} = 1.47[M_h/(M_h)_{\min}]^{3/8}$. This relation is equivalent to the “velocity dispersion tracing” relation according to which the velocity dispersion in the core $v_c^2 \sim GM_c/R_c$ is of the same order as the velocity dispersion in the halo $v_h^2 \sim GM_h/r_h$. We provide therefore a justification of this relation from thermodynamical arguments. The fermion ball represents a large quantum bulge which is either present now or may have, in the past, triggered the collapse of the surrounding gas, leading to a supermassive black hole and a quasar. When $M_h > (M_h)_{\text{MCP}}$, the quantum core-halo solution is microcanonically unstable. Large dark matter halos may undergo a gravothermal catastrophe leading ultimately to the formation of a small out-of-equilibrium condensed core or, in the case of very large dark matter halos with $M_h > M_{\text{OV}}$, to a supermassive black hole when the core mass overcomes the Oppenheimer-Volkoff (OV) limit. The isothermal halo is left undisturbed and is in agreement with the Burkert profile. Our model has no free parameter (the mass $m = 165 \text{ eV}/c^2$ of the fermionic particle is determined by the minimum halo) so it is completely predictive. It predicts that the Milky Way should harbor a fermionic dark matter bulge of mass $M_c = 9.45 \times 10^9 M_\odot$ and radius $R_c = 240 \text{ pc}$ in possible agreement with the observations. We also consider another model involving a larger fermion mass $m = 54.6 \text{ keV}/c^2$. In this model, a fermion ball of mass $M_c = 4.2 \times 10^6 M_\odot$ and radius $R_c = 6 \times 10^{-4} \text{ pc}$ could mimic the effect of a supermassive black hole at the center of the Milky Way (Sagittarius A*). In bigger galaxies, the fermion ball should be replaced by a supermassive black hole of mass $M_{\text{BH}} = 2.10 \times 10^8 M_\odot$ which could account for active galactic nuclei. For an even larger fermion mass $m = 386 \text{ keV}/c^2$, a supermassive black hole of mass $M_{\text{BH}} = 4.2 \times 10^6 M_\odot$ should be formed in the

Milky Way instead of a fermion ball. However, models with a fermion mass $m = 54.6 \text{ keV}/c^2$ predict that ultracompact dark matter halos of mass $\sim 10^8 M_\odot$ should contain a fermionic core of mass $M_c \sim 10^4 M_\odot$ and radius $R_c \sim 5 \text{ mpc}$ similar to intermediate mass black holes, a prediction which may be challenged by observations.

DOI: [10.1103/PhysRevD.106.043538](https://doi.org/10.1103/PhysRevD.106.043538)

I. INTRODUCTION

The cold dark matter (CDM) model of cosmology is remarkably successful in explaining the large scale structure of the Universe but it experiences several difficulties at the scale of DM halos: (i) classical CDM simulations lead to a universal cuspy density profile—the Navarro-Frenk-White (NFW) profile [1] which decreases as r^{-3} at large distances and diverges as r^{-1} at the center, while observations rather favor corelike centers—the Burkert [2] profile which also decreases as r^{-3} at large distances but tends to a constant at the center; (ii) the number of subhalos obtained in CDM simulations is much larger than the number of satellites observed in the Galaxy [3–5]; (iii) dissipationless CDM simulations predict that the majority of the most massive subhalos of the Milky Way are too dense to host any of its bright satellites; (iv) the stellar velocity dispersions measured in CDM simulations are larger than those observed in the satellites of the Galaxy [6]. These problems are called the core-cusp problem [7], the missing satellites problem [3–5] and the “too big to fail” problem [8]. They are responsible for the small-scale crisis of CDM [9]. To solve these problem one solution might be to take into account baryonic feedback that can transform cusps into cores [10–12]. A possible alternative is to take into account the quantum (or wave) nature of the particles. Indeed, quantum mechanics creates an effective pressure which can balance gravitational attraction and lead to cores instead of cusps. Moreover, the quantum Jeans length is finite even at $T = 0$ (contrary to the classical Jeans length) and this may solve the missing satellites problem and other small-scale problems experienced by the classical CDM model.

If the DM particle is a boson,¹ like an ultralight axion [14], the quantum pressure is due to the Heisenberg uncertainty principle which is equivalent to an anisotropic pressure or to a quantum potential. If the bosons are self-interacting, there is an additional (isotropic) pressure arising from the self-interaction. At $T = 0$, bosons form Bose-Einstein condensates (BECs). Newtonian self-gravitating BECs are described by the Schrödinger-Poisson (SP) if they are noninteracting or by the Gross-Pitaevskii-Poisson (GPP) equations if they are self-interacting [15]. Numerical simulations of the SP equations [16–24] show that Bose-Einstein condensate dark matter (BECDM) halos typically have a

¹See the Introduction of Ref. [13] for a short review and an exhaustive list of references on bosonic DM.

core-halo structure with a quantum core (soliton) surrounded by an extended halo made of quantum interferences. The halo typically has a NFW or Burkert density profile decreasing as r^{-3} . It can be approximated in certain cases by an isothermal density profile decreasing as r^{-2} (see Sec. III C of [25]). The halo leads to approximately flat rotation curves and the quantum core solves the core-cusp problem. This core-halo structure results from a process of gravitational cooling [26–29] or from a collisional relaxation of nongravitational origin if the bosons are self-interacting.

If the DM particle is a fermion,² like a sterile neutrino, the quantum pressure is due to the Pauli exclusion principle which creates an effective isotropic pressure. Fermionic DM halos are described by the Fermi-Dirac distribution at finite (effective) temperature which may be justified by Lynden-Bell’s theory of violent relaxation [31,32] as argued in [33,34]. They typically have a core-halo structure with a quantum core (fermion ball) surrounded by an isothermal halo [32]. An isothermal halo is not very different from the NFW or Burkert profile and may provide a good approximation of it in certain cases.³ The isothermal halo leads to flat rotation curves and the quantum core solves the core-cusp problem. This core-halo structure results from a process of violent collisionless relaxation [31,32] or from a collisional relaxation of nongravitational origin if the fermions are self-interacting (see Sec. II).⁴

The analogy between bosonic and fermionic DM halos suggests that (i) the process of gravitational cooling is

²See the Introduction of Ref. [30] for a short review and an exhaustive list of references on fermionic DM.

³It is shown in Figs. 5 and 6 of [25] that the isothermal profile is almost indistinguishable from the empirical Burkert profile up to a few halo radii. This is even more true if we account for tidal effects by using the fermionic King model [33,34]. It is shown in [33] that the critical (marginal) King profile triggering the gravothermal catastrophe at the turning point of energy is relatively close to the Burkert profile (see Fig. 1). It may therefore provide a physical justification of this empirical profile. Observations reveal that many real DM halos are close to the point of marginal stability (see Fig. 8 of [35]) as predicted in [33,34].

⁴Fermions and bosons behave antisymmetrically regarding their collisional relaxation. The Pauli blocking $f(\eta_0 - f)$ for fermions has the tendency to slow down the relaxation and the Bose enhancement $f(\eta_0 + f)$ for bosons, leading to the formation of “granules” or “quasiparticles”, has the tendency to accelerate the relaxation. Gravitational encounters (“collisions”) are completely negligible in fermionic DM halos. In bosonic DM halos, they manifest themselves on a secular timescale of the order of the age of the Universe (see [36] and references therein).

similar to the process of violent relaxation (they may even correspond to the same phenomenon); (ii) the NFW profile (excluding the cusp) and the Burkert profile, which are similar to the isothermal profile, may be physically justified by Lynden-Bell’s theory of violent relaxation; (iii) the fermion ball in the fermionic model is the counterpart of the soliton in the BEC model.

A problem of considerable interest in the physics of quantum (fermionic and bosonic) DM halos is to construct core-halo profiles of DM halos and predict the quantum core mass—halo mass relation $M_c(M_h)$. One can then compare theoretical predictions with direct numerical simulations and observations.

In a previous paper [25], we have developed a predictive model of BECDM halos in the case where the bosons have a strong repulsive self-interaction so that the Thomas-Fermi (TF) approximation can be implemented. We considered a generalized GPP equation⁵ which provides a parametrization of the complicated processes of violent relaxation and gravitational cooling. With respect to the ordinary GPP equation, this new wave equation includes an effective thermal term and a source of dissipation. We determined the equilibrium states of this equation and obtained core-halo profiles with a quantum core and an isothermal halo similar to those observed in direct numerical simulations of BECDM. We obtained the core mass—halo mass relation $M_c(M_h)$ from an effective thermodynamical approach by maximizing the entropy at fixed mass and energy. We showed that this relation is equivalent to the velocity-dispersion tracing relation stating that the velocity dispersion in the core $v_c^2 \sim GM_c/R_c$ is of the same order as the velocity dispersion in the halo $v_h^2 \sim GM_h/r_h$. We could therefore provide a justification of this relation from thermodynamical arguments (maximum entropy principle) [25]. In subsequent papers [38–40], we derived the core mass—halo mass relation $M_c(M_h)$ from a simple analytical model again based on a maximum entropy principle and we obtained a general formula for $M_c(M_h)$ valid for noninteracting bosons, for bosons with a repulsive or attractive self-interaction, and for fermions. We showed that the velocity dispersion tracing relation is fulfilled in all cases. In the present paper, we adapt the bosonic model developed in [25] to the case of fermions.⁶

In the recent years, three types of studies have been conducted in the context of fermionic DM:

- (i) Chavanis and coworkers studied phase transitions in the self-gravitating Fermi gas in Newtonian gravity [32,34,41–45] and general relativity [46–48]. They showed that three possibilities can arise in the caloric

curve depending on the size of the system (measured by the so-called “degeneracy parameter” μ). For small systems $\mu < \mu_{\text{CCP}}$, no phase transition occur. For intermediate size systems $\mu_{\text{CCP}} < \mu < \mu_{\text{MCP}}$, phase transitions can occur in the canonical ensemble but not in the microcanonical ensemble. For large systems $\mu > \mu_{\text{MCP}}$, both canonical and microcanonical phase transitions can occur. They also showed that above the Oppenheimer-Volkoff (OV) limit $N > N_{\text{OV}}$, a new turning point of energy appears in the caloric curve and triggers a general relativistic instability leading to the formation of a black hole by gravitational collapse.

- (ii) de Vega and coworkers [49–54] constructed models of DM halos in Newtonian gravity adopting a fermion mass of the order of 1 keV/ c^2 . This mass determines a minimum halo of mass $(M_h)_{\text{min}} = 0.39 \times 10^6 M_\odot$ and size $(r_h)_{\text{min}} = 33$ pc corresponding to Willman I assumed to be completely degenerate. They argued that larger halos are nondegenerate (without quantum core) so they coincide with the well-known classical isothermal sphere [55].
- (iii) Argüelles and coworkers [56–62] constructed general relativistic models of DM halos adopting a fermion mass of the order of 48 keV/ c^2 and applied these models to the Milky Way. Their system has a core-halo structure made of a small quantum core (fermion ball) surrounded by an isothermal atmosphere. Reviving the original idea of Bilic and coworkers [63–67], they argued that the fermion ball could mimic a supermassive black hole (SMBH) that is purported to exist at the center of the Galaxy.

In the present paper, we develop a general model valid for fermions of arbitrary mass m . Then, we consider specifically the case of a “small” mass $m = 165$ eV/ c^2 or $m \sim 1$ keV/ c^2 and the case of a “large” mass $m = 54.6$ keV/ c^2 or $m = 386$ keV/ c^2 and discuss the connection with previous works. A brief and synthetic presentation of our results is given in Ref. [68] that the readers may consult in a first reading. The present paper provides a justification and a detailed description of these results.

The paper is organized as follows. In Sec. II, we explain why fermionic DM halos may be in a maximum entropy state described by the Fermi-Dirac distribution at finite (effective) temperature. In Sec. III, we recall basic results concerning the thermodynamics of a self-gravitating Fermi gas in a box. In Sec. IV, we consider the nondegenerate limit of the self-gravitating Fermi gas which explains the external structure of large DM halos. In Sec. V, we consider the completely degenerate limit of the self-gravitating Fermi gas which explains the structure of ultracompact DM halos and the cores of large DM halos. In Sec. VI, we consider partially degenerate DM halos. We show that they have a core-halo structure with a quantum core (fermion ball) surrounded by an isothermal halo. The isothermal halo

⁵This equation was introduced heuristically in [37] and justified with more precise arguments in [29] from a coarse graining of the Wigner-Poisson equations.

⁶The fact that the results obtained for bosons can be transposed to fermions was mentioned in [25]. Conversely, some of the results obtained here for fermions can be exported to bosons and can complete the discussion given in [25].

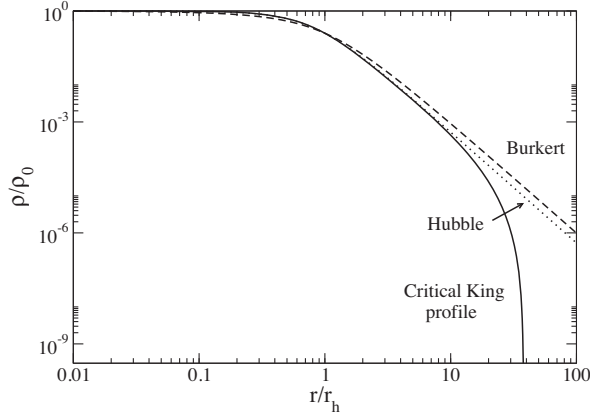


FIG. 1. Normalized density profiles in logarithmic scales (zoom of Fig. 18 in [33]). Solid line: Critical (marginal) King profile; Dotted line: Modified Hubble profile; Dashed line: Burkert profile. The critical King profile is relatively close to the Burkert profile for $r \lesssim 5r_h$ [33].

leads to flat rotation curves and the quantum core solves the core-cusp problem. We determine the core-halo mass relation $M_c(M_h)$ from thermodynamical arguments. In Sec. VII, we consider astrophysical applications of our model for a fermion mass $m = 165 \text{ eV}/c^2$. We evidence a bifurcation above a canonical critical point $(M_h)_{\text{CCP}} = 6.73 \times 10^8 M_\odot$ between purely gaseous states and core-halo states containing a fermion ball. For the core-halo states, we also evidence a transition at a microcanonical critical point $(M_h)_{\text{MCP}} = 1.08 \times 10^{10} M_\odot$. We argue that small DM halos with $M_h < (M_h)_{\text{MCP}}$ should contain a large quantum bulge while large DM halos with $M_h > (M_h)_{\text{MCP}}$ should rather contain a small out-of-equilibrium quantum core resulting from a gravothermal catastrophe arrested by quantum effects. For very large DM halos, when the core mass M_c passes above the Oppenheimer-Volkoff limit M_{OV} , quantum mechanics cannot prevent gravitational collapse and the gravothermal catastrophe leads to the formation of a SMBH. The isothermal halo is left undisturbed and is in agreement with the Burkert profile (see Fig. 1). We argue that the Milky Way should contain a large fermionic bulge of mass $M_c = 9.45 \times 10^9 M_\odot$ and radius $R_c = 240 \text{ pc}$ in possible agreement with the observations. In Sec. VIII, we consider another model with a fermion mass $m = 54.6 \text{ keV}/c^2$ in which the fermion ball could mimic a SMBH at the center of the Milky Way. We argue that, for larger DM halos or for a larger fermion mass, the fermion ball should be replaced by a true SMBH. In Sec. IX, we propose possible solutions to an apparent paradox related to the universal surface density of DM halos. In Sec. X we discuss the difference between isothermal and quantum cores and their formation process. In Sec. XII, we summarize our main results and conclude.

II. FORMATION AND EVOLUTION OF DM HALOS

In this section, we recall basic elements of kinetic theory related to the formation and the evolution of fermionic DM

halos in order to justify our thermodynamical approach (we refer to [36] for a more detailed discussion).

It is well known that self-gravitating systems experience two successive types of relaxation:

- (i) In a first regime, gravitational encounters can be neglected and the evolution of the system is described by the Vlasov (or collisionless Boltzmann) equation. The Vlasov-Poisson equations experience a complicated process of collisionless violent relaxation as described by Lynden-Bell [31] in the context of stellar systems. Through violent relaxation, the system reaches a quasistationary state (virialized state) on the coarse-grained scale which is a stable stationary solution of the Vlasov equation. The Vlasov-Poisson equations admit an infinite number of stationary solutions. In addition, all spherical distribution functions (DFs) of the form $f = f(\epsilon)$ with $f'(\epsilon) < 0$, where $\epsilon = v^2/2 + \Phi(\mathbf{r})$ is the energy of a particle, are dynamically (Vlasov) stable in Newtonian gravity [69].⁷ Lynden-Bell proposed determining the “most probable state” of the system resulting from a collisionless relaxation by using arguments of statistical mechanics and thermodynamics. This equilibrium state is obtained by maximizing a mixing entropy while taking into account all the constraints of the Vlasov equation. In the single-level approximation, the Lynden-Bell entropy is similar to the Fermi-Dirac entropy and the constraints of the Vlasov equation reduce to the conservation of mass and energy. In addition, if the particles are fermions, the Lynden-Bell exclusion principle $\bar{f} \leq \eta_0$, where η_0 is the initial DF, coincides with the Pauli exclusion principle $f \leq 2m^4/h^3$ up to a numerical factor of order unity (see footnote 34 of [33]). In order to select the most probable structure arising from a violent collisionless relaxation, one has therefore to maximize the Lynden-Bell (or Fermi-Dirac) entropy at fixed mass and energy. The extremization problem leads to the Lynden-Bell (or Fermi-Dirac) DF. Then, we have to make sure that the equilibrium state is an entropy maximum (most probable state), not an entropy minimum or a saddle point.⁸

⁷This is no more true in general relativity (see the discussion in [30]).

⁸If several stable equilibrium states (entropy maxima) are found for the same values of mass and energy, they may all be equally relevant. Indeed, metastable states (local entropy maxima) have a very long lifetime and are as much relevant as fully stable states (global entropy maxima). Their selection is related to a notion of basin of attraction and cannot be decided simply by comparing their entropies. Finally, we note that the predictive power of Lynden-Bell’s theory is limited by the problem of incomplete relaxation; the system may reach a dynamically stable stationary state of the Vlasov equation that is not a maximum entropy state.

- (ii) In a second regime, collisions must be taken into account.⁹ The collisional relaxation of the system is described by a kinetic equation such as the gravitational Boltzmann, Landau or Lenard-Balescu equation.¹⁰ If the particles are fermions, the collisional relaxation leads to a statistical equilibrium state described by the ordinary Fermi-Dirac distribution which maximizes the Fermi-Dirac entropy at fixed mass and energy. This corresponds to the “most probable state” of the system resulting from a collisional relaxation. This is also a stable stationary solution of the kinetic equation.¹¹

In the two situations described above we are led to maximizing the Lynden-Bell or Fermi-Dirac entropy at fixed mass and energy. We stress that the justification of this maximization problem is different in the collisionless (Lynden-Bell) and collisional (Fermi-Dirac) regimes. If the system is collisionless, the temperature is effective. We also note that the proper thermodynamical ensemble to consider is the microcanonical ensemble. Indeed, the system is assumed to be isolated so that the energy and the mass are conserved. This remark is important since statistical ensembles may be inequivalent for systems with long-range interactions such as self-gravitating systems [43,73,74].

If the particles interact only via (weak) two-body gravitational encounters, the collisional relaxation time is extremely long, scaling as $t_R \sim (N/\ln N)t_D$ [69], where N is the number of particles and $t_D \sim R/v \sim 1/\sqrt{G\rho} \sim 0.1$ Gyrs is the dynamical time (we have taken $R \sim 20.1$ kpc, $\rho \sim 7.02 \times 10^{-3} M_\odot/\text{pc}^3$ and $v \sim 146$ km/s in a galaxy of mass $M \sim 10^{12} M_\odot$ like the Milky Way). For fermionic DM halos, N is huge ($N \sim 10^{75}$ for keV fermions) so the relaxation time is much larger than the age of the Universe $t_U \sim 13.8$ Gyrs by many orders of magnitude (the Pauli blocking even increases this relaxation time). In that case, the system is essentially collisionless and only the Lynden-Bell type of relaxation is relevant. However, in order to be more general, we consider the possibility that the particles have a (strong) self-interaction that can cause a faster collisional evolution of

⁹We consider collisions of all sorts. They may correspond to weak gravitational encounters or strong (hard corelike) collisions if the particles have a self-interaction, leading to the notion of self-interacting dark matter (SIDM) halos. DM halos may also experience a stochastic forcing due to the presence of baryons or other external sources that can induce a secular relaxation of the system (see Appendix B of [25]).

¹⁰See the introduction of Ref. [70] for a short review and an exhaustive list of references on the kinetic theory of self-gravitating systems.

¹¹Actually, because of evaporation and because of its interaction with nearby galaxies, the system is tidally truncated and the Fermi-Dirac distribution must be replaced by the fermionic King distribution [71,72]. This DF can be derived from a kinetic theory based on the fermionic Landau equation [72]. The fermionic King model has been studied in [34] in Newtonian gravity and in [60–62] in general relativity.

nongravitational origin. This allows us to consider the possibility of a collisional relaxation (especially in the core of the system where the density is high and the relaxation time short) towards a Fermi-Dirac equilibrium state on a timescale smaller than the age of the Universe. For example, if the particles have a cross section per unit mass $\sigma_m \equiv \sigma/m = 1.25 \text{ cm}^2/\text{g}$ consistent with the Bullet Cluster constraint [75] we get $t_{\text{self}} \sim 1/(\rho\sigma_m v) \sim 3.66$ Gyrs $< t_U$. In that case, fermionic DM halos behave similarly to globular clusters with additional quantum effects. Because of collisions and evaporation, they follow a series of equilibria towards configurations of higher and higher central density. If the equilibrium state becomes thermodynamically unstable (after a turning point of energy), a fermionic DM halo may experience a phase transition from a gaseous phase to a condensed phase (with a quantum core and an isothermal envelope) associated with a form of gravothermal catastrophe [76] stopped by quantum degeneracy [32]. This may be followed by a dynamical instability of general relativity origin leading to the formation of a SMBH [46–48].

III. SELF-GRAVITATING FERMIONIC GAS IN A BOX

In this section we consider the statistical mechanics of a self-gravitating Fermi gas in a box. We summarize the main results obtained in our previous papers [32,41–43] and detail the theoretical framework that will be needed in the present study.

A. Theoretical framework

We consider a gas of nonrelativistic fermions interacting via Newtonian gravity. Let $f(\mathbf{r}, \mathbf{v}, t)$ denote its distribution function (DF) in phase space giving the mass density of fermions with position \mathbf{r} and velocity \mathbf{v} at time t . The mass density in configuration space is $\rho = \int f d\mathbf{v}$. The total mass of the system is

$$M = \int f d\mathbf{r} d\mathbf{v} \quad (1)$$

and its total energy is

$$E = \int f \frac{v^2}{2} d\mathbf{r} d\mathbf{v} + \frac{1}{2} \int \rho \Phi d\mathbf{r}, \quad (2)$$

where the first term is the kinetic energy and the second term is the gravitational energy ($E = E_{\text{kin}} + W$). We introduce the Fermi-Dirac entropy

$$\frac{S}{k_B} = -\frac{\eta_0}{m} \int \left\{ \frac{f}{\eta_0} \ln \frac{f}{\eta_0} + \left(1 - \frac{f}{\eta_0}\right) \ln \left(1 - \frac{f}{\eta_0}\right) \right\} d\mathbf{r} d\mathbf{v}, \quad (3)$$

where

$$\eta_0 = \frac{2m^4}{h^3} \quad (4)$$

is the maximum value of the DF fixed by the Pauli exclusion principle (the factor 2 accounts for the multiplicity $2s + 1$ of quantum states for particles of spin $s = 1/2$). The Fermi-Dirac entropy is equal to the logarithm of the number of microstates, specified by the precise position and velocity $\{\mathbf{r}_i, \mathbf{v}_i\}$ of all the fermions, corresponding to a given macrostate specified by the DF $f(\mathbf{r}, \mathbf{v})$ giving the density of fermions around the point (\mathbf{r}, \mathbf{v}) in phase space.

In the microcanonical ensemble, the statistical equilibrium state of a self-gravitating gas of fermions is obtained by maximizing the Fermi-Dirac entropy S at fixed energy E and mass M . One has therefore to solve the optimization problem

$$\max\{S|E, M \text{ fixed}\}. \quad (5)$$

This thermodynamic approach is justified in a mean field approximation which is exact in a proper thermodynamic limit $N \rightarrow +\infty$ (see Sec. 7.1 of [43] and Appendix B of [46]).

An extremum of entropy at fixed energy and mass is determined by the variational principle

$$\frac{\delta S}{k_B} - \beta \delta E + \frac{\alpha}{m} \delta M = 0, \quad (6)$$

where $\beta = 1/(k_B T)$ and $\alpha = \mu/(k_B T)$ are Lagrange multipliers (T is the temperature and μ is the global chemical potential). This leads to the Fermi-Dirac distribution

$$f = \frac{\eta_0}{1 + e^{[mv^2/2 + m\Phi(\mathbf{r}) - \mu]/k_B T}}. \quad (7)$$

The density of particles $\rho = \int f d\mathbf{v}$ and the pressure $P = \frac{1}{3} \int f v^2 d\mathbf{v}$ are related to the gravitational potential $\Phi(\mathbf{r})$ by

$$\rho(\mathbf{r}) = \frac{4\pi\sqrt{2}\eta_0}{(\beta m)^{3/2}} I_{1/2}[\lambda e^{\beta m \Phi(\mathbf{r})}], \quad (8)$$

$$P(\mathbf{r}) = \frac{8\pi\sqrt{2}\eta_0}{3(\beta m)^{5/2}} I_{3/2}[\lambda e^{\beta m \Phi(\mathbf{r})}], \quad (9)$$

where $\lambda = e^{-\beta\mu}$ and $I_n(t)$ denotes the Fermi integrals

$$I_n(t) = \int_0^{+\infty} \frac{x^n}{1 + te^x} dx. \quad (10)$$

We recall the identity

$$I'_n(t) = -\frac{n}{t} I_{n-1}(t) \quad (n > 0), \quad (11)$$

which can be established from Eq. (10) by an integration by parts. Eliminating $\lambda e^{\beta m \Phi(\mathbf{r})}$ between Eqs. (8) and (9), we

obtain the equation of state $P(\rho)$ of the nonrelativistic Fermi gas at finite temperature in parametric form (see also Appendix A).

Combining the condition of hydrostatic equilibrium

$$\nabla P + \rho \nabla \Phi = \mathbf{0} \quad (12)$$

with the Poisson equation

$$\Delta \Phi = 4\pi G \rho, \quad (13)$$

we obtain the fundamental differential equation of hydrostatic equilibrium

$$\nabla \cdot \left(\frac{\nabla P}{\rho} \right) = -4\pi G \rho. \quad (14)$$

Together with the barotropic equation of state $P(\rho)$ specified by Eqs. (8) and (9) this equation determines the density profile of the self-gravitating Fermi gas at statistical equilibrium.

Alternatively, substituting the density-potential relation from Eq. (8) into the Poisson equation (13), we obtain a differential equation determining the gravitational potential

$$\Delta \Phi = \frac{16\pi^2 \sqrt{2} G \eta_0}{(\beta m)^{3/2}} I_{1/2}[\lambda e^{\beta m \Phi(\mathbf{r})}], \quad (15)$$

which is called the Fermi-Poisson equation or the finite temperature Thomas-Fermi equation. The density is then obtained from Eq. (8). The two equations (14) and (15) are equivalent.

We now assume that the system is spherically symmetric and introduce the dimensionless variables

$$\psi = \beta m (\Phi - \Phi_0), \quad k = \lambda e^{\beta m \Phi_0}, \quad (16)$$

and

$$\xi = \left[\frac{16\pi^2 \sqrt{2} G \eta_0}{(\beta m)^{1/2}} \right]^{1/2} r, \quad (17)$$

where Φ_0 is the central value of the gravitational potential. We can then rewrite the density and the pressure under the form

$$\rho(r) = \frac{4\pi\sqrt{2}\eta_0}{(\beta m)^{3/2}} I_{1/2}[k e^{\psi(\xi)}], \quad (18)$$

$$P(r) = \frac{8\pi\sqrt{2}\eta_0}{3(\beta m)^{5/2}} I_{3/2}[k e^{\psi(\xi)}]. \quad (19)$$

On the other hand, Eqs. (14) and (15) lead to the fermionic Emden equation

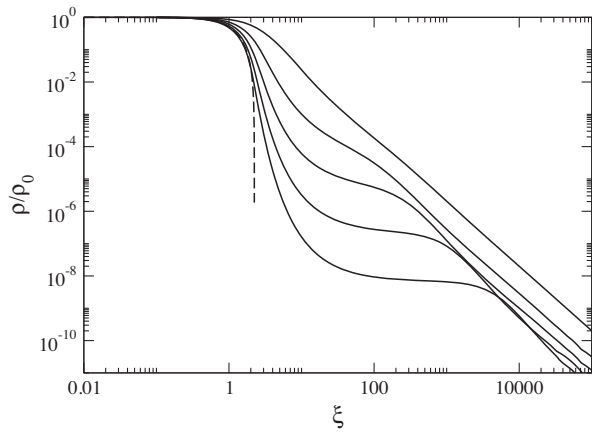


FIG. 2. Normalized density profiles of fermionic DM halos for different values of k ($k = 10^{-8}, 10^{-6}, 10^{-4}, 10^{-2}$ from bottom to top). The dashed line corresponds to a completely degenerate fermion ball. The upper curve corresponds to a nondegenerate isothermal DM halo.

$$\frac{1}{\xi^2} \frac{d}{d\xi} \left(\xi^2 \frac{d\psi}{d\xi} \right) = I_{1/2}(ke^\psi) \quad (20)$$

with the boundary conditions

$$\psi(0) = \psi'(0) = 0. \quad (21)$$

This equation determines the structure of the system as a function of the parameter k . For $k \rightarrow +\infty$, the system is nondegenerate; this corresponds to the gaseous phase (see Sec. IV). For $k \rightarrow 0$, the system is completely degenerate; this corresponds to the condensed phase (see Sec. V). For intermediate values of k , the system is partially degenerate; it typically has a core-halo structure with a quantum core (fermion ball) surrounded by a classical isothermal halo (see Sec. VI).¹² Some density profiles are plotted in Fig. 2 for different values of k .

As is well known, self-gravitating systems at nonzero temperature have the tendency to evaporate. Therefore, there is no equilibrium state in a strict sense and the statistical mechanics of self-gravitating systems is essentially an out-of-equilibrium problem. However, the evaporation rate is small in general and the system can be found in a quasi-equilibrium state for a relatively long time. In order to describe the thermodynamics of the self-gravitating Fermi gas rigorously, we shall use an artifice and enclose the system within a spherical box of radius R .¹³ The box typically represents the size of the cluster under

¹²See Ref. [32] for a description of this core-halo configuration and some analytical approximations. See also Sec. V of Ref. [25] for similar results obtained in the case of bosonic DM halos which can be directly exported to the case of fermionic DM halos.

¹³A more rigorous approach would be to use a truncated model (fermionic King model) like in [33,34].

consideration (see Sec. VI). In that case, the solution of Eq. (20) is terminated by the box at the normalized radius

$$\alpha = \left[\frac{16\pi^2 \sqrt{2} G \eta_0}{(\beta m)^{1/2}} \right]^{1/2} R. \quad (22)$$

Since α is the value of ξ at the box radius R we can write

$$\xi = \alpha \frac{r}{R}. \quad (23)$$

Let us first calculate the normalized inverse temperature

$$\eta = \frac{\beta G M m}{R}. \quad (24)$$

For a spherically symmetric distribution of matter, the Poisson equation (13) is equivalent to Newton's law

$$\frac{d\Phi}{dr} = \frac{GM(r)}{r^2}, \quad (25)$$

where $M(r) = \int_0^r \rho(r') 4\pi r'^2 dr'$ is the mass contained within the sphere of radius r . Applying Newton's law at $r = R$ and using Eqs. (16), (23), and (24), we get

$$\eta = \alpha \psi'_k(\alpha). \quad (26)$$

This equation relates the dimensionless box radius α and the concentration variable k to the dimensionless inverse temperature η .

On the other hand, according to Eqs. (22) and (24), α and k are linked to each other by the relation

$$\alpha^2 \sqrt{\eta} = \mu \quad (27)$$

or, more explicitly [using Eq. (26)]

$$\alpha^5 \psi'_k(\alpha) = \mu^2, \quad (28)$$

where

$$\mu = \eta_0 \sqrt{512\pi^4 G^3 M R^3} \quad (29)$$

is the so-called degeneracy parameter [43].¹⁴ We shall give a physical interpretation of this parameter in Sec. VI.

The calculation of the energy is a little more intricate. The kinetic energy of a nonrelativistic gas can be written as

$$E_{\text{kin}} = \frac{3}{2} \int P dr. \quad (30)$$

¹⁴It should not be confused with the chemical potential which is denoted by the same symbol. In principle, no confusion should arise.

Using Eq. (19), we obtain

$$\frac{E_{\text{kin}}R}{GM^2} = \frac{\alpha^7}{\mu^4} \int_0^\alpha I_{3/2}[ke^{\psi_k(\xi)}] \xi^2 d\xi. \quad (31)$$

In order to determine the potential energy, we can use the virial theorem (see, e.g., [30])

$$2E_{\text{kin}} + W = 3P_b V, \quad (32)$$

where $P_b = P(R)$ is the pressure on the boundary of the box and $V = \frac{4}{3}\pi R^3$ is the volume of the spherical box. Using the expression of the pressure from Eq. (19) at the box radius R , we get

$$\frac{WR}{GM^2} = \frac{2\alpha^{10}}{3\mu^4} I_{3/2}[ke^{\psi_k(\alpha)}] - \frac{2E_{\text{kin}}R}{GM^2}. \quad (33)$$

Introducing the normalized energy

$$\Lambda = -\frac{ER}{GM^2} \quad (34)$$

and combining Eqs. (31) and (33), we finally obtain

$$\Lambda = \frac{\alpha^7}{\mu^4} \int_0^\alpha I_{3/2}[ke^{\psi_k(\xi)}] \xi^2 d\xi - \frac{2\alpha^{10}}{3\mu^4} I_{3/2}[ke^{\psi_k(\alpha)}]. \quad (35)$$

The expression of the entropy is derived in Appendix B. Finally, using Eqs. (16), (18), (24), (25), (29), and (C7) the normalized density and velocity profiles can be written as

$$\frac{\rho(r)}{M/R^3} = \frac{\mu}{4\pi\eta^{3/2}} I_{1/2}[ke^{\psi(\xi)}], \quad (36)$$

$$\frac{v^2(r)}{GM/R} = \frac{1}{\eta} \xi \psi'(\xi). \quad (37)$$

B. Caloric curves and ensemble inequivalence

Using the foregoing formulas, we can obtain the caloric curve $\eta(\Lambda)$ of the self-gravitating Fermi gas for a specified value of μ as follows. For a given value of k , we can solve the ordinary differential equation (20) with the initial conditions (21) until the value of α at which the relation (28) is satisfied. Then, Eqs. (26) and (35) determine the normalized inverse temperature η and the normalized energy Λ of the configuration. By varying the parameter k from 0 to $+\infty$, we can determine the full caloric curve $\eta(\Lambda)$ for the specified value of the degeneracy parameter μ (see Fig. 3). We can then study the occurrence of phase transitions as a function of μ . This study has been made in detail in [43].¹⁵ Below, we summarize the main results of this study that will be useful in the following.

We have to be careful that, for self-gravitating systems (which have a long-range interaction), the statistical

¹⁵Very similar results apply to the case of tidally-truncated systems described by the fermionic King model [33,34].

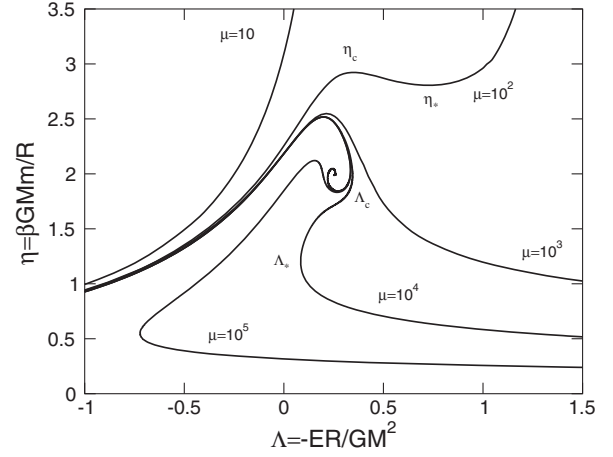


FIG. 3. Caloric curves (series of equilibria) of the self-gravitating Fermi gas for different values of μ .

ensembles are inequivalent. In the previous section, we have worked in the microcanonical ensemble. This is the statistical ensemble associated with isolated systems where the energy E is fixed. By contrast, systems in contact with a heat bath fixing the temperature T are described by the canonical ensemble. In the canonical ensemble, the statistical equilibrium state of a self-gravitating gas of fermions is obtained by minimizing the Fermi-Dirac free energy $F = E - TS$ at fixed mass M . One has therefore to solve the optimization problem

$$\min\{F|M \text{ fixed}\}. \quad (38)$$

One can easily show that the equilibrium states in the microcanonical and in the canonical ensembles are the same; an extremum of free energy at fixed mass is also an extremum of entropy at fixed mass and energy, and conversely [77]. However, their stability may be different in the two ensembles. An equilibrium state that is canonically stable is always microcanonically stable (a minimum of free energy at fixed mass is always a maximum of entropy at fixed mass and energy), but the converse is wrong; a maximum of entropy at fixed mass and energy is not necessarily a minimum of free energy at fixed mass [77]. For example, equilibrium states with a negative specific heat are always unstable in the canonical ensemble while they may be stable in the microcanonical ensemble. This corresponds to the concept of ensemble inequivalence for systems with long-range interactions [43,73,74]. As a result, we may miss important solutions if we use the canonical ensemble instead of the microcanonical one.¹⁶

¹⁶In particular, as shown in [38] and further discussed in Sec. VII, the core-halo solution that possibly describes real DM halos is unstable in the canonical ensemble while it is stable in the microcanonical ensemble. This suggests that the microcanonical ensemble is more adapted to DM halos than the canonical ensemble. Since DM halos are isolated instead of being in contact with a thermal bath, the use of the microcanonical ensemble is physically justified [33,34].

The self-gravitating Fermi gas presents two critical points, one in each ensemble; the function $\Lambda(\eta)$ becomes multivalued at the canonical critical point μ_{CCP} and the function $\eta(\Lambda)$ becomes multivalued at the microcanonical critical point μ_{MCP} whose values are [43]

$$\mu_{\text{CCP}} = 83, \quad \mu_{\text{MCP}} = 2670. \quad (39)$$

For $\mu < \mu_{\text{CCP}}$ the series of equilibria $\eta(\Lambda)$ is monotonic (see the curve $\mu = 10$ in Fig. 3; see also Fig. 11 below). The equilibrium states are stable in both canonical and microcanonical ensembles.

For $\mu > \mu_{\text{CCP}}$ the series of equilibria $\eta(\Lambda)$ presents turning points of temperature (see the curves $\mu = 10^2$ – 10^5 in Fig. 3; see also Figs. 12 and 14 below). Following the series of equilibria towards higher and higher density contrasts, and using the Poincaré-Katz [78,79] criterion, one can show that the equilibrium states are canonically stable before the first turning point of temperature η_c (gaseous phase) and after the last turning point of temperature η_* (condensed phase). They are canonically unstable in between. In the canonical ensemble, the system undergoes an isothermal collapse at η_c from the gaseous phase to the condensed phase and an explosion at η_* from the condensed phase to the gaseous phase. The first-order phase transition that is expected at η_t (at which the free energy of the two phases coincides) does not take place in practice because of the very long lifetime of metastable states for systems with long-range interactions scaling as e^N [80].

For $\mu > \mu_{\text{MCP}}$ the series of equilibria $\eta(\Lambda)$ presents turning points of energy (see the curves $\mu = 10^4$ and 10^5 in Fig. 3; see also Fig. 14 below). Following the series of equilibria towards higher and higher density contrasts, and using the Poincaré-Katz [78,79] criterion, one can show that the equilibrium states are microcanonically stable before the first turning point of energy Λ_c (gaseous phase) and after the last turning point of energy Λ_* (condensed phase). They are microcanonically unstable in between. In the microcanonical ensemble, the system undergoes a gravothermal catastrophe at Λ_c from the gaseous phase to the condensed phase and an explosion at Λ_* from the condensed phase to the gaseous phase. The first-order phase transition that is expected at Λ_t (at which the entropy of the two phases coincides) does not take place in practice because of the very long lifetime of metastable states for systems with long-range interactions scaling as e^N [80].

For $\mu \rightarrow +\infty$ we recover the series of equilibria $\eta(\Lambda)$ of a classical isothermal self-gravitating gas (see Fig. 6 below). It has a snail-like structure (spiral). Using the Poincaré-Katz [78,79] criterion, one can show that the equilibrium states become (and remain) unstable after the first turning point of temperature in the canonical ensemble and after the first turning point of energy in the microcanonical ensemble.

For $\mu_{\text{CCP}} < \mu < \mu_{\text{MCP}}$ (see the curves $\mu = 10^2$ and 10^3 in Fig. 3; see also Fig. 12 below) all the equilibrium states are

stable in the microcanonical ensemble while the equilibrium states between the first turning point of temperature η_c and the last turning point of temperature η_* (core-halo solution) are unstable in the canonical ensemble. They have a core-halo structure and a negative specific heat. The region of negative specific heat that is allowed in the microcanonical ensemble is replaced by a phase transition in the canonical ensemble. This corresponds to a region of ensemble inequivalence.¹⁷

We now apply these results to DM halos. We have explained that metastable states (local entropy maxima) are as much relevant as fully stable states (global entropy maxima) since they are robust and long-lived. Therefore, we shall not make a distinction between fully stable and metastable states in our study. We shall treat them on the same footing.

IV. NONDEGENERATE LIMIT: EXTERNAL STRUCTURE OF LARGE DM HALOS

Let us first consider the nondegenerate limit of the self-gravitating Fermi gas which describes the external structure (envelope) of large DM halos.

A. Isothermal equation of state

In the nondegenerate limit $T \rightarrow +\infty$ (or $T \gg T_F$ where $T_F \sim \hbar^2 \rho^{2/3} / m^{5/3} k_B$ is the Fermi temperature) the Fermi-Dirac DF (7) reduces to the Maxwell-Boltzmann distribution

$$f = \eta_0 e^{\beta\mu} e^{-\beta m \left[\frac{v^2}{2} + \Phi(\mathbf{r}) \right]}. \quad (40)$$

In that case, the density and the pressure are given by

$$\rho = \eta_0 e^{\beta\mu} \left(\frac{2\pi}{\beta m} \right)^{3/2} e^{-\beta m \Phi(\mathbf{r})}, \quad (41)$$

$$P = \eta_0 e^{\beta\mu} \left(\frac{2\pi}{\beta m} \right)^{3/2} \frac{1}{\beta m} e^{-\beta m \Phi(\mathbf{r})}, \quad (42)$$

leading to the classical isothermal equation of state

$$P(\mathbf{r}) = \rho(\mathbf{r}) \frac{k_B T}{m}. \quad (43)$$

¹⁷The physical nature of the core-halo solution is very different in the two ensembles. In the canonical ensemble, the degenerate core represents a ‘‘germ’’ or a ‘‘critical droplet’’ (in the language of phase transitions and nucleation) that the system must form to pass from the gaseous phase to the condensed phase. This is a saddle point of free energy at fixed mass. The probability to form this configuration is very low, scaling with the number of particles as e^{-N} . This is a rare event. This explains why metastable gaseous states have a very long lifetime scaling as e^N [43,80]. By contrast, in the microcanonical ensemble, the core-halo solution is fully stable and corresponds to the most probable state of the system for the corresponding energy. It is therefore expected to be physically selected by the system.

The fundamental differential equation (14) of hydrostatic equilibrium takes the form

$$-\frac{k_B T}{m} \Delta \ln \rho = 4\pi G \rho. \quad (44)$$

It describes the balance between the gravitational attraction and the thermal pressure. It is equivalent to the Boltzmann-Poisson equation

$$\Delta \Phi = 4\pi G \eta_0 e^{\beta\mu} \left(\frac{2\pi}{\beta m}\right)^{3/2} e^{-\beta m \Phi(r)} \quad (45)$$

obtained by combining Eqs. (13) and (41). Equations (44) and (45) can be reduced to the Emden equation (D5) [55].

B. Flat rotation curves

The differential equation of hydrostatic equilibrium (44) has no simple analytical solution and must be solved numerically. However, its asymptotic behavior is known analytically [55,69]. The density of a self-gravitating isothermal halo decreases as

$$\rho(r) \sim \frac{k_B T}{2\pi G m r^2} \quad (46)$$

for $r \rightarrow +\infty$, corresponding to an accumulated mass $M(r) \sim 2k_B \text{Tr}/(Gm)$ increasing linearly with r . This leads to flat rotation curves

$$v^2(r) = \frac{GM(r)}{r} \rightarrow v_\infty^2 = \frac{2k_B T}{m}, \quad (47)$$

in agreement with the observations [69].

C. Thermal core radius

The isothermal density profile has not a compact support so it extends to infinity. Furthermore, its total mass is infinite [69]. As a result, self-gravitating systems have no statistical equilibrium state in an unbounded domain. In practice, the isothermal equation of state is not valid at arbitrarily large distances and the expansion of the halo is limited by tidal effects [33,34,81] or by incomplete relaxation [31,82] (see Sec. XI).

From the scaling of Eq. (44) we can define a characteristic radius

$$r_0 = \left(\frac{k_B T}{4\pi G \rho_0 m}\right)^{1/2} \quad (48)$$

that we shall call the thermal core radius.¹⁸ It represents the typical radius of an isothermal halo of central density ρ_0 . The halo mass M_h , the halo radius r_h , the temperature T

¹⁸This is the scale radius that is used in Eq. (D4) to obtain the Emden equation (D5). We add the word ‘‘thermal’’ to avoid confusion with the quantum core radius considered later (see the discussion in Sec. X).

and the circular velocity v_h at the halo radius are defined in Appendix C. For an isothermal profile they are given by (see Appendix D)

$$\frac{r_h}{r_0} = 3.63, \quad \frac{M_h}{\rho_0 r_h^3} = 1.76, \quad (49)$$

$$\frac{k_B T}{G m \rho_0 r_h^2} = 0.954, \quad \frac{v_h^2}{4\pi G \rho_0 r_h^2} = 0.140. \quad (50)$$

We note that the dimensionless inverse temperature has the value

$$\eta_v = \frac{\beta G M_h m}{r_h} = 1.84. \quad (51)$$

This is essentially a consequence of the virial theorem. Equation (51) will be called the ‘‘virial condition’’.

The density and circular velocity profiles of a purely isothermal halo are plotted in Figs. 2–6 of [25]. The isothermal profile is relatively close to the empirical (observational) Burkert profile [2] up to $r/r_h = 6$.

D. The constant surface density

It is an observational evidence that the surface density of DM halos is independent of their mass and size and has the universal value [83–85]

$$\Sigma_0 = \rho_0 r_h = 141_{-52}^{+83} M_\odot/\text{pc}^2. \quad (52)$$

This result is valid for all the galaxies even if their sizes and masses vary by several orders of magnitude (up to 14 orders of magnitude in luminosity). The reason for this universality is not known but it is crucial to take this result into account in any modeling of DM halos. Therefore, we shall assume this relation as an empirical fact.¹⁹

E. Halo mass-radius relation

Substituting the constraint (52) of a constant surface density into Eqs. (49) and (50), we obtain the relations

$$M_h = 1.76 \Sigma_0 r_h^2, \quad \frac{k_B T}{m} = 0.954 G \Sigma_0 r_h, \quad (53)$$

$$v_h^2 = 1.76 G \Sigma_0 r_h, \quad \rho_0 = \frac{\Sigma_0}{r_h}. \quad (54)$$

They determine the halo mass, the halo temperature, the halo velocity, and the halo central density as a function of the halo radius. The halo mass scales with the size as $M_h \propto r_h^2$ and the temperature as $k_B T/m \propto r_h$ (basically,

¹⁹In Refs. [86–91] we have explained this universal value, without adjustable parameter, from a logotropic model of DM halos.

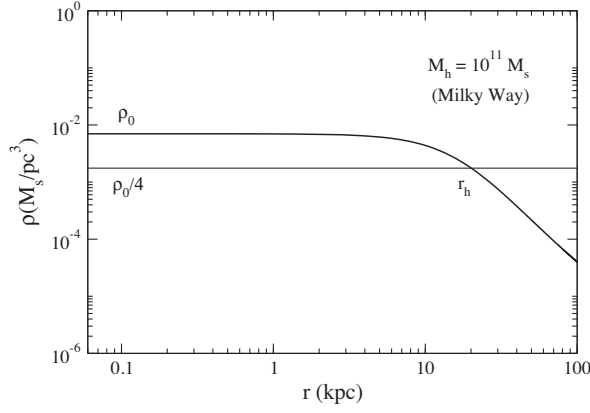


FIG. 4. Density profile of a classical isothermal DM halo of mass $M_h = 10^{11} M_\odot$ (Milky Way).

these scalings stem from the universality of the surface density of DM halos $M_h/r_h^2 \sim \Sigma_0$ and from the virial theorem $k_B T/m \sim v_h^2 \sim GM_h/r_h \sim G\Sigma_0 r_h$.

For a halo of mass $M_h = 10^{11} M_\odot$, similar to the halo that surrounds our Galaxy, we find $r_h = 20.1$ kpc, $\rho_0 = 7.02 \times 10^{-3} M_\odot/\text{pc}^3$, $(k_B T/m)^{1/2} = 108$ km/s, and $v_h = (GM_h/r_h)^{1/2} = 146$ km/s (we also have $v_\infty = 153$ km/s). We stress that these results are independent of the characteristics of the DM particle. The corresponding density and velocity profiles are plotted in Figs. 4 and 5.

Remark: The (effective) temperature of the DM halos depends on the fermion mass m and on the halo mass M_h through the law $k_B T = 0.719 Gm \sqrt{\Sigma_0 M_h}$. Let us consider a halo mass $M_h = 10^{11} M_\odot$ as above. For $m = 165$ eV/ c^2 (see Sec. V C), we get $T = 0.247$ K. For $m = 1$ keV/ c^2 (see Sec. V C), we get $T = 1.50$ K. For $m = 54.6$ keV/ c^2 (see Sec. VIII), we get $T = 81.9$ K. These values, which are of the order of the Kelvin scale, are much more physical than those obtained in the case of bosonic DM, which are of the order of $T \sim 10^{-25}$ K for a boson mass $m \sim 10^{-22}$ eV/ c^2 [25].

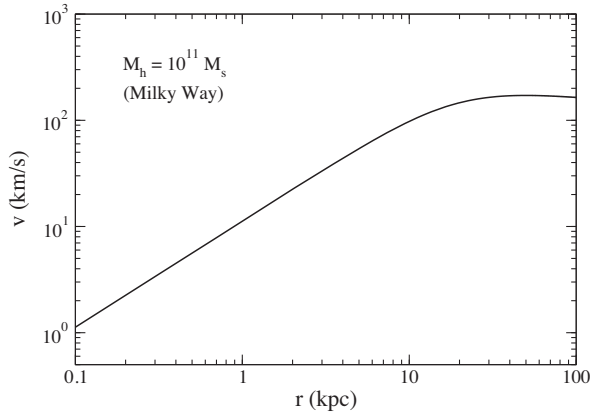


FIG. 5. Rotation curve of a classical isothermal DM halo of mass $M_h = 10^{11} M_\odot$ (Milky Way).

F. Classical isothermal gas in a box

Let us finally derive the equations determining the caloric curve of a self-gravitating isothermal gas in a box. The density profile (41) can be written as

$$\rho(r) = \rho_0 e^{-\beta m(\Phi(r) - \Phi_0)}, \quad (55)$$

where ρ_0 is the central density and Φ_0 is the central potential. The Boltzmann-Poisson equation (45) then becomes

$$\Delta\Phi = 4\pi G\rho_0 e^{-\beta m(\Phi - \Phi_0)}. \quad (56)$$

If we assume that the system is spherically symmetric and introduce the dimensionless variables

$$\rho = \rho_0 e^{-\psi(\xi)}, \quad \psi = \beta m(\Phi - \Phi_0), \quad (57)$$

and

$$\xi = (4\pi G\beta m\rho_0)^{1/2} r \quad (58)$$

into Eq. (56), we obtain the Emden equation (D5). If we denote by α the value of ξ at the edge of the box, we have

$$\alpha = (4\pi G\beta m\rho_0)^{1/2} R \quad \text{and} \quad \xi = \alpha \frac{r}{R}. \quad (59)$$

Introducing the inverse normalized temperature from Eq. (24) and applying Newton's law (25) at $r = R$, we get

$$\eta = \alpha\psi'(\alpha). \quad (60)$$

To compute the energy, we proceed as follows. The kinetic energy of an isothermal gas is

$$E_{\text{kin}} = \frac{3}{2} N k_B T. \quad (61)$$

Using the virial theorem from Eq. (32) we can compute the gravitational energy. We find

$$W = -2E_{\text{kin}} + 3P_b V = -3Nk_B T + \frac{4\pi R^3 \rho(R) k_B T}{m}. \quad (62)$$

The total energy is $E = E_{\text{kin}} + W$. Introducing the normalized energy from Eq. (34) we obtain

$$\Lambda = \frac{3}{2\alpha\psi'(\alpha)} - \frac{e^{-\psi(\alpha)}}{\psi'(\alpha)^2}. \quad (63)$$

The expression of the entropy is derived in Appendix B. The caloric curve $\eta(\Lambda)$ of the classical self-gravitating gas [76,79,92] is represented in Fig. 6. It has the form of a spiral (see Sec. III B). It leads to an isothermal collapse [93] in the canonical ensemble above $\eta_c = 2.52$ and to a gravothermal

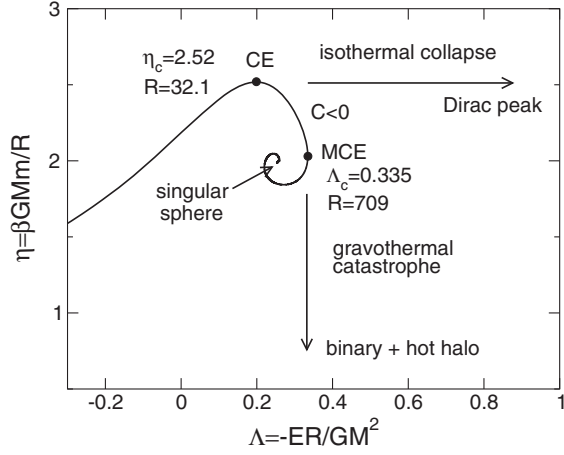


FIG. 6. Caloric curve of the classical self-gravitating gas.

catastrophe [76] in the microcanonical ensemble above $\Lambda_c = 0.335$.

Remark: The equations of this section can be recovered from the general equations of Sec. III by taking the nondegenerate limit $k \rightarrow +\infty$ and replacing the Fermi integrals by their asymptotic expressions

$$I_n(t) \sim \frac{1}{t} \Gamma(n+1), \quad (t \rightarrow +\infty). \quad (64)$$

V. COMPLETELY DEGENERATE LIMIT: MINIMUM HALO (GROUND STATE) AND QUANTUM CORE OF DM HALOS

We now consider the completely degenerate limit of the self-gravitating Fermi gas which describes (i) ultracompact dwarf spheroidals (dSphs) like Fornax or Willman I and (ii) the quantum core of bigger DM halos.

A. Polytropic equation of state

In the completely degenerate limit $T = 0$ (or $T \ll T_F$), the Fermi-Dirac DF (7) reduces to the step function

$$\begin{aligned} f(\mathbf{r}, \mathbf{v}) &= \eta_0 & v \leq v_F(\mathbf{r}), \\ f(\mathbf{r}, \mathbf{v}) &= 0 & v \geq v_F(\mathbf{r}), \end{aligned} \quad (65)$$

where

$$v_F(\mathbf{r}) = \sqrt{2 \left[\frac{\mu}{m} - \Phi(\mathbf{r}) \right]} \quad (66)$$

is the Fermi velocity.²⁰ The density and the pressure are explicitly given by

²⁰The Fermi energy is given by $\epsilon_F(\mathbf{r}) = \frac{1}{2} m v_F^2(\mathbf{r}) = \mu - m\Phi(\mathbf{r})$. It is equal to the local chemical potential $\mu(\mathbf{r}) = \mu - m\Phi(\mathbf{r})$.

$$\rho = \int f d\mathbf{v} = \int_0^{v_F} \eta_0 4\pi v^2 dv = \frac{4\pi}{3} \eta_0 v_F^3(\mathbf{r}), \quad (67)$$

$$P = \frac{1}{3} \int f v^2 d\mathbf{v} = \frac{1}{3} \int_0^{v_F} \eta_0 v^2 4\pi v^2 dv = \frac{4\pi}{15} \eta_0 v_F^5(\mathbf{r}). \quad (68)$$

Eliminating the Fermi velocity between these two expressions, we find that the equation of state of a cold Fermi gas is [55]

$$P = \frac{1}{20} \left(\frac{3}{\pi} \right)^{2/3} \frac{h^2}{m^{8/3}} \rho^{5/3}. \quad (69)$$

This is a polytropic equation of state $P = K_1 \rho^{5/3}$ of index $\gamma = 5/3$ (i.e., $n = 3/2$). The fundamental differential equation of hydrostatic equilibrium determining the density profile of a fermion ball at $T = 0$ with the equation of state (69) reads [see Eq. (14)]

$$\frac{1}{3} \left(\frac{3}{\pi} \right)^{2/3} \frac{h^2}{m^{8/3}} \Delta \rho^{2/3} = -4\pi G \rho. \quad (70)$$

It describes the balance between the gravitational attraction and the quantum pressure. It is equivalent to the Thomas-Fermi equation

$$\Delta \Phi = \frac{16}{3} \pi^2 G \eta_0 \left[2 \left(\frac{\mu}{m} - \Phi \right) \right]^{3/2} \quad (71)$$

obtained by combining Eqs. (13) and (67) with Eq. (66). Equations (70) and (71) can be reduced to the Lane-Emden equation (E5) of index $n = 3/2$.

B. Mass-radius relation

The density profile of a fermion ball at $T = 0$ (corresponding to a polytrope of index $n = 3/2$) has a compact support: the density vanishes at a finite distance $r = R$ representing the radius of the object (see Fig. 7 below). The radius, the mass and the central density of the object satisfy the relations (see Appendix E)

$$R = 0.359 \frac{h}{m^{4/3} G^{1/2} \rho_0^{1/6}}, \quad (72)$$

$$M = 0.699 \rho_0 R^3, \quad (73)$$

$$MR^3 = 0.00149 \frac{h^6}{G^3 m^8}. \quad (74)$$

Similarly, the halo mass, the halo radius and the central density satisfy the relations (see Appendix E)

$$r_h = 0.223 \frac{h}{m^{4/3} G^{1/2} \rho_0^{1/6}}, \quad (75)$$

$$M_h = 1.99\rho_0 r_h^3, \quad (76)$$

$$M_h r_h^3 = 2.45 \times 10^{-4} \frac{\hbar^6}{G^3 m^8}. \quad (77)$$

Therefore

$$\frac{M}{M_h} = 1.46, \quad \frac{R}{r_h} = 1.61, \quad (78)$$

yielding $GM/R = 0.907GM_h/r_h$.

C. Minimum halo

The foregoing equations determine the ground state ($T = 0$) of the self-gravitating Fermi gas. This fermion ball corresponds either to the smallest and most compact DM halo of the Universe (which has no isothermal atmosphere) that we call the ‘‘minimum halo’’, or to the quantum cores of larger DM halos (which are surrounded by an isothermal atmosphere) [38]. We consider here the first possibility (minimum halo). Using Eqs. (75)–(77) and the constraint from Eq. (52), we obtain [38]

$$(r_h)_{\min} = 1.50 \left(\frac{\hbar^6}{G^3 m^8 \Sigma_0} \right)^{1/5}, \quad (79)$$

$$(M_h)_{\min} = 4.47 \left(\frac{\hbar^{12} \Sigma_0^3}{G^6 m^{16}} \right)^{1/5}, \quad (80)$$

$$(\rho_0)_{\max} = 0.667 \left(\frac{\Sigma_0 m^{4/3} G^{1/2}}{\hbar} \right)^{6/5}, \quad (81)$$

$$(v_h^2)_{\min} = 2.98 \left(\frac{\Sigma_0^4 G^2 \hbar^6}{m^8} \right)^{1/5}. \quad (82)$$

These equations determine the radius, the mass, the central density and the velocity of the minimum halo as a function of the fermion mass m and the universal surface density Σ_0 . In practice, they are used the other way round in order to determine the fermion mass m . Assuming that the mass $(M_h)_{\min}$ of the minimum halo is known, we obtain

$$m = 1.60 \frac{\hbar^{3/4} \Sigma_0^{3/16}}{G^{3/8} (M_h)_{\min}^{5/16}}. \quad (83)$$

If we take $(M_h)_{\min} = 10^8 M_\odot$ we find $m = 165 \text{ eV}/c^2$. We then obtain $(r_h)_{\min} = 597 \text{ pc}$, $(\rho_0)_{\max} = 0.236 M_\odot/\text{pc}^3$, and $(v_h)_{\min} = 26.8 \text{ km/s}$. Using Eq. (78), we also have $M_{\min} = 1.46 \times 10^8 M_\odot$ and $R_{\min} = 961 \text{ pc}$. The corresponding density and velocity profiles are plotted in Figs. 7 and 8.

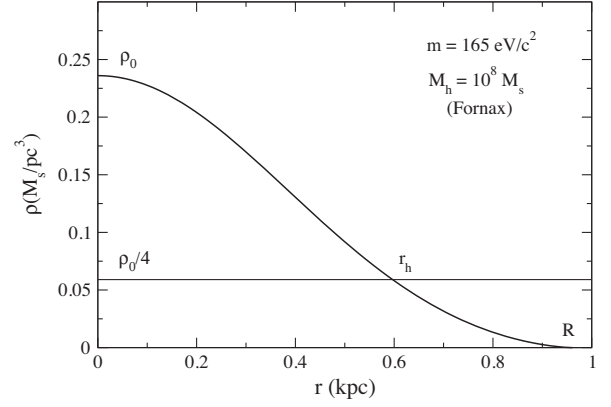


FIG. 7. Density profile of a completely degenerate DM halo of mass $M_h = 10^8 M_\odot$ (Fornax). We have taken $m = 165 \text{ eV}/c^2$.

The Fermi temperature is defined by

$$k_B T_F = \frac{\hbar^2 \rho^{2/3}}{m^{5/3}}. \quad (84)$$

It can be obtained qualitatively by equating Eqs. (43) and (69). For the minimum halo, using Eq. (81), it reads

$$k_B T_F = \left(\frac{\hbar^6 \Sigma_0^4 G^2}{m^3} \right)^{1/5}. \quad (85)$$

For $m = 165 \text{ eV}/c^2$, we get $T_F = 5.15 \times 10^{-3} \text{ K}$. We note that the minimum halo is determined by the condition $T \sim T_F$, where T is the temperature given by Eq. (53).

Remark: The choice of the mass $(M_h)_{\min} = 10^8 M_\odot$ (Fornax) for the minimum halo is a little bit arbitrary and open to criticism. We shall adopt this value, however, in order to be consistent with our other papers [25,38,40,94]. Nevertheless, our model is perfectible. If a more relevant minimum halo mass is considered, our analytical results remain valid but the numerical applications must be

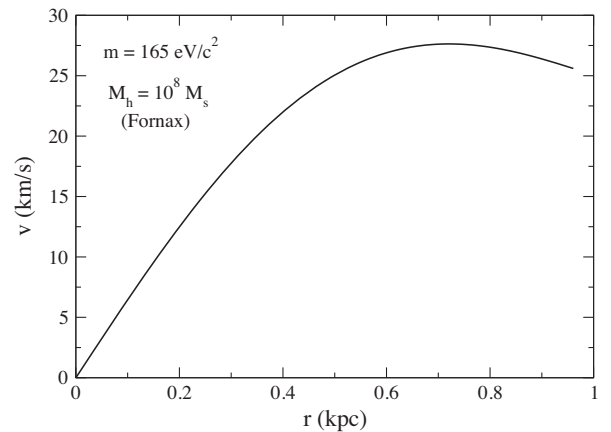


FIG. 8. Rotation curve of a completely degenerate DM halo of mass $M_h = 10^8 M_\odot$ (Fornax). We have taken $m = 165 \text{ eV}/c^2$.

reconsidered. For example, if we take a minimum halo mass $(M_h)_{\min} = 0.39 \times 10^6 M_\odot$ corresponding to Willman I (as in Refs. [49–54] and Refs. [34,95]) we obtain $m \sim 1 \text{ keV}/c^2$. We then obtain $(r_h)_{\min} \sim 33 \text{ pc}$ (in very good agreement with the measured value reported in Ref. [49]), $(\rho_0)_{\max} \sim 4.3 M_\odot/\text{pc}^3$, and $(v_h)_{\min} = 6.35 \text{ km/s}$. It is also possible that the concept of a “minimum halo” which is completely degenerate is wrong (see Sec. VIII). In that case, our general results remain valid but the fermion mass cannot be obtained from the considerations of this section.

D. Quantum core of DM halos

The relations from Eqs. (72)–(83) apply to the minimum halo which is a pure fermion ball without isothermal atmosphere. The relations from Eqs. (72)–(74) also apply to the quantum core of larger DM halos. If we normalize the core mass M_c by the minimum halo mass $(M_h)_{\min}$ and the core radius R_c by the minimum halo radius $(r_h)_{\min}$, we get

$$\frac{M_c}{(M_h)_{\min}} \left[\frac{R_c}{(r_h)_{\min}} \right]^3 = 6.09. \quad (86)$$

We can check that Eq. (86) is verified for the minimum halo for which $M_c = 1.46(M_h)_{\min}$ and $R_c = 1.61(r_h)_{\min}$ [see Eq. (78)].

E. Maximum mass due to general relativity

The maximum mass and the minimum radius of a fermion ball at $T = 0$ set by general relativity are

$$M_{\text{OV}} = 0.384 \left(\frac{\hbar c}{G} \right)^{3/2} \frac{1}{m^2}, \quad R_{\text{OV}} = 8.73 \frac{GM_{\text{max}}}{c^2}. \quad (87)$$

They were first determined by Oppenheimer and Volkoff [96] in the context of neutron stars. For a fermion of mass $m = 165 \text{ eV}/c^2$, we obtain $M_{\text{OV}} = 2.30 \times 10^{13} M_\odot$ and $R_{\text{OV}} = 9.61 \text{ pc}$. For $m = 1 \text{ keV}/c^2$, we get $M_{\text{OV}} = 6.26 \times 10^{11} M_\odot$ and $R_{\text{OV}} = 0.262 \text{ pc}$. The maximum mass is much larger than the typical core mass of any DM halo. Assuming that a fermion ball at $T = 0$ describes the quantum core of a DM halo, we conclude that such cores are nonrelativistic since $M_c \ll M_{\text{max}}$ in general. Since the maximum mass is much larger than the core mass, gravity can be treated within a Newtonian framework.²¹

F. Energy of a fermion ball

Let us finally derive the energy of a completely degenerate fermion ball.

A nonrelativistic fermion ball at $T = 0$ is equivalent to a polytrope of index $n = 3/2$ [see Eq. (69)]. Its kinetic energy is given by [see Eq. (30)]

$$E_{\text{kin}} = \frac{3}{2} \int P d\mathbf{r} = \frac{3}{2} K_1 \int \rho^{5/3} d\mathbf{r}. \quad (88)$$

Its gravitational energy is given by the Betti-Ritter formula [55]

$$W = -\frac{6}{7} \frac{GM^2}{R} \quad (89)$$

with the mass-radius relation from Eq. (74). The virial theorem reduces to [see Eq. (32)]

$$2E_{\text{kin}} + W = 0 \quad (90)$$

since the pressure vanishes on the boundary of the fermion ball. Therefore, the total energy $E = E_{\text{kin}} + W$ of the fermion ball is

$$E = -E_{\text{kin}} = \frac{W}{2} = -\frac{3}{7} \frac{GM^2}{R}. \quad (91)$$

This is the minimum energy E_{\min} of the self-gravitating Fermi gas (ground state). Using the mass-radius relation (74), we obtain

$$E_{\min} = -3.750 \frac{G^2 m^{8/3}}{h^2} M^{7/3}. \quad (92)$$

Considering the box model of Sec. III and introducing the normalized energy from Eq. (34) we get

$$\Lambda_{\text{max}} = 0.0642 \mu^{2/3}. \quad (93)$$

Remark: The equations of this section can be recovered from the general equations of Sec. III by taking the completely degenerate limit $k \rightarrow 0$ and replacing the Fermi integrals by their asymptotic expressions

$$I_n(t) \sim \frac{(-\ln t)^{n+1}}{n+1}, \quad (t \rightarrow 0). \quad (94)$$

VI. PARTIALLY DEGENERATE DM HALOS: CORE-HALO STRUCTURE

To study partially degenerate DM halos with a core-halo structure, we shall use the box model of Sec. III. In order to apply this model to real DM halos, we identify the mass M with the halo mass M_h and the box radius R with the halo radius r_h :

$$M = M_h, \quad R = r_h. \quad (95)$$

We first have to determine the relation between the degeneracy parameter μ and the halo mass M_h .

A. Relation between the degeneracy parameter μ and the halo mass M_h

Sufficiently large DM halos are dominated by their classical isothermal envelope (the quantum core of mass

²¹This statement is valid for the fermion mass $m = 165 \text{ eV}/c^2$ that we consider here. It is only marginally valid for the larger fermion mass $m = 48 \text{ keV}/c^2$ considered in Sec. VIII.

$M_c \ll M_h$ does not affect their external structure). As a result, the halo mass is related to the halo radius by [see Eq. (53)]

$$M_h = 1.76 \Sigma_0 r_h^2. \quad (96)$$

Using this relation, the degeneracy parameter defined by Eq. (29) can be written as

$$\mu = 1.18 \frac{G^{3/2} m^4 M_h^{5/4}}{\hbar^3 \Sigma_0^{3/4}}. \quad (97)$$

Normalizing the halo mass M_h by the minimum halo mass $(M_h)_{\min}$ given by Eq. (80) we obtain

$$\mu = 7.66 \left[\frac{M_h}{(M_h)_{\min}} \right]^{5/4}. \quad (98)$$

This equation relates the degeneracy parameter μ to the halo mass M_h . As a result, the canonical and microcanonical critical points given by Eq. (39) may be expressed in terms of the halo mass by using $(M_h)_{\text{CCP}} = (\mu_{\text{CCP}}/7.66)^{4/5} (M_h)_{\min}$ and $(M_h)_{\text{MCP}} = (\mu_{\text{MCP}}/7.66)^{4/5} (M_h)_{\min}$ yielding

$$(M_h)_{\text{CCP}} = 6.73 (M_h)_{\min} = 30.1 \left(\frac{\hbar^{12} \Sigma_0^3}{G^6 m^{16}} \right)^{1/5}, \quad (99)$$

$$(M_h)_{\text{MCP}} = 108 (M_h)_{\min} = 483 \left(\frac{\hbar^{12} \Sigma_0^3}{G^6 m^{16}} \right)^{1/5}. \quad (100)$$

Taking $(M_h)_{\min} = 10^8 M_\odot$ (Fornax), corresponding to a fermion mass $m = 165 \text{ eV}/c^2$, we get

$$(M_h)_{\text{CCP}} = 6.73 \times 10^8 M_\odot, \quad (M_h)_{\text{MCP}} = 1.08 \times 10^{10} M_\odot. \quad (101)$$

If we take $(M_h)_{\min} = 0.39 \times 10^6 M_\odot$ (Willman I) instead, corresponding to a fermion mass $m \sim 1 \text{ keV}/c^2$, we get $(M_h)_{\text{CCP}} = 2.62 \times 10^6 M_\odot$ and $(M_h)_{\text{MCP}} = 4.21 \times 10^7 M_\odot$. We note that $(M_h)_{\text{CCP}}$ and $(M_h)_{\text{MCP}}$ are very sensitive to the value of m since it occurs in their expressions [see Eqs. (99) and (100)] with the power 16/5.

Remark: We can also write the degeneracy parameter μ under the form [43]

$$\mu = 17.3 \left[\frac{R}{R_F(M)} \right]^{3/2}, \quad (102)$$

where $R_F(M)$ is the (Fermi) radius of a completely degenerate fermion ball of mass M given by Eq. (74). The condition $R > R_c$ imposes $R > R_F(M)$, hence $\mu > \mu_{\min} = 17.3$. Applying this inequality to real DM halos, using Eq. (98), we find that $M_h > 1.92 (M_h)_{\min}$. Up to a factor of order unity, we recover the fact that the ground state of the self-gravitating

Fermi gas ($T = 0$) determines the existence of a minimum halo mass $(M_h)_{\min}$.

B. Virial condition

We have seen in Sec. IV that the normalized inverse temperature of an isothermal DM halo is $\eta_v = 1.84$.²² Therefore, if we want to make the connection between the box model and real DM halos, we should consider a value of η equal to 1.84. It is reassuring to note that $\eta_v = 1.84$ is smaller than $\eta_c \simeq 2.52$, corresponding to the maximum inverse temperature of the classical isothermal spiral, implying that there always exists a gaseous (nondegenerate) equilibrium state with $\eta_v = 1.84$. Actually, we should not give too much importance on the precise value of η_v . It is sufficient to consider that η_v is of the order of unity. Therefore, we shall take

$$\eta_v \sim 1. \quad (103)$$

The intersections between the series of equilibria $\eta(\Lambda)$ and the line level $\eta = \eta_v \sim 1$ determine the possible equilibrium states of our system of self-gravitating fermions. We can generically have three kinds of solutions: (i) a gaseous solution (G) which is purely isothermal without quantum core; (ii) a core-halo solution (CH) with a quantum core (fermion ball) surrounded by a classical isothermal atmosphere; (iii) a condensed solution (C) which is an essentially quantum object with a tenuous isothermal atmosphere. The gaseous solution has been discussed in Sec. IV. The condensed solution is not physical in the case of large DM halos because it would imply that the halo is completely degenerate, which is not the case. This solution only applies to the minimum halo (see Sec. V). The core-halo solution is the most important one for our purposes. It is similar to the gaseous solution at sufficiently large distances but it contains a small nucleus (fermion ball) at its center. An important question is to determine the core mass M_c as a function of the halo mass M_h .

C. The $M_c - M_h$ relation for the CH solution

The core mass-halo mass relation $M_c(M_h)$ can be obtained from the box model as follows. The halo mass M_h determines the value of the degeneracy parameter μ . We can then plot the series of equilibria $\eta(\Lambda)$ parametrized by the concentration parameter k (see Figs. 11, 12, and 14 below). For $\mu > \mu_{\text{CCP}}$, the intersections between the caloric curve $\eta(\Lambda)$ and the virial condition $\eta = \eta_v \sim 1$ determine three solutions G, CH, and C (see Fig. 9 for an illustration). We select the core-halo solution and compute the corresponding concentration parameter $k = k_{\text{CH}}(\mu, \eta_v)$. The density profile of the core-halo solution is then given by Eq. (18). Its central density is

²²Coincidentally, this value turns out to be very close to the value $\eta_2 = 1.84$ corresponding to the minimum inverse temperature of the classical isothermal spiral (see Sec. IV F).

$$\rho_0 = \frac{4\pi\sqrt{2}\eta_0}{(\beta m)^{3/2}} I_{1/2}(k). \quad (104)$$

Introducing the dimensionless variables defined in Sec. III A, we get

$$\frac{4\pi\rho_0 R^3}{M} = \frac{\mu}{\eta^{3/2}} I_{1/2}(k). \quad (105)$$

Now, the core-halo configuration can be decomposed into a fermion ball at $T = 0$ and a classical isothermal atmosphere. For a completely degenerate fermion ball, representing the quantum core of the DM halo, the relation between the core mass and the central density is given by [see Eqs. (72)–(74)]

$$M_c = 8.01 \frac{\hbar^3 \rho_0^{1/2}}{G^{3/2} m^4}. \quad (106)$$

Combining Eqs. (105) and (106) we obtain

$$\frac{M_c}{M} = 4.07 \frac{\sqrt{I_{1/2}(k)}}{\mu^{1/2} \eta^{3/4}}. \quad (107)$$

Recalling that $M = M_h$, $\eta = \eta_v \sim 1$ and $k = k_{\text{CH}}(\mu, \eta_v)$ we get

$$\frac{M_c}{M_h} = 4.07 \frac{\sqrt{I_{1/2}[k_{\text{CH}}(\mu, \eta_v)]}}{\mu^{1/2} \eta_v^{3/4}}. \quad (108)$$

Together with the relation (98) between μ and M_h , Eq. (108) determines the core mass-halo mass relation $M_c(M_h)$. In principle, the function $I_{1/2}[k_{\text{CH}}(\mu, \eta_v)]$ has to be determined numerically as a function of μ . However, it turns out that, for the CH solution, $I_{1/2}[k_{\text{CH}}(\mu, \eta_v)]$ changes slowly (logarithmically) with μ . As a result, up to logarithmic corrections (see Sec. VID), it can be assumed to be constant. Therefore, we obtain the scaling

$$\frac{M_c}{M_h} \propto \frac{1}{\mu^{1/2}}. \quad (109)$$

More precisely, recalling Eq. (98), Eq. (108) can be written as

$$\frac{M_c}{(M_h)_{\min}} = 1.47 \frac{\sqrt{I_{1/2}[k_{\text{CH}}(\mu, \eta_v)]}}{\eta_v^{3/4}} \left[\frac{M_h}{(M_h)_{\min}} \right]^{3/8}. \quad (110)$$

If we take $\eta_v = 1$ and $I_{1/2}(k_{\text{CH}}) = 1$, we get

$$\frac{M_c}{(M_h)_{\min}} = 1.47 \left[\frac{M_h}{(M_h)_{\min}} \right]^{3/8}. \quad (111)$$

This relation shows that the core mass M_c scales with the halo mass as $M_h^{3/8}$. The prefactor, obtained from our model,

is of order unity implying that $M_c \sim M_h$ for the minimum halo, as expected. Actually, for $M_h = (M_h)_{\min}$ we get $M_c = 1.47(M_h)_{\min}$ in very good agreement with Eq. (78). Returning to the original variables, using Eq. (80), we can rewrite Eq. (111) as

$$M_c = 3.75 \frac{\hbar^{3/2}}{m^2} \left(\frac{M_h \Sigma_0}{G^2} \right)^{3/8}. \quad (112)$$

Once we have M_c by Eq. (111) or (112) we can get R_c by Eq. (74) or (86) and ρ_0 by Eq. (106). Explicitly,

$$R_c = 4.51 \frac{\hbar^2}{G m^{8/3} M_c^{1/3}} = 2.90 \frac{\hbar^{3/2}}{G^{3/4} m^2 M_h^{1/8} \Sigma_0^{1/8}}, \quad (113)$$

$$\rho_0 = 0.0156 \frac{G^3 m^8 M_c^2}{\hbar^6} = 0.219 \frac{G^{3/2} m^4 M_h^{3/4} \Sigma_0^{3/4}}{\hbar^3}. \quad (114)$$

Remark: In this paper, we have defined the halo mass M_h such that the density at the halo radius r_h is equal to the central density divided by 4 (see Appendix C). However, other authors work in terms of a halo mass M_v defined in another manner as explained in Sec. VC of [38]. The relation between M_h and M_v is [see Eq. (146) of Ref. [38]]

$$\frac{M_h}{M_\odot} = 6.01 \times 10^{-6} \left(\frac{M_v}{M_\odot} \right)^{4/3}. \quad (115)$$

Combining Eqs. (112) and (115), we obtain the core mass—halo mass relation $M_c(M_v)$. It exhibits the fundamental scaling $M_c \propto M_v^{1/2}$. This theoretical scaling, first obtained in the form of Eq. (112) in Appendix H of [34], is consistent with the scaling found numerically by Ruffini *et al.* [59] (they find an exponent equal to 0.52 instead of 1/2).

D. Logarithmic corrections

In the previous section, we have assumed that $I_{1/2}(k_{\text{CH}})$ is approximately constant and we have taken $I_{1/2}(k_{\text{CH}}) \simeq 1$. A more precise expression of $I_{1/2}(k_{\text{CH}})$ can be obtained as follows: We see on Fig. 9 that $k_{\text{CH}} \sim 1/\mu$ for large values of μ .²³ Using the asymptotic expression $I_{1/2}(k) \sim \frac{2}{3} (-\ln k)^{3/2}$ of the Fermi integral $I_{1/2}(k)$ for $k \rightarrow 0$ [see Eq. (94)], we obtain $I_{1/2}(k_{\text{CH}}) \sim \frac{2}{3} (\ln \mu)^{3/2}$. This behavior is confirmed by the plot of Fig. 10. If we take this logarithmic correction into account we have to multiply M_c [given by Eq. (111) or (112)] by the factor

$$\mathcal{A} = \sqrt{\frac{2}{3}} (\ln \mu)^{3/4}. \quad (116)$$

²³This is not rigorously the case but this approximation is sufficient for our purposes since k arises in a logarithm.

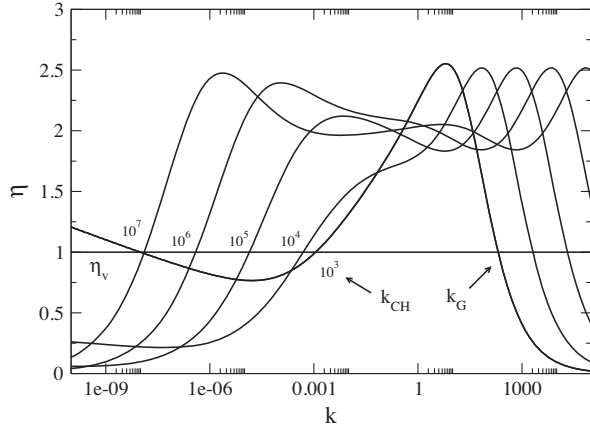


FIG. 9. Inverse temperature η as a function of k for different values of $\mu = 10^3$ – 10^7 . The intersection between the curve $\eta(k)$ and the line $\eta = \eta_v = 1$ selects three solutions G, CH, and C. Only the physical solutions G and CH are visible on the figure.

Similarly, R_c [given by Eq. (113)] has to be divided by $\mathcal{A}^{1/3}$ and ρ_0 [given by Eq. (114)] has to be multiplied by \mathcal{A}^2 .

E. Velocity dispersion tracing relation

The core mass—halo mass relation can also be obtained from a simple analytical model of self-gravitating fermions enclosed within a box as detailed in Sec. IV of [38]. In that model, the fermion ball is represented by a polytrope of index $n = 3/2$ and the classical isothermal atmosphere is assumed to be uniform. Under these approximations, one can compute the energy and the entropy analytically. The mass of the fermion ball M_c is then obtained by maximizing the entropy $S(M_c)$ for a given value of E_h , M_h , and r_h . This leads to a relation $M_c(M_h)$ similar to that of Eq. (109) with Eq. (116) [see Eq. (123) of Ref. [38]]. This relation is obtained from a thermodynamical approach (maximum entropy principle) determining the “most probable” core mass M_c . It is furthermore shown in Sec. V of [38] that this

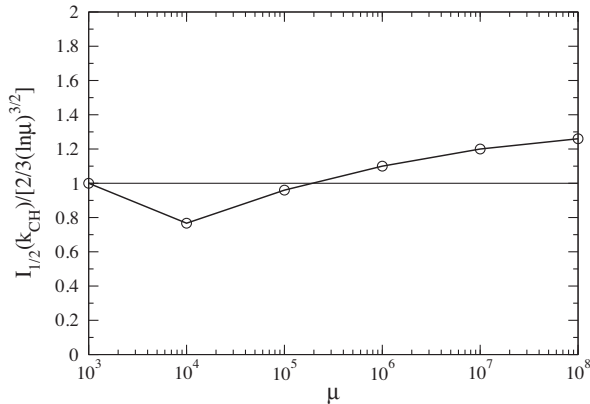


FIG. 10. This curve confirms that $I_{1/2}(k_{CH}) \sim \frac{2}{3}(\ln \mu)^{3/2}$ in good approximation.

relation is equivalent to the “velocity dispersion tracing” relation [19,25,97]

$$v_c^2 \sim v_h^2 \quad \text{or} \quad M_c \sim \frac{R_c}{r_h} M_h \quad (117)$$

stating that the velocity dispersion in the core $v_c^2 \sim GM_c/R_c$ is of the same order as the velocity dispersion in the halo $v_h^2 \sim GM_h/r_h$. This is the reason why Eq. (111) is similar to Eq. (169) of [38]. It is interesting to note that the prefactors appearing in these relations are almost the same although these relations are obtained from substantially different calculations. Therefore, the present approach provides an additional justification of the “velocity dispersion tracing” relation from thermodynamical arguments.

VII. ASTROPHYSICAL APPLICATIONS

We now consider astrophysical applications of our model and discuss several scenarios that are suggested by the previous results.

A. Minimum halo with $M_h = (M_h)_{\min}$

The minimum halo has a mass $(M_h)_{\min} = 10^8 M_\odot$ and a radius $(r_h)_{\min} = 597$ pc. It corresponds to the ground state (minimum energy state) of the self-gravitating Fermi gas. A completely degenerate fermion ball at $T = 0$ is equivalent to a polytrope of index $n = 3/2$ (see Figs. 7 and 8). This solution is fully stable in all statistical ensembles.

B. Ultracompact DM halos with $(M_h)_{\min} < M_h < (M_h)_{\text{CCP}}$

Ultracompact DM halos have a mass in the range $(M_h)_{\min} = 10^8 M_\odot < M_h < (M_h)_{\text{CCP}} = 6.73 \times 10^8 M_\odot$. Since $\mu < \mu_{\text{CCP}}$ the caloric curve $\eta(\Lambda)$ is monotonic (see Fig. 11). There is only one equilibrium state with $\eta_v \sim 1$.

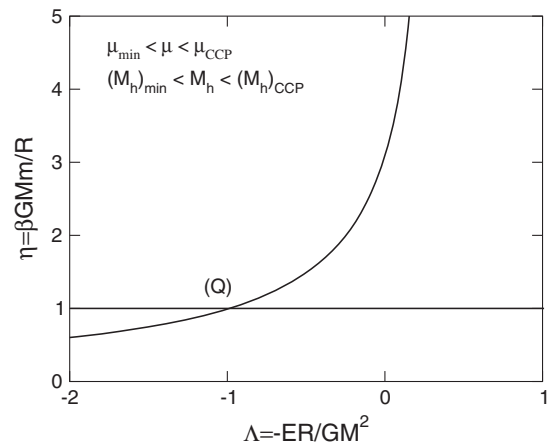


FIG. 11. Caloric curve of self-gravitating fermions for $\mu = 10$. When $(M_h)_{\min} < M_h < (M_h)_{\text{CCP}}$, the caloric curve is monotonic. The quantum solution (Q) is thermodynamically stable in all statistical ensembles.

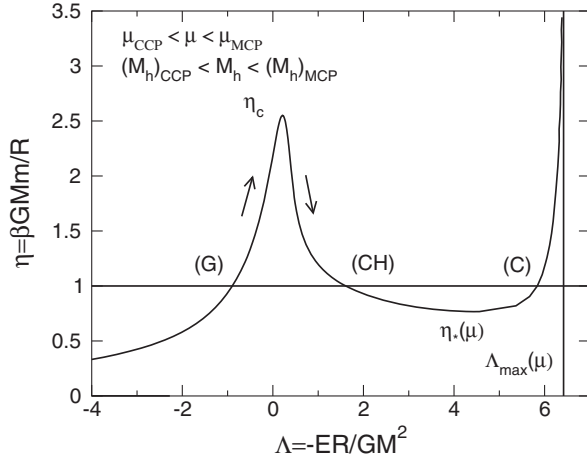


FIG. 12. Caloric curve of self-gravitating fermions for $\mu = 10^3$. When $(M_h)_{\text{CCP}} < M_h < (M_h)_{\text{MCP}}$, the caloric curve has an N -shape structure. In the canonical ensemble, the gaseous phase and the condensed phase are stable while the core-halo phase is unstable (it represents a “critical droplet” that the system must create to pass from one phase to the other). In the microcanonical ensemble, all the equilibrium states are stable. The system may directly reach the core-halo phase through a process of collisionless violent relaxation. It may also evolve collisionally, following the arrows, from the gaseous solution to the core-halo solution.

It corresponds to a completely degenerate fermion ball surrounded by a tenuous classical isothermal atmosphere. This quantum solution (Q) is thermodynamically stable in all statistical ensembles.

C. Small DM halos with $(M_h)_{\text{CCP}} < M_h < (M_h)_{\text{MCP}}$

Small DM halos have a mass in the range $(M_h)_{\text{CCP}} = 6.73 \times 10^8 M_\odot < M_h < (M_h)_{\text{MCP}} = 1.08 \times 10^{10} M_\odot$. Specifically, we consider a DM halo characterized by a degeneracy parameter $\mu = 10^3$. It has a mass $M_h = 4.93 \times 10^9 M_\odot$ [see Eq. (98)] and a radius $r_h = 4.46$ kpc [see Eq. (96)]. The corresponding caloric curve (see Sec. III A) is represented in Fig. 12. Since $\mu_{\text{CCP}} < \mu < \mu_{\text{MCP}}$, the caloric curve has an N -shape structure (see Sec. III B). The intersection of this curve with the line $\eta_v \sim 1$ (see Sec. VI B) determines three solutions: a gaseous solution, a core-halo solution and a condensed solution that we do not consider here (see Sec. VI B). The gaseous solution has a concentration parameter $k_G = 206$ (see Fig. 9). The corresponding density profile is plotted as a dashed line in Fig. 13. It represents a purely classical isothermal DM halo without quantum core as investigated in Sec. IV. This solution lies in the region of the caloric curve where the specific heat is positive ($C = dE/dT > 0$). It is thermodynamically stable in all statistical ensembles (maximum entropy state at fixed mass and energy and minimum free energy state at fixed mass). The core-halo solution has a concentration parameter $k_{\text{CH}} = 1.12 \times 10^{-3}$ (see Fig. 9). The corresponding density profile (see Sec. III A) is plotted as a solid line in

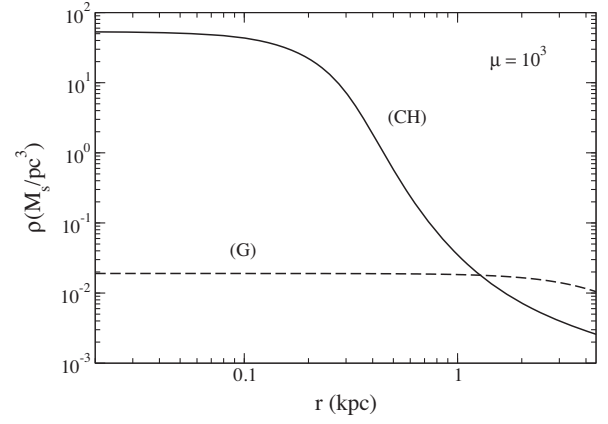


FIG. 13. Density profile of the core-halo solution ($k_{\text{CH}} = 1.12 \times 10^{-3}$) for $\mu = 10^3$. For comparison, we have represented in dashed line the gaseous solution which corresponds to a classical isothermal halo ($k_G = 206$).

Fig. 13. It represents a DM halo with a quantum core (fermion ball) of mass $M_c = 2.21 \times 10^9 M_\odot$, radius $R_c = 389$ pc and central density $\rho_0 = 53.6 M_\odot/\text{pc}^3$ [we have used Eq. (111) to obtain M_c , Eqs. (113) and (114) to obtain R_c and ρ_0 , and we have taken into account the logarithmic correction $\mathcal{A} = 3.48$ from Eq. (116)] surrounded by a classical isothermal atmosphere. This core-halo solution lies in the region of the caloric curve where the specific heat is negative ($C = dE/dT < 0$). It is thermodynamically unstable in the canonical ensemble (saddle point of free energy at fixed mass) but it is thermodynamically stable in the microcanonical ensemble (entropy maximum at fixed mass and energy) which is the relevant ensemble to consider (see Sec. II).²⁴

For small DM halos with $(M_h)_{\text{CCP}} < M_h < (M_h)_{\text{MCP}}$, the gaseous solution and the core-halo solution are both thermodynamically stable in the microcanonical ensemble (maximum entropy state at fixed mass and energy). Therefore, they are both likely to result from a natural evolution in a thermodynamical sense. Let us consider different scenarios of formation and evolution in line with the general discussion given in Sec. II:

- (1) The core-halo solution may arise naturally from a process of violent collisionless relaxation (following Jeans instability and free fall) since it is a maximum entropy state in the sense of Lynden-Bell. This is a fast process taking place on a dynamical timescale. If the evolution is collisionless, the system remains in that state.

²⁴The solutions G, CH, and C that we consider have different energies but the same temperature. Indeed, the temperature is more relevant than the energy to characterize a DM halo since, according to the virial theorem, $\eta \sim 1$. However, we stress that we must analyze the thermodynamical stability of the system in the microcanonical ensemble, not in the canonical ensemble.

- (2) The gaseous solution may also arise naturally from a process of violent collisionless relaxation since it is a maximum entropy state in the sense of Lynden-Bell. Then, there are two possibilities:
- If the evolution is collisionless, the system remains in that state.
 - If the evolution is collisional, the system may evolve along the series of equilibria (see Fig. 12). Indeed, because of collisions²⁵ and evaporation the central density increases and the energy decreases. The temperature first decreases in the region of positive specific heat ($C = dE/dT > 0$) then increases in the region of negative specific heat ($C = dE/dT < 0$). The whole series of equilibria represented in Fig. 12 is stable in the microcanonical ensemble. Therefore, if the DM halo evolves adiabatically under the effect of collisions, it can progressively pass from the gaseous solution to the core-halo solution. This is a slow relaxation taking place on a secular timescale. This may be a mechanism—alternative to violent relaxation—which explains how the system reaches the core-halo solution.

In conclusion, small DM halos with $(M_h)_{CCP} < M_h < (M_h)_{MCP}$ can be in two types of configuration:

- The gaseous solution coinciding with the classical isothermal sphere. This simple solution is consistent with the observations because we have shown in Sec. III C of [25] that an isothermal DM halo is almost indistinguishable from the observational Burkert profile.
- The core-halo solution made of a quantum core (fermion ball) of mass $M_c = 2.21 \times 10^9 M_\odot$ and radius $R_c = 389$ pc surrounded by a classical isothermal atmosphere. The quantum core cannot mimic a SMBH because it is too big (its radius $R_c = 389$ pc is much larger than its Schwarzschild radius $R_S = 2GM/c^2 = 2.11 \times 10^{-4}$ pc). However, it can represent a large quantum bulge made of DM. This quantum bulge may possibly exist at present at the center of certain galaxies or may have existed in the past as a temporary state, and has disappeared since then. Indeed, a large bulge may provide a favorable environment for triggering the formation of a SMBH that can then grow by accretion. The final outcome of this scenario would then be a classical isothermal halo containing either a quantum bulge (large fermion ball) or a SMBH that would be the remnant of the original bulge.

²⁵These collisions between DM particles are not two-body gravitational encounters because the relaxation time would be too long [33,34], but they can have another origin such as short-range interactions (SIDM model) like in, e.g., Ref. [98].

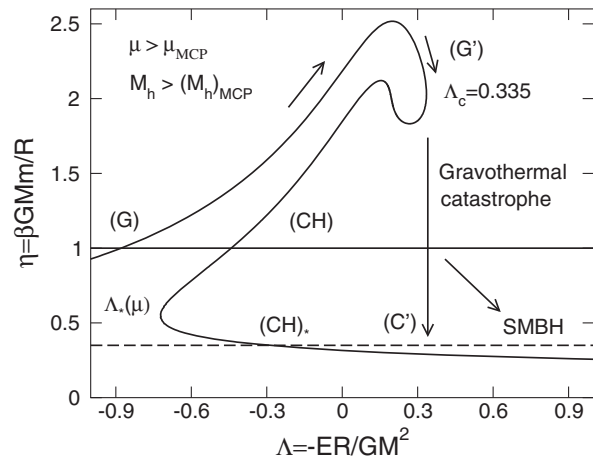


FIG. 14. Caloric curve of self-gravitating fermions for $\mu = 10^5$. For $M_h > (M_h)_{MCP}$, the caloric curve has a Z-shape structure (dinosaur's neck). In the microcanonical ensemble, the gaseous phase G and G' before the first turning point of energy and the condensed phase C' and C after the last turning point of energy are stable. By contrast, the core-halo phase CH in the intermediate branch between the first and the last turning points of energy is unstable. The system can evolve collisionally in the gaseous phase G and G' up to the turning point of energy E_c and collapse in the condensed phase C' (see arrows). This corresponds to the gravothermal catastrophe [76] arrested by quantum effects. Another possibility is that the gravothermal catastrophe triggers a dynamical instability of general relativistic origin leading to the formation of a SMBH [98] (see Fig. 16 below).

D. Large DM halos with $M_h > (M_h)_{MCP}$

Large DM halos have a mass $M_h > (M_h)_{MCP} = 1.08 \times 10^{10} M_\odot$. Specifically, we consider a DM halo characterized by a degeneracy parameter $\mu = 10^5$. It has a mass $M_h = 1.96 \times 10^{11} M_\odot$ [see Eq. (98)] and a radius $r_h = 28.1$ kpc [see Eq. (96)]. The corresponding caloric curve (see Sec. III A) is represented in Fig. 14. Since $\mu > \mu_{MCP}$, the caloric curve has a Z-shape structure similar to a dinosaur's neck (see Sec. III B). As before, the intersection of this curve with the line $\eta_v \sim 1$ (see Sec. VI B) determines two physical solutions: a gaseous solution and a core-halo solution. The gaseous solution has a concentration parameter $k_G = 2.05 \times 10^4$ (see Fig. 9). The corresponding density profile is plotted as a dashed line in Fig. 15. It represents a purely classical isothermal DM halo of mass M_h and radius r_h without quantum core as investigated in Sec. IV. It lies in a region of positive specific heat. It is thermodynamically stable in all statistical ensembles (maximum entropy state at fixed mass and energy and minimum free energy state at fixed mass). The core-halo solution has a concentration parameter $k_{CH} = 1.38 \times 10^{-5}$ (see Fig. 9). The corresponding density profile (see Sec. III A) is plotted as a solid line in Fig. 15. It represents a DM halo with a quantum core (fermion ball) of mass $M_c = 1.29 \times 10^{10} M_\odot$, radius $R_c = 216$ pc and central density $\rho_0 = 1820 M_\odot/\text{pc}^3$ [we have used Eq. (111) to

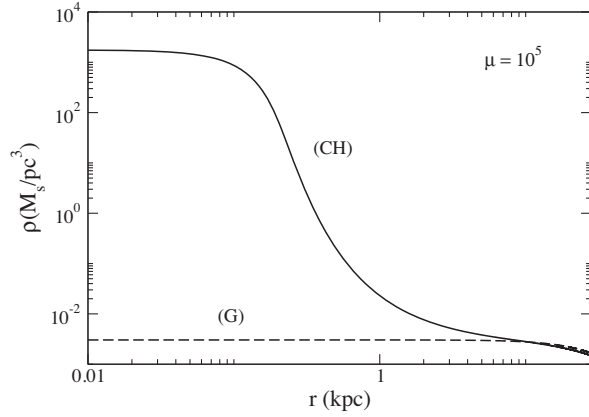


FIG. 15. Density profile of the core-halo solution ($k_{\text{CH}} = 1.38 \times 10^{-5}$) for $\mu = 10^5$. For comparison, we have represented in dashed line the gaseous solution which corresponds to a classical isothermal halo ($k_G = 2.05 \times 10^4$).

obtain M_c , Eqs. (113) and (114) to obtain R_c and ρ_0 , and we have taken into account the logarithmic correction $\mathcal{A} = 5.10$ from Eq. (116)] surrounded by a classical isothermal atmosphere of mass $\sim M_h$ and radius r_h . Since this solution is located between the first and the last turning points of energy, it is thermodynamically unstable in all statistical ensembles (saddle point of entropy at fixed mass and energy and saddle point of free energy at fixed mass). Note that it lies in a region of the caloric curve with a positive specific heat, showing that a positive specific heat does not necessarily imply that the system is stable.

For large DM halos with $M_h > (M_h)_{\text{MCP}} = 1.08 \times 10^{10} M_\odot$ the gaseous solution is thermodynamically stable but the core-halo solution is thermodynamically unstable. Therefore, the gaseous solution is likely to result from a natural evolution in a thermodynamical sense while the core-halo solution should not be observed.²⁶ Let us consider different scenarios of formation and evolution in line with the general discussion given in Sec. II.

The gaseous solution may arise naturally from a process of violent collisionless relaxation (following Jeans instability and free fall) since it is a maximum entropy state in the sense of Lynden-Bell. This is a fast process taking place on a few dynamical times. Then, there are two possibilities:

- (1) If the evolution is collisionless, the system remains in that state.

²⁶This statement could be alleviated by the following considerations. On the one hand, the core-halo solution would be stable if η_v is smaller than the value $\eta_v = 1$ that we have somehow arbitrarily chosen (see the dashed line in Fig. 14). For example, the core-halo solution CH_* located just after the last turning point of energy Λ_* is stable. On the other hand, it is always possible that the process of *incomplete relaxation* [31,82] leads to a Vlasov stable core-halo profile that is not of the Lynden-Bell (or Fermi-Dirac) type. Indeed, we have seen that all DFs $f = f(\epsilon)$ with $f'(\epsilon) < 0$ are dynamically stable in Newtonian gravity even those that are thermodynamically unstable.

- (2) If the evolution is collisional, the system may slowly evolve along the series of equilibria (see Fig. 14). The beginning of the collisional evolution is similar to that described previously. The temperature first decreases in the region of positive specific heat ($C = dE/dT > 0$) then increases in the region of negative specific heat ($C = dE/dT < 0$). However, when the system reaches the turning point of energy (corresponding to the minimum energy E_c) it becomes thermodynamically unstable and undergoes the gravothermal catastrophe [76]. At that point, there are several possibilities:

- (a) We first assume that the gravothermal catastrophe is eventually halted by quantum mechanics (Pauli's exclusion principle) and that the system reaches an equilibrium state. This takes the system from the gaseous phase (G') to the condensed phase (C') in which only a fraction (typically $\sim 1/4$) of the mass of the DM halo forms a compact fermion ball while the rest of the mass constitutes a hot halo. The hot halo has a uniform density so that it is strongly held by the box (see Fig. 16 in [43]). As discussed in [43,46], if we remove the box, the halo should be expelled at large distances in a process reminiscent of a supernova explosion [99–101]. This is because the collapse of the core heats the halo which thus extends at large distances. Although this mechanism could be at work for fermion stars such as white dwarfs and neutron stars, it may not be relevant for DM halos. Therefore, we shall prefer the following scenarios.

- (b) We assume that the gravothermal catastrophe is eventually halted by quantum mechanics as before, but the system does not reach the equilibrium solution C'. It may reach an out-of-equilibrium core-halo structure that is not described by the Fermi-Dirac distribution. This out-of-equilibrium state (CH_{out}) may be made of a slowly evolving quantum core surrounded by a classical atmosphere that is not as much extended as the classical atmosphere of the equilibrium solution C'. Actually, in this scenario, the initial isothermal halo (at criticality) is essentially left undisturbed. Since the solution CH_{out} is an out-of-equilibrium structure, we expect that the core-halo mass relation $M_c(M_h)$ is different from the one predicted by Eq. (111). In particular, the quantum core resulting from the gravothermal catastrophe should be more compact and more massive than the quantum core composing the CH solution. The occurrence of this CH_{out} is due to the fact that the exchange of energy between the core and the halo, and the process of thermalization, may take a very long time. Therefore, the equilibrium state C' of scenario (a) may not be reached on relevant timescales.

(c) Finally, we assume that the halo undergoes a gravothermal catastrophe at E_c but we consider another evolution in which quantum mechanics cannot prevent gravitational collapse (the validity of this hypothesis is considered in Sec. VII E). This scenario, already advocated in Refs. [33,34], is based on the SIDM model of Balberg *et al.* [98] who developed the idea of an “avalanche-type contraction” towards a SMBH initially suggested by Zeldovich and Podurets [102], improved by Fackerell *et al.* [103], and confirmed numerically by Shapiro and Teukolsky [104–106]. The initial stage of the gravothermal catastrophe is well known. The core collapses and reaches high densities and high temperatures while the halo is not sensibly affected by the collapse of the core and maintains its initial structure. Now, Balberg *et al.* [98] argue that during the gravothermal catastrophe, when the central density and the temperature increase above a critical value, the system undergoes a dynamical instability of general relativistic origin leading to the formation of a SMBH on a dynamical time scale. Only the central region of the DM halo (not its outer part) is affected by this collapse so the final outcome of this scenario is a classical isothermal halo at criticality containing a central SMBH.

In conclusion, large DM halos with $M_h > (M_h)_{\text{MCP}}$ can be in three types of configuration:

- (1) A purely classical isothermal halo, G, without quantum core.
- (2) An out-of-equilibrium core-halo solution, resulting from the gravothermal catastrophe, which is different from the CH solution that is unstable or from the C' solution that is unphysical. It is made of a compact (small and massive) quantum core surrounded by a classical isothermal atmosphere at criticality.
- (3) A classical isothermal halo at criticality containing a SMBH resulting from the gravothermal catastrophe followed by a dynamical instability of general relativity origin.

It is also possible that, following the gravothermal catastrophe, the system first forms a fermion ball then a SMBH (see Secs. VII E and VIII D).

Remark: The scenarios (2) and (3) may be particularly interesting especially if we account for tidal effects. Indeed, it has been shown in [33,34] that the King profile at criticality (i.e., at the verge of the gravothermal catastrophe) is very close to the observational Burkert profile (see, e.g., Figs. 18 and 27 of [33] and Fig. 1). Therefore, the structure of large DM halos could consist in a fermion ball or a SMBH surrounded by an envelope with a marginal (critical) King profile unaffected by the collapse of the core [33,34]. The conditions for forming a SMBH at the center of a DM halo are discussed in Sec. VII E based on the results of Alberti and Chavanis [46,47].

E. Criterion for the existence of a SMBH at the center of a galaxy

According to the above scenario, the formation of a SMBH at the center of a galaxy is possible only if the system can experience the gravothermal catastrophe and if, during core collapse, the core can reach sufficiently high densities and high temperatures to trigger a general relativistic dynamical instability leading to the formation of a SMBH. This may happen in sufficiently large systems. By contrast, in small systems, quantum mechanics (Pauli's exclusion principle for fermions) prevents the gravothermal catastrophe and leads to a large fermion ball (bulge) instead of a SMBH. In conclusion, a SMBH can form only if the degeneracy parameter μ is sufficiently large so that the gravothermal catastrophe is efficient. Therefore, we expect that DM halos harbor a SMBH if $\mu \gg \mu_{\text{MCP}} = 2670$ i.e.,

$$M_h \gg (M_h)_{\text{MCP}} = 1.08 \times 10^{10} M_\odot, \quad (118)$$

and we expect that DM halos harbor a large quantum bulge (fermion ball) in the opposite case.²⁷

This result is qualitatively consistent with the conclusion reached by Ferrarese [107] on the basis of observations. She found that black holes can form only in sufficiently large galaxies, above a typical mass $\sim 5 \times 10^{11} M_\odot$. This limit may correspond to the microcanonical critical point $(M_h)_{\text{MCP}}$ of our model. To facilitate further comparisons, using Eq. (97), we rewrite this criterion as²⁸

$$M_h \gg (M_h)_{\text{MCP}} = 483 \left(\frac{\hbar^3 \Sigma_0^{3/4}}{G^{3/2} m^4} \right)^{4/5}. \quad (119)$$

Actually, things are more complicated than the scenario just exposed. Indeed, as shown by Alberti and Chavanis [46,47], when general relativity is taken into account, the caloric curves of the self-gravitating Fermi gas depend not only on μ , but also on the value of the particle number N with respect to N_{OV} . When $N < N_{\text{OV}}$, the caloric curve is similar to the one reported in Fig. 14. In particular, there is an equilibrium state for any value of the energy since quantum mechanics (Pauli's exclusion principle) can prevent gravitational collapse even at $T = 0$. By contrast, when $N > N_{\text{OV}}$, a new turning point of energy appears [46,47] as shown in Fig. 16. In that case, there is no equilibrium state below a minimum energy E_c'' and the system collapses towards a black hole. These results

²⁷Large DM halos may contain a SMBH but they should not contain a fermion ball because the core-halo solution is thermodynamically unstable. By contrast, small DM halos may contain a large quantum bulge (fermion ball) but they should not contain a SMBH because the gravothermal catastrophe is inhibited by quantum mechanics.

²⁸Equation (119) is in good agreement with the criterion $H > 8.24$ obtained in Appendix H of [34] where H is defined by Eq. (E4) of that paper.

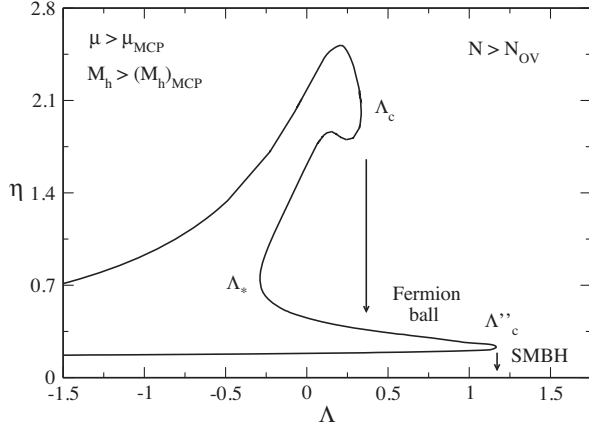


FIG. 16. Caloric curve for $M_h > (M_h)_{\text{MCP}}$ and $N > N_{\text{OV}}$ (from [46,47]). As energy decreases, the system first experiences a gravothermal catastrophe at Λ_c leading to a fermion ball stabilized by quantum degeneracy, then a gravitational collapse at Λ''_c leading to a SMBH. They are both surrounded by a classical isothermal envelope.

suggest that the correct criterion for the existence of a SMBH at the center of a galaxy is that $\mu \gg \mu_{\text{MCP}}$ (in order to trigger the gravothermal catastrophe) and $N > N_{\text{OV}}$ (in order to have a gravitational collapse towards a SMBH). The first condition yields Eq. (119). It signals the instability of the core-halo solution with respect to the gravothermal catastrophe. If we approximate the second condition by $M_h > M_{\text{OV}}$, where M_{OV} is given by Eq. (87), we obtain the condition

$$M_h > M_{\text{OV}} = 0.384 \left(\frac{\hbar c}{G} \right)^{3/2} \frac{1}{m^2}. \quad (120)$$

If $(M_h)_{\text{MCP}} < M_h < M_{\text{OV}}$ we expect that the halo experiences the gravothermal catastrophe but does not form a SMBH. It may rather form an out-of-equilibrium fermion ball (scenario b). By contrast, if $M_h > M_{\text{OV}}$, the halo may form either an out-of-equilibrium fermion ball (scenario b) or a SMBH (scenario c). A necessary condition to form a SMBH is that $M_{\text{OV}} > (M_h)_{\text{MCP}}$. This yields

$$m > 383 \frac{\hbar^{3/4} \sum_0^{1/2} G^{1/4}}{c^{5/4}} = 0.278 \text{ eV}/c^2. \quad (121)$$

This condition is always fulfilled in practice.

For $m = 165 \text{ eV}/c^2$ we find that $(M_h)_{\text{MCP}} = 1.08 \times 10^{10} M_\odot$ and $M_{\text{OV}} = 2.30 \times 10^{13} M_\odot$. In that case, the OV mass is very large, much larger than the mass $M_h = 10^{11} M_\odot$ of a DM halo comparable to the Milky Way. As a result, the gravothermal catastrophe should be stopped by quantum mechanics and a SMBH cannot be formed. This suggests that the Milky Way contains an out-of-equilibrium fermion ball rather than a SMBH. However, if we consider a larger fermion mass $m \sim 1 \text{ keV}/c^2$ we find

$(M_h)_{\text{MCP}} = 3.38 \times 10^7 M_\odot$ and $M_{\text{OV}} = 6.26 \times 10^{11} M_\odot$, which are closer to the conditions required to form a SMBH (see, however, the Remark below).

Remark: It is natural to expect that the gravitational collapse at E'_c leads to a SMBH of mass M_{OV} because the instability of the DM halo occurs precisely at the moment where the core mass becomes critical ($M_c = M_{\text{OV}}$) [46,62]. In that case, we find for $m = 165 \text{ eV}/c^2$ and $m \sim 1 \text{ keV}/c^2$ that the SMBH mass would be $M_{\text{OV}} = 2.30 \times 10^{13} M_\odot$ and $M_{\text{OV}} = 6.26 \times 10^{11} M_\odot$ respectively. These very large masses are not consistent with the observations of SMBHs. The OV mass is more relevant if the fermion has a larger mass m as considered in Sec. VIII. For example, for $m = 54.6 \text{ keV}/c^2$, we get $M_{\text{OV}} = 2.10 \times 10^8 M_\odot$ which is of the order of the mass of SMBHs observed in active galactic nuclei (AGNs). On the other hand, for $m = 386 \text{ keV}/c^2$ we get $M_{\text{OV}} = 4.2 \times 10^6 M_\odot$, which is of the order of the mass of Sagittarius A*. In that case, according to the scenario (3) discussed above, the Milky Way could consist in a SMBH of mass $M_{\text{OV}} = 4.2 \times 10^6 M_\odot$ (Sagittarius A*) resulting from the gravothermal catastrophe surrounded by an envelope with a marginal King profile similar to the Burkert profile (see Sec. VIII D).

F. Application to the Milky Way

We now specifically apply our fermionic model to the Milky Way. We consider a DM particle mass $m = 165 \text{ eV}/c^2$ so that the minimum halo has a mass $(M_h)_{\text{min}} = 10^8 M_\odot$ and a radius $(r_h)_{\text{min}} = 597 \text{ pc}$ (see Sec. V). To be specific, we consider a DM halo of mass $M_h = 10^{11} M_\odot$ (corresponding to $M_v \sim 10^{12} M_\odot$) and radius $r_h = 20.1 \text{ kpc}$ similar to the one that surrounds our Galaxy (see Sec. IV). Using Eq. (98) we find that the corresponding degeneracy parameter is $\mu = 4.31 \times 10^4$. The corresponding caloric curve has a Z-shape structure like in Fig. 14. The gaseous solution corresponding to a purely classical isothermal halo, is plotted as a dashed line in Figs. 17 and 18. Then, considering the core-halo solution and using Eqs. (86), (106), (111), and (116), we find that the DM halo should contain a quantum core of mass $M_c = 9.45 \times 10^9 M_\odot$, radius $R_c = 240 \text{ pc}$ and central density $\rho_0 = 983 M_\odot/\text{pc}^3$.²⁹ The density and velocity profiles given by Eqs. (36) and (37) are represented as solid lines in Figs. 17 and 18. Clearly, the fermion ball is too extended to mimic a black hole. It is more likely to represent a large quantum bulge as discussed in Sec. VII C.

The halo mass $M_h = 10^{11} M_\odot$ is above the micro-canonical critical point $(M_h)_{\text{MCP}} = 1.08 \times 10^{10} M_\odot$. The gaseous solution is thermodynamically stable and could result from a process of violent relaxation. The core-halo solution is thermodynamically unstable and should not be observed. It should be replaced by an out-of-equilibrium

²⁹Comparatively, for $m = 1 \text{ keV}/c^2$ we get $\mu = 4.42 \times 10^7$, $M_c = 4.30 \times 10^8 M_\odot$, $R_c = 5.84 \text{ pc}$, and $\rho_0 = 3.71 \times 10^6 M_\odot/\text{pc}^3$.

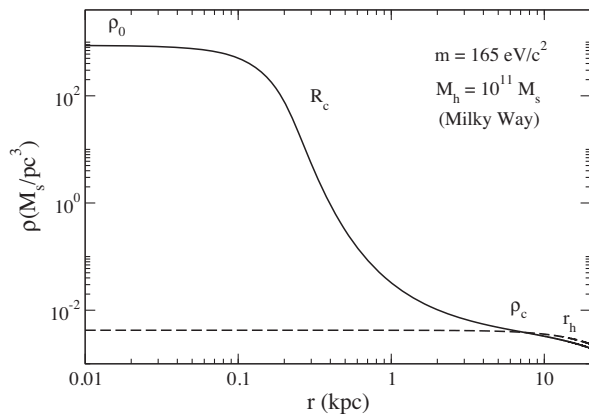


FIG. 17. Density profile of the core-halo solution ($k_{\text{CH}} = 5.21 \times 10^{-5}$) for a DM halo of mass $M_h = 10^{11} M_\odot$ (Milky Way) up to the halo radius $r_h = 20.1$ kpc. We have taken $m = 165$ eV/ c^2 . For comparison, we have represented in dashed line the gaseous solution which corresponds to a classical isothermal halo ($k_G = 8.85 \times 10^3$).

core-halo structure CH_{out} with a compact quantum core as discussed in Sec. VII D. However, since we are relatively close to the microcanonical critical point, the core-halo solution may be marginally relevant, especially if η_v is smaller than expected, e.g., if we select the CH_* solution of Fig. 14 (see footnote 26).

Remark: We may wonder if there is evidence of a large quantum bulge at the center of the Milky Way. If we make the analogy with bosonic models of DM halos, the fermion ball is the equivalent of the soliton [16,17]. The mass and size of the fermion ball that we find correspond to the typical mass and size of the solitons that have been predicted theoretically or observed in numerical simulations of BECDM [16,17]. In addition, De Martino *et al.* [108] have suggested that a large soliton, forming a quantum bulge of mass $\simeq 10^9 M_\odot$ and radius $\simeq 100$ pc, may be present at the center of the Milky Way and may account for the observed dispersion velocity peak (see the discussion in Sec. VII E. of [25]). If this result is confirmed, we could argue that this quantum bulge may correspond to a fermion ball rather than a bosonic soliton since our model yields the same characteristic mass and radius.³⁰

G. Problems with a fermionic model involving a mass $m = 165$ eV/ c^2 or $m \sim 1$ keV/ c^2

In this section, we mention some problems with a fermionic DM halo model involving a “small” fermion mass $m = 165$ eV/ c^2 or $m \sim 1$ keV/ c^2 :

³⁰In that case, we must also add a primordial black hole in the model in order to account for the observation of a large central mass at the center of the Milky Way corresponding to Sgr A*.

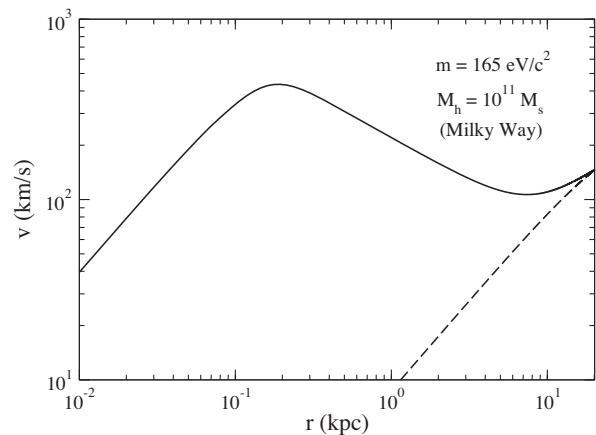


FIG. 18. Velocity profile of the core-halo solution ($k_{\text{CH}} = 5.21 \times 10^{-5}$) for a DM halo of mass $M_h = 10^{11} M_\odot$ (Milky Way) up to the halo radius $r_h = 20.1$ kpc. We have taken $m = 165$ eV/ c^2 . For comparison, we have represented in dashed line the gaseous solution which corresponds to a classical isothermal halo ($k_G = 8.85 \times 10^3$).

- (i) Argüelles *et al.* [60] show in their Figs. 3 and 4 that a fermion mass $m \sim 0.6$ keV/ c^2 is not consistent with the structure of the Milky Way. A much larger mass $m \sim 48$ keV/ c^2 is necessary to reproduce the rotation curve of the Milky Way. Therefore, the study of Argüelles *et al.* [60] rules out the possibility to have a large DM bulge of mass $\simeq 10^9 M_\odot$ and radius $\simeq 100$ pc at the center of the Milky Way. This is in contradiction with our claim and with the claim of De Martino *et al.* [108] that a large DM bulge may account for the dispersion velocity peak observed in the Milky Way.³¹ It would be extremely important to clarify this issue.
- (ii) A warm dark matter fermionic particle with a mass $m < 3$ keV/ c^2 is ruled out by cosmological observations [110,111]. Likewise, a boson of mass $m = 1.44 \times 10^{-22}$ eV/ c^2 which produces results similar to a fermion of mass $m = 165$ eV/ c^2 (the soliton in the BEC model being the counterpart of the fermion ball) is in tension with cosmological observations such as the Lyman α forest (it is one or two orders of magnitude smaller than the required value) [112]. This suggests that a minimum halo mass $(M_h)_{\text{min}} = 0.39 \times 10^6 M_\odot$ (Willman I) leading to a fermion mass $m \sim 1$ keV/ c^2 and a boson mass $m = 9.22 \times 10^{-21}$ eV/ c^2 [95] may be more relevant than a

³¹As noted by C. Argüelles (private communication), De Martino *et al.* [108] have to add “by hand” a Plummer component of bulge stars to reduce the central dispersion because otherwise the BECDM model overestimates the data. On the other hand, Bar *et al.* [109] argue in their Sec. III that the central mass component could well be due to ordinary baryonic matter rather than a DM soliton.

minimum halo mass $(M_h)_{\min} = 10^8 M_\odot$ (Fornax) leading to a fermion mass $m = 165 \text{ eV}/c^2$ and a boson mass $m = 1.44 \times 10^{-22} \text{ eV}/c^2$ (see [38] for the determination of the DM particle mass).

- (iii) The OV mass $M_{\text{OV}} = 2.30 \times 10^{13} M_\odot$ or $M_{\text{OV}} = 6.26 \times 10^{11} M_\odot$ associated with a fermion of mass $m = 165 \text{ eV}/c^2$ or $m \sim 1 \text{ keV}/c^2$ seems to be too large to be of much astrophysical interest (see the discussion in Sec. VII E).

VIII. CAN A FERMION BALL MIMIC A SMBH?

A. Sagittarius A*

The detailed study of the motion of S-stars near the Galactic center has revealed the presence of a very massive central object, Sagittarius A* (Sgr A*). This central object is usually associated with a SMBH of mass $M = 4.2 \times 10^6 M_\odot$ and Schwarzschild radius $R_S = 4.02 \times 10^{-7} \text{ pc}$. Whatever the object may be, its radius must be smaller than $R_P = 6 \times 10^{-4} \text{ pc}$ ($R_P = 1492 R_S$), the S2 star pericenter [113]. Similar objects are expected to reside at the center of most spiral and elliptical galaxies, in active galactic nuclei (AGN). Although it is commonly believed that these objects are SMBHs [113–116], this is not yet established on a firm observational basis in all cases. Some authors have proposed that such objects could be fermion balls [59,60,63,65–67] or boson stars [117,118] that could mimic a SMBH.

Let us consider this possibility in the framework of the fermionic model. More precisely, let us investigate if a fermion ball can mimic a SMBH at the center of the Galaxy.

B. Standard Fermi-Dirac distribution

Bilic *et al.* [67] developed a general relativistic model of fermionic DM halos at finite temperature with a fermion mass $m = 15 \text{ keV}/c^2$ that describes both the center and the halo of the Galaxy in a unified manner. The density profile has a core-halo structure with a quantum core (fermion ball) and a classical isothermal atmosphere. By using the usual Fermi-Dirac distribution and choosing parameters so as to fit observational data at large distances, they found a fermion ball of mass $M_c = 2.27 \times 10^6 M_\odot$ and radius $R_c = 18 \text{ mpc}$.³² Unfortunately, its radius is larger by a factor 100 than the bound $R_P = 6 \times 10^{-4} \text{ pc}$ set by observations [113]. This is why Bilic and coworkers abandoned this fermion ball scenario (R. Viollier, private communication). The same problem was encountered later by Ruffini *et al.* [59] who developed a similar model with a fermion mass $m \sim 10 \text{ keV}/c^2$.

Let us check that their results are consistent with our analytical box model. Following Bilic *et al.* [67], we take a

³²The fermion ball is weakly general relativistic because $M_c = 2.27 \times 10^6 M_\odot \ll M_{\text{OV}} = 2.78 \times 10^9 M_\odot$ [see Eq. (87)].

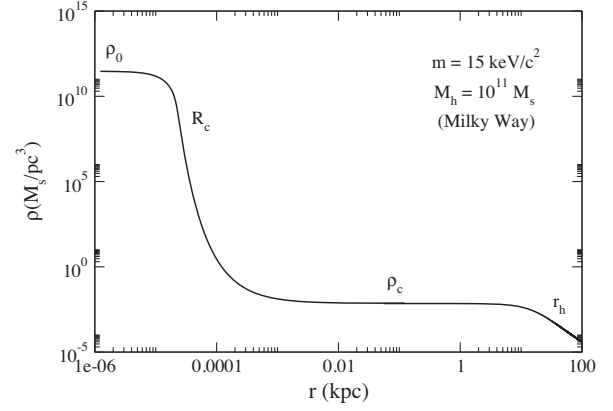


FIG. 19. Density profile of a DM halo of mass $M_h = 10^{11} M_\odot$ (Milky Way) assuming a fermion mass $m = 15 \text{ keV}/c^2$.

DM particle mass $m = 15 \text{ keV}/c^2$. The corresponding minimum halo (see Sec. V) has a mass $(M_h)_{\min} = 54.0 M_\odot$ and a radius $(r_h)_{\min} = 0.439 \text{ pc}$. If we consider a DM halo of mass $M_h = 10^{11} M_\odot$ and radius $r_h = 20.1 \text{ kpc}$ similar to the one that surrounds our Galaxy (see Sec. IV) we find that the corresponding degeneracy parameter is $\mu = 2.94 \times 10^{12}$ [see Eq. (98)]. Considering the core-halo solution and using Eqs. (86), (106), (111), and (116), we find that this DM halo should contain a quantum core of mass $M_c = 2.39 \times 10^6 M_\odot$, radius $R_c = 22.7 \text{ mpc}$ and central density $\rho_0 = 2.95 \times 10^{11} M_\odot/\text{pc}^3$ in good agreement with the numerical results of Bilic *et al.* [67] and Ruffini *et al.* [59]. The corresponding density and velocity profiles given by Eqs. (36) and (37) are represented in Figs. 19 and 20. They are in good agreement with Fig. 3 of Bilic *et al.* [67] and Figs. 1 and 3 of Ruffini *et al.* [59]. Therefore, our semianalytical model [see in particular Eq. (111)] can reproduce their numerical results.

Let us now discuss the thermodynamical stability of the core-halo solution considered by Bilic *et al.* [67] and Ruffini *et al.* [59]. The caloric curve (see Sec. III A)

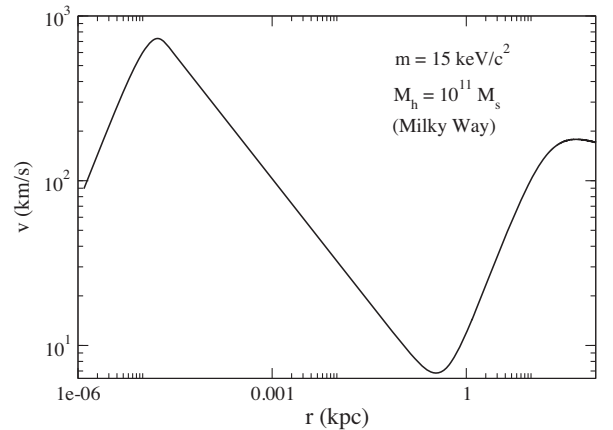


FIG. 20. Velocity profile of a DM halo of mass $M_h = 10^{11} M_\odot$ (Milky Way) assuming a fermion mass $m = 15 \text{ keV}/c^2$.

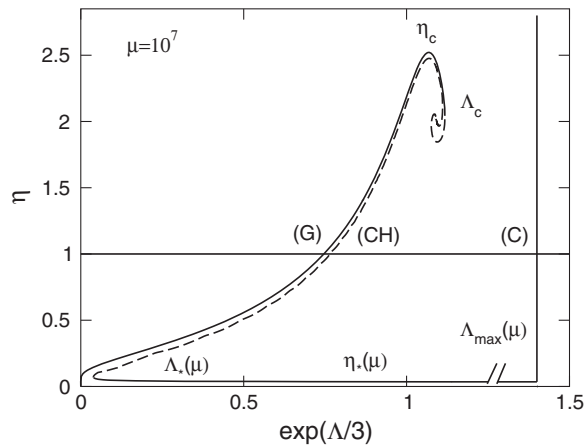


FIG. 21. Caloric curve for $M_h \gg (M_h)_{\text{MCP}}$.

corresponding to $\mu = 2.94 \times 10^{12}$ is similar to the one represented in Fig. 21. For large values of μ , a spiral appears in the caloric curve at the location of the “head” of the dinosaur. As μ increases, the spiral winds more and more before unwinding. For $\mu \gg 1$ the direct and reversed spirals are very close to each other. The intersections of the caloric curve with the line $\eta_v \sim 1$ (see Sec. VIB) determines two physical solutions a before: a gaseous solution and a core-halo solution. The gaseous solution represents a purely classical isothermal DM halo of mass M_h and radius r_h without quantum core as investigated in Sec. IV (see Figs. 4 and 5). This solution lies on the caloric curve in the region of positive specific heat. This gaseous solution is thermodynamically stable in all statistical ensembles (maximum entropy state at fixed mass and energy and minimum free energy state at fixed mass). The core-halo solution (see Sec. III A) represents a DM halo with a quantum core (fermion ball) of mass $M_c = 2.39 \times 10^6 M_\odot$, radius $R_c = 22.7$ mpc and central density $\rho_0 = 2.95 \times 10^{11} M_\odot/\text{pc}^3$ surrounded by a classical isothermal atmosphere of mass $\sim M_h = 10^{11} M_\odot$ and radius $r_h = 20.1$ kpc. The corresponding density and velocity profiles are plotted in Figs. 19 and 20. Since this solution lies between the first and the last turning points of energy, it is thermodynamically unstable in all statistical ensembles (saddle point of entropy at fixed mass and energy and saddle point of free energy at fixed mass). This solution lies in a region of the caloric curve with a positive specific heat.

The discussion about the thermodynamical stability of the core-halo solution is essentially the same as in Sec. VII D. The main differences are the followings:

- (i) According to the Poincaré-Katz [78,79] criterion, the system loses more and more modes of stability, one at each turning point of energy, as we progress clockwise into the spiral. However, when the spiral unwinds the modes of stability are progressively regained. Indeed, one mode of stability is regained at each turning point

of energy as we follow the spiral anticlockwise.³³ As a consequence, the core-halo solutions that lie on the spiral are very unstable since they have several modes of instability. We note, however, that the core-halo solution has only one mode of instability as before.

- (ii) The energy of the core-halo solution almost coincides with the energy of the gaseous solution. This is because their external structure is exactly the same. The core-halo solution only differs from the gaseous solution by the presence of a small core with a small mass, a small radius and a very high density (see Fig. 19). The core and the halo are separated by a large plateau where the density is approximately constant.³⁴ Therefore, when $\mu \gg \mu_{\text{MCP}}$, the core-halo solution almost coincides with the gaseous solution except that it contains a small nucleus (fermion ball). For smaller values of μ , the plateau is reduced and finally disappears. For example, in Fig. 15, the core-halo solution does not show a very pronounced separation between the quantum core and the halo. Furthermore, the halo is perturbed by the presence of the core (unlike in Fig. 19). As a result, the energy of the core-halo and gaseous solutions on the caloric curve of Fig. 14 are relatively different (unlike in Fig. 21).

In conclusion, the models of Bilic *et al.* [67] and Ruffini *et al.* [59] that are based on the standard Fermi-Dirac DF lead to DM halos with a core-halo structure made of a small quantum core (fermion ball) of mass $M_c = 2.39 \times 10^6 M_\odot$ and radius $R_c = 22.7$ mpc surrounded by a classical isothermal atmosphere. The core and the halo are separated by an extended plateau. The quantum core describes a very compact central object not very different from Sagittarius A*. However, the quantum core is not small enough to account for the observational constraints. Furthermore, this core-halo configuration is thermodynamically unstable so it is not expected to result from a natural evolution (in the sense of Lynden-Bell). Therefore, the original models of Bilic *et al.* [67] and Ruffini *et al.* [59] have to be rejected.³⁵

C. Fermionic King model

More recently, Argüelles *et al.* [60] considered the general relativistic fermionic King model accounting for

³³See [43] and Appendix C of [46] for a detailed discussion of the Poincaré-Katz criterion.

³⁴See Sec. V of [25] for a detailed discussion of the structure of quantum DM halos involving a quantum core, a plateau, and a classical isothermal atmosphere. The core-halo profiles of DM halos with a “small” μ do not show a plateau while an extended plateau is present in DM halos with $\mu \gg \mu_{\text{MCP}}$.

³⁵The claim that the core-halo solution of Refs. [59,67] is thermodynamically unstable was first made in [25,34,46].

a tidal confinement.³⁶ They applied this model to the Milky Way and determined the parameters by fitting the core-halo profile to the observations. For a fermion mass $m = 48 \text{ keV}/c^2$ they obtained a fermion ball of mass $M_c = 4.2 \times 10^6 M_\odot$ and radius $R_c = R_p = 6 \times 10^{-4} \text{ pc}$ which, this time, is consistent with the observational constraints.³⁷

Let us see if their results are consistent with our analytical box model. Following Argüelles *et al.* [60], we take a DM particle mass $m = 48 \text{ keV}/c^2$. The corresponding minimum halo (see Sec. V) has a mass $(M_h)_{\min} = 1.30 M_\odot$ and a radius $(r_h)_{\min} = 0.0683 \text{ pc}$. If we consider a DM halo of mass $M_h = 10^{11} M_\odot$ and radius $r_h = 20.1 \text{ kpc}$ similar to the one that surrounds our Galaxy (see Sec. IV) we find that the corresponding degeneracy parameter is $\mu = 3.09 \times 10^{14}$ [see Eq. (98)]. Considering the core-halo solution and using Eqs. (86), (106), (111), and (116), we find that this halo should contain a quantum core of mass $M_c = 2.61 \times 10^5 M_\odot$, radius $R_c = 2.13 \text{ mpc}$ and central density $\rho_0 = 3.87 \times 10^{13} M_\odot/\text{pc}^3$. Our analytical results are *not* consistent with the results of Argüelles *et al.* [60] because we find that the mass M_c of the fermion ball is about 10 times smaller than their value. Since our analytical model is consistent with the results of Bilic *et al.* [67] and Ruffini *et al.* [59] that are based on the usual Fermi-Dirac DF but not with the results of Argüelles *et al.* [60] that are based on the fermionic King model we deduce that the difference comes from the fact that tidal effects—which are not taken into account in our analytical model—are important (*a priori*, the difference does not come from general relativity effects which are small as we have indicated in footnote 37).

Therefore, in order to obtain accurate results, it is important to use the fermionic King model [34,60] instead of the usual fermionic model [43,59,67]. Argüelles *et al.* [60] managed to fit the density profile and the rotation curve of the Milky Way with the fermionic King distribution and argued that a fermion ball can mimic the effect of a SMBH. This scenario is very attractive because it can explain the whole structure of the galaxy, the supermassive central object and the isothermal halo, by a single DF; the fermionic King model [71,72].

Let us now discuss the thermodynamical stability of the core-halo solution considered by Argüelles *et al.* [60].

³⁶The fermionic King model was heuristically introduced by Ruffini and Stella [71] as a generalization of the classical King model [81]. It was also introduced independently by Chavanis [72] who derived it from a kinetic theory based on the fermionic Landau equation. The nonrelativistic fermionic King model was studied by Chavanis *et al.* [34] who showed that the density profiles typically have a core-halo structure with a quantum core (fermion ball) and a tidally-truncated isothermal halo leading to flat rotation curves. They also studied the caloric curves and the thermodynamical stability of the equilibrium states. The name “fermionic King model” was introduced in [34,44].

³⁷The fermion ball is weakly general relativistic because $M_c = 4.2 \times 10^6 M_\odot \ll M_{\text{OV}} = 2.71 \times 10^8 M_\odot$ [see Eq. (87)].

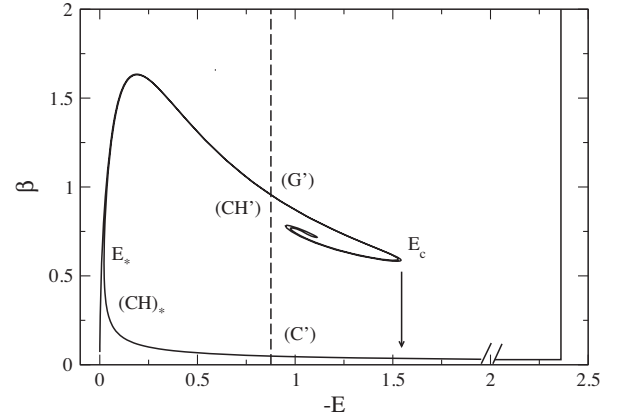


FIG. 22. Caloric curve of the fermionic King model for large DM halos (from [34]). CH' considered in [34] is unstable. CH_{*} considered in [62] has a similar structure and is stable (being located just after the last turning point of energy E_*). It may account for the structure of the Milky Way in which the fermion ball mimics a SMBH.

The caloric curves of the fermionic King model in Newtonian gravity for arbitrary values of μ were first studied by Chavanis *et al.* [34]. The caloric curve corresponding to a large value of μ (i.e., having the characteristics of the Milky Way) is plotted in Fig. 30 of [34]. In that paper, we have focused on the density profiles of the solutions located in the region of the spiral (see Fig. 44 of [34]). For a given energy in that region, we found a gaseous solution G', a core-halo solution CH' and a condensed solution C'. These results are reproduced in Figs. 22 and 23 for convenience. G' corresponds to the classical isothermal sphere. Since it lies before the first turning point of energy, it is thermodynamically stable in the microcanonical ensemble (maximum entropy state at fixed mass and energy). C' is also stable in the microcanonical ensemble because it lies after the last turning point of energy. However, this solution is not astrophysically relevant because it has a too extended halo that is not consistent

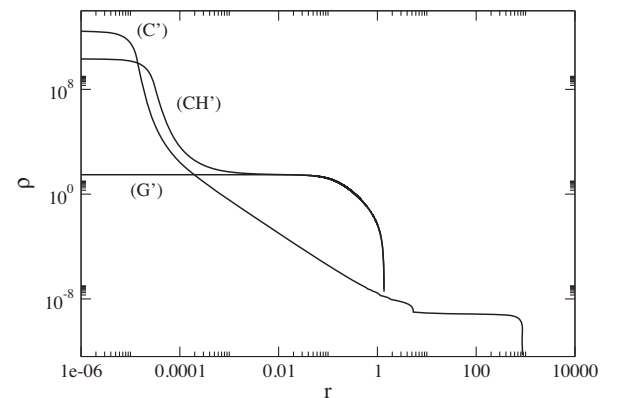


FIG. 23. Density profiles of G', CH' and C' solutions identified in Fig. 22 (from [34]).

with the structure of DM halos (see Fig. 23). CH' is similar to the solution found by Ruffini *et al.* [59] which was claimed to reproduce the structure of the Milky Way. It consists in a large nondegenerate isothermal atmosphere harboring a small “fermion ball” with a high density, a large mass and a small radius that could mimic a SMBH. Since this solution lies between the first and the last turning points of energy, it is thermodynamically unstable in the microcanonical ensemble (saddle point of entropy at fixed mass and energy). Therefore, we concluded in [34] that this type of solution is not likely to result from a natural evolution and, consequently, we questioned the possibility that a fermion ball could mimic a central SMBH.

However, in our analysis, we did not consider the stable solution CH_{*} located just after the turning point of energy E_* , believing that this solution would be unreachable by a natural evolution or that it would look like the solution C' which has a too extended halo. Recently, Argüelles *et al.* [62] computed the caloric curves of the fermionic King model in general relativity. For not too negative energies³⁸ they obtained a caloric curve similar to the one represented in Fig. 22. They confirmed the instability of the CH' solution in the region of the spiral previously considered by Chavanis *et al.* [34] but they also investigated the CH_{*} solution close to E_* and showed that this solution actually corresponds to the density profile obtained in their previous work [60] which provides a good agreement with the structure of the Milky Way.³⁹ Since this solution is located after the last turning point of energy it is thermodynamically stable in the microcanonical ensemble. This is a very interesting result because it shows that the core-halo structure found by Argüelles *et al.* [60] is thermodynamically stable and can, therefore, arise from a natural evolution.

In conclusion, when we use the ordinary Fermi-Dirac DF, the core-halo solution purported to reproduce the structure of the Milky Way is thermodynamically unstable but when we use the fermionic King model, this core-halo solution is thermodynamically stable. Therefore, this core-halo configuration may result from a natural evolution in the sense of Lynden-Bell. This gives further support to the scenario according to which a fermion ball could mimic a SMBH at the center of the galaxies.

³⁸For smaller energies, it becomes crucial to take general relativity into account (see Sec. VIII D). In that case, a new turning point of energy appears which was first evidenced by Alberti and Chavanis [46,47] in the framework of the box model (see Fig. 16). Below this critical energy the system collapses towards a SMBH as discussed in Sec. VIII D.

³⁹We note, however, that Argüelles *et al.* [62] considered a DM halo with a mass about 10 times smaller than the mass of the Milky Way. Therefore, it is not straightforward to compare their results with those of their previous works [60]. It would be interesting to repeat their study with the correct Milky Way mass to see if their conclusion remains valid.

Remark: The discovery [62] that the CH_{*} solution with a compact fermion ball mimicking a SMBH is thermodynamically stable is a very important result. However, it does not prove that this structure will effectively arise from a natural evolution. The reason is that violent relaxation is in general incomplete [31,82]. In particular, the fluctuations of the gravitational potential that are the engine of the collisionless relaxation can die out before the system has reached statistical equilibrium in the sense of Lynden-Bell. Therefore, it is not clear if violent relaxation can produce this type of structures with a very high central density.⁴⁰ In order to vindicate this scenario, the next step would be to perform direct numerical simulations of collisionless fermionic matter to see if they spontaneously generate fermion balls with the characteristics of SMBHs. *Indeed, it is not clear why the system should spontaneously reach an equilibrium state that is just in the bend after the turning point of energy Λ_* .* The purely gaseous solution without a quantum core, which is also a maximum entropy state, may be easier to reach through a violent relaxation process and is consistent with the observations. However, it does not account for a massive central object at the center of the galaxies. In that case, we either have to introduce a primordial SMBH “by hand” or advocate a scenario of gravitational collapse such as the one discussed in the following section.

D. General relativistic collapse towards a SMBH

For a fermion mass $m = 48 \text{ keV}/c^2$, the mass $M_h = 10^{11} M_\odot$ of the Milky Way is larger than the OV mass $M_{\text{OV}} = 2.71 \times 10^8 M_\odot$, so we have to take into account general relativity effects in the caloric curve. As first shown by Alberti and Chavanis [46,47] for box-confined systems, and recovered by Argüelles *et al.* [62] for tidally-truncated models, relativistic effects create a new turning point of energy in the caloric curve at which the condensed branch terminates (see Fig. 16). Below E'_c the system collapses towards a black hole. As we have seen previously, two stable equilibrium states are relevant in the structure of DM halos; G' equivalent to the classical isothermal sphere and CH_{*} which contains a fermion ball mimicking a SMBH. Only direct numerical simulations can tell us which metaequilibrium state will be reached in practice from a violent collisionless relaxation. Since these numerical results are not available yet, we shall consider the two possibilities. If the system were truly collisionless, the DM halo would remain in the metaequilibrium state G' or CH_{*} forever. In order to be more general, we consider below the possibility that the system slowly evolves dynamically due

⁴⁰It may be easier to form core-halo configurations with a very high central density if the fermions are self-interacting and if the Fermi-Dirac equilibrium state results from a collisional evolution of nongravitational origin as discussed in Sec. II.

to collisions and evaporation. There are then two situations to consider:

(A) Suppose that violent relaxation selects G' . On a secular timescale, the system follows the upper series of equilibria from point G' to the point of minimum energy E_c . At that point, it becomes thermodynamically unstable and undergoes a gravothermal catastrophe up to point C' where the collapse is stopped by quantum mechanics, leading to the formation of a fermion ball. Then, if the energy keeps decreasing, the system follows the lower series of equilibria up to the point of minimum energy E'_c where it becomes thermodynamically and dynamically unstable (in a general relativistic sense) and collapses towards a SMBH.⁴¹ As discussed in [46], there are two possible evolutions: (i) If the particle number N is below a critical value N'_* , then $\Lambda_c < \Lambda''_c$ and the system is first arrested by quantum mechanics (it forms a fermion ball) before becoming unstable and collapsing towards a SMBH. (ii) If the particle number N is above a critical value N'_* , then $\Lambda_c > \Lambda''_c$ and the system directly collapses towards a SMBH without forming a fermion ball. These two possibilities are illustrated in Fig. 24.

(B) Suppose that violent relaxation selects CH_* where the fermion ball mimics a SMBH. On a secular timescale, the system follows the series of equilibria from point CH_* to the point of minimum energy E'_c . At that point, it becomes thermodynamically and dynamically unstable (in a general relativistic sense) and collapses towards a SMBH.

In the two cases, the ultimate fate of the system is to form a SMBH surrounded by an envelope. This picture may be just qualitative because it is not clear if the lower branch of equilibrium states is astrophysically relevant. Indeed, we have indicated that the envelope of the solutions C' is too much extended to match the characteristics of DM halos. Therefore, the collisional evolution of the system from point G' or from point CH_* up to the formation of a SMBH at E'_c may involve out-of-equilibrium states CH_{out} instead of following the series of equilibrium states C' .

For a fermion mass $m = 48 \text{ keV}/c^2$, the OV mass $M_{OV} = 2.71 \times 10^8 M_\odot$ is too large to account for the mass of a SMBH like Sgr A* at the center of the Milky Way. Either the mass of the SMBH resulting from gravitational collapse is smaller than M_{OV} or there is no gravitational collapse and Sgr A* is a fermion ball CH_* as suggested by Argüelles *et al.* [62]. Therefore, a fermion ball is favored in medium size galaxies like the Milky Way. However, for very large halos it is shown by Alberti and Chavanis [46] that the condensed branch disappears

⁴¹This requires that the core mass increases until it reaches the critical OV value. The increase of the core mass may take place through an accretion process.

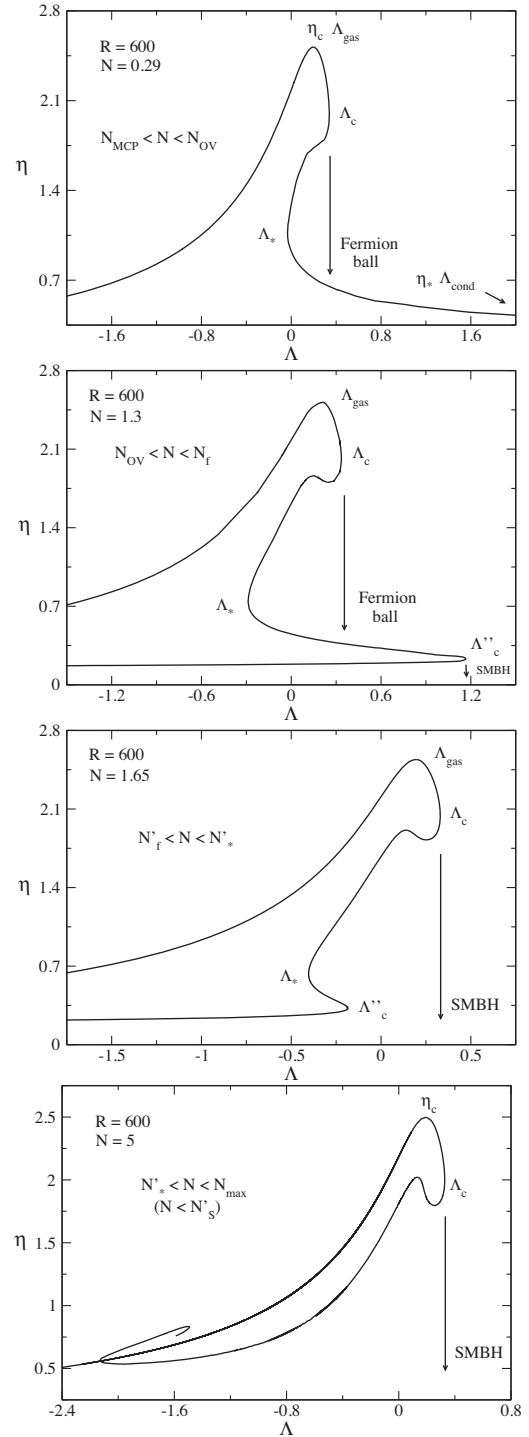


FIG. 24. Caloric curve of the general relativistic Fermi gas in a box as a function of the particle number N (adapted from [46]). For $N < N_{OV}$, the gravothermal catastrophe at E_c leads to a fermion ball surrounded by a hot halo. For $N_{OV} < N < N'_*$ the system first takes a quantum core-halo structure resulting from the gravothermal catastrophe at E_c (as before) then collapses towards a SMBH at E'_c . For $N > N'_*$ the condensed branch disappears so that only the collapse at E_c towards a SMBH is possible. These caloric curves are valid for relatively small DM halos. For larger halos a spiral develops in the head of the dinosaur but the phenomenology remains the same.

(see the last panel of Fig. 24).⁴² In that case, there is no solution with a fermion ball such as CH_* and the system necessarily collapses towards a SMBH. Therefore, medium size galaxies ($N < N'_*$) like the Milky Way may harbor a fermion ball of mass $M = 4.2 \times 10^6 M_\odot$ while very large galaxies ($N > N'_*$) like ellipticals may harbor a SMBH of mass $M_{\text{OV}} = 2.71 \times 10^8 M_\odot$ that could even grow by accretion. This could account for the mass of SMBHs in AGNs like the one recently photographed in M87 ($M_h \sim 10^{13} M_\odot$ and $M_{\text{BH}} \sim 10^{10} M_\odot$).

For a fermion mass $m = 386 \text{ keV}/c^2$, the OV mass $M_{\text{OV}} = 4.2 \times 10^6 M_\odot$ is comparable to the mass of Sgr A*. Furthermore, the caloric curve is similar to the one reported in the last panel of Fig. 24 and there is no possibility to have a CH_* solution involving a fermion ball. In that case, the Milky Way could have undergone a gravitational collapse leading to a SMBH of mass $M_{\text{OV}} = 4.2 \times 10^6 M_\odot$. The halo surrounding the SMBH is left undisturbed and could correspond to a marginal classical King profile which gives a good agreement with the Burkert profile (see Ref. [33] and Fig. 1).

E. Potential problems with a DM model involving a fermion mass $m = 48 \text{ keV}/c^2$ or $m = 386 \text{ keV}/c^2$

In Sec. V C we have determined the mass m of the DM particle by arguing that the smallest halo observed in the Universe (“minimum halo”) with a typical mass $M \sim 10^8 M_\odot$ and a typical radius $R \sim 1 \text{ kpc}$ (Fornax) represents the ground state of the self-gravitating Fermi gas at $T = 0$. This yields $m = 165 \text{ eV}/c^2$. This value (previously given in Appendix D of [94]) is of the order of magnitude of the fermion mass obtained by other authors [119–121] using more detailed comparisons with observations.⁴³ Alternatively, Argüelles *et al.* [60,62] determined the mass of the fermionic DM particle in such a way that the fermion ball that composes the core-halo structure of a large DM halo like the Milky Way, obtained in the framework of the fermionic King model, mimics the effect of a SMBH at the center of the Galaxy. This leads to a much

⁴²It would be interesting to determine precisely the condition of disappearance of the condensed branch in the framework of the relativistic fermionic King model, i.e., the value of N'_* . In the framework of the box model, we find $N'_* \sim 3.73 N_{\text{OV}}$ [46] but the prefactor may be substantially larger in more realistic models.

⁴³Domcke and Urbano [119] model dSphs as completely degenerate fermionic systems and find that $m = 200 \text{ eV}/c^2$ provides the best fit to observations of velocity dispersion. Randall *et al.* [120] show that self-gravitating fermions under full degeneracy do not fit well the velocity dispersion data of some local dwarfs and introduce by hand a Boltzmannian tail (i.e., finite temperature effects) in order to better reproduce the data. They find good agreement for $70 \text{ eV}/c^2 < m < 400 \text{ eV}/c^2$. Bar *et al.* [121] study the globular cluster timing problem in Fornax assuming that the core is a completely degenerate fermion ball. They find $m = 135 \text{ eV}/c^2$ but point out that this mass violates the Lyman α limit.

larger mass $m = 48 \text{ keV}/c^2$.⁴⁴ In very recent works, Becerra-Vergara *et al.* [122,123] showed that the gravitational potential of a fermion ball (with a particle mass $m = 56 \text{ keV}/c^2$) leads to a better fit of the orbits of all the 17 best resolved S-stars orbiting Sgr A* (including the S2 and G3 objects) than the one obtained by the central SMBH model.

A possible problem with this model is the following. If the DM particle had a mass $m = 48 \text{ keV}/c^2$, the minimum halo (ground state) would be too small: it would have a mass $(M_h)_{\text{min}} = 1.30 M_\odot$ and a radius $(r_h)_{\text{min}} = 0.0683 \text{ pc}$. This would imply the formation of structures at very small scales, up to $\sim 1 M_\odot$. Therefore, DM halos should exist up to very small scales, like in the CDM model. Indeed, (bosonic or fermionic) quantum models with a large particle mass m behave essentially as classical CDM since the quantum parameter $\hbar/m \ll 1$. This is not what we observe. There are apparently no DM halos with a mass below $\sim 10^8 M_\odot$ (missing satellite problem) [3–5]. This is why quantum models of DM with a *small* particle mass have been introduced. Namely, they have been introduced precisely in order to have a ground state (minimum halo) with a typical mass $M \sim 10^8 M_\odot$ and a typical radius $R \sim 1 \text{ kpc}$, corresponding to dSphs like Fornax, not smaller. Accordingly, a fermionic model with $m = 48 \text{ keV}/c^2$ may not be able to solve the missing satellite problem.

If we disregard this difficulty, another consequence of the model of Argüelles *et al.* [60,62] is that dSphs should have a very pronounced core-halo structure (since they do not correspond to the ground state of the self-gravitating Fermi gas). For example, a compact DM halo of mass $M_h = 10^8 M_\odot$ (Fornax) should have a core-halo structure with a small central fermion ball (possibly mimicking an intermediate mass BH) and an atmosphere. Using Eqs. (86), (106), (111), and (116), we find that this DM halo should contain a quantum core of mass $M_c = 1.57 \times 10^4 M_\odot$, radius $R_c = 5.42 \text{ mpc}$ and central density $\rho_0 = 1.40 \times 10^{11} M_\odot/\text{pc}^3$.⁴⁵ The corresponding density and velocity profiles are plotted in Figs. 25 and 26. To our knowledge, this core-halo structure has not been observed in ultracompact DM halos.⁴⁶ dSphs are rather expected to

⁴⁴If we use the nonrelativistic mass-radius relation (74) of a fermion ball at $T = 0$ and take $M_c = 4.2 \times 10^6 M_\odot$ and $R_c = 6 \times 10^{-4} \text{ pc}$, corresponding to the characteristics of the massive object at the center of our Galaxy (see Sec. VIII A), we get $m = 54.6 \text{ keV}/c^2$.

⁴⁵Interestingly, these values obtained from our semianalytical model [see in particular Eq. (111)] are comparable to the values obtained numerically in [61].

⁴⁶Recently, C. Argüelles drew our attention to the works [124–126] that report observations supporting the existence of intermediate mass BHs ($M_{\text{BH}} \sim 10^4\text{--}10^6 M_\odot$) in ultracompact dwarf galaxies ($M_h \sim 10^9\text{--}10^{10} M_\odot$). However, these galaxies are not DM dominated, so it is not clear if their massive cores could correspond to fermion balls.

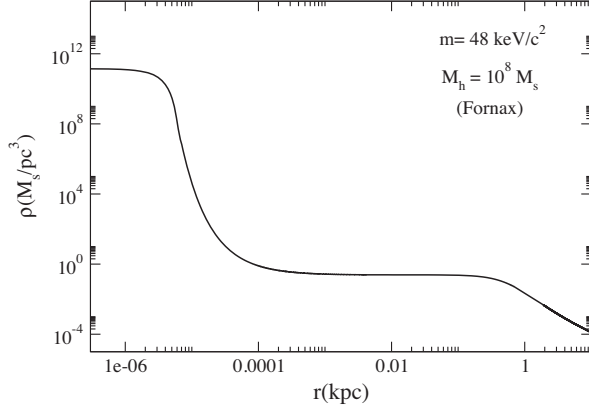


FIG. 25. Density profile of a DM halo of mass $M_h = 10^8 M_\odot$ (Fornax) assuming that the fermion mass is $m = 48 \text{ keV}/c^2$. It presents a core-halo structure.

correspond to pure fermion balls at $T = 0$ (possibly surrounded by a tenuous atmosphere). Therefore, they are expected to have a profile similar to Figs. 7 and 8 instead of Figs. 25 and 26. It would be extremely important to clarify this issue by applying the model of Argüelles *et al.* [60] to ultracompact halos in order to determine which of the two scenarios (the scenario of Argüelles *et al.* [60,62] with $m = 48 \text{ keV}/c^2$ or the one developed in the present paper with $m = 165 \text{ eV}/c^2$ or $m \sim 1 \text{ keV}/c^2$) is the most relevant.

There is also a problem related to the validity of the Fermi-Dirac (or Lynden-Bell) DF as discussed further in Sec. X. Indeed, for a large fermion mass $m \gg 1 \text{ keV}/c^2$, the DM halo is essentially classical except in a very small quantum core (fermion ball). Away from the core, we should recover the NFW profile leading to cusps. It is precisely in order to avoid these cusps that quantum models of DM with a *small* particle mass $m \lesssim 1 \text{ keV}/c^2$ have been introduced. A fermionic model with a mass $m = 48 \text{ keV}/c^2$ may not be able to solve the core-cusp problem.

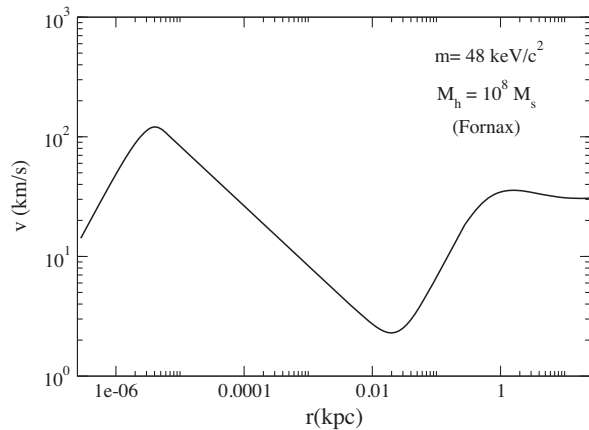


FIG. 26. Velocity profile of a DM halo of mass $M_h = 10^8 M_\odot$ (Fornax) assuming that the fermion mass is $m = 48 \text{ keV}/c^2$.

IX. POSSIBLE SOLUTIONS TO AN APPARENT PARADOX RELATED TO THE UNIVERSAL SURFACE DENSITY OF DM HALOS

A. The apparent paradox

The mass-radius relation of a completely degenerate fermion ball (ground state of the self-gravitating Fermi gas at $T = 0$) is given by [see Eq. (74)]

$$R = 0.114 \frac{h^2}{Gm^{8/3}M^{1/3}}. \quad (122)$$

The radius decreases like $M^{-1/3}$ as the mass increases. Therefore, if we identify M with the halo mass M_h and R with the halo radius r_h , this result is in contradiction with the universality of the surface density of DM halos [see Eq. (52)] implying that the radius increases with the mass as $M^{1/2}$ [see Eq. (53)]. A similar problem arises in the BECDM model [25].

This apparent paradox was pointed out by the author at several occasions in the case of fermions and bosons (see, e.g., Appendix F of Ref. [34], the Introduction of Ref. [37] and Appendix L of [25]). It has also been recently emphasized by Deng *et al.* [127] and Burkert [128] in the case of bosons. A possible implication of this paradox is that the quantum (fermionic and bosonic) models of DM are ruled out because they are not consistent with the constraint from Eq. (52). This is essentially the conclusion reached by Deng *et al.* [127] and Burkert [128] for the BECDM model. Below, we discuss several possible solutions to this apparent paradox that were suggested in [25] for bosonic DM and that can be straightforwardly adapted to fermionic DM.

Remark: The constant surface density of DM halos $\Sigma_0 = \rho_0 r_h = 141_{-52}^{+83} M_\odot/\text{pc}^2$ may be explained by the logotropic model developed in [86–91] which involves a logotropic envelope instead of an isothermal one. This model not only explains why the surface density of DM halos is constant but it also determines its universal value in terms of the fundamental constants of physics according to the relation $\Sigma_0^{\text{th}} = 0.01955c\sqrt{\Lambda}/G = 133 M_\odot/\text{pc}^2$ without adjustable parameter. This relation is consistent with the observational result. At the same time, in a cosmological context, the logotropic model correctly accounts for the accelerating expansion of the Universe with a single dark fluid and suggests that the present ratio of dark energy and dark matter is equal to the Euler number $\Omega_{\text{de},0}^{\text{th}}/\Omega_{\text{dm},0}^{\text{th}} = e = 2.71828\dots$ in agreement with the empirical value $\Omega_{\text{de},0}^{\text{obs}}/\Omega_{\text{dm},0}^{\text{obs}} = 2.669 \pm 0.08$ within the error bars.

B. Model I: Purely gaseous solution

A first possible solution to this problem is that DM halos do not have a quantum core such as a fermion ball or such as a soliton (in the BECDM model). Indeed, the DM halos

could be in the purely gaseous phase corresponding to the classical isothermal sphere (see Sec. IV). This solution is always thermodynamically stable (maximum entropy state) so it represents the most probable state of the system. Furthermore, it is always possible to satisfy the constraint from Eq. (52) by adapting the temperature [see Eq. (53)]. This leads to the mass-radius relation from Eq. (53). As shown in [25], the classical isothermal distribution (without quantum core) is fully consistent with the observational Burkert profile and can therefore represent a satisfying description of DM halos. It is nevertheless crucial to take quantum mechanics into account in the case of ultracompact DM halos with a small mass, corresponding to dSphs like Fornax. This leads to the Model I of Ref. [25] in which the DM halos are purely isothermal (without quantum core) except near the ground state. More precisely:

- (i) At $(M_h)_{\min}$ the DM halo is completely degenerate (see Sec. V). The values of M_h and r_h for this minimum halo are consistent with the constraint from Eq. (52).
- (ii) Ultracompact DM halos with a mass $(M_h)_{\min} \leq M_h \leq (M_h)_{\text{CCP}}$ have a quantum core surrounded by a tenuous isothermal atmosphere. The presence of a small isothermal halo allows us to satisfy the constraint from Eq. (52) as discussed in Sec. VI of [25] for BECDM halos. All the profiles constructed in Sec. VI of [25] satisfy the constraint from Eq. (52). The same results apply to fermionic DM halos.
- (iii) DM halos with a mass $M_h \geq (M_h)_{\text{CCP}}$ are purely isothermal without quantum core. Indeed, as shown in [25] for BECDM halos, if we enforce the constraint from Eq. (52) in Model I we find that

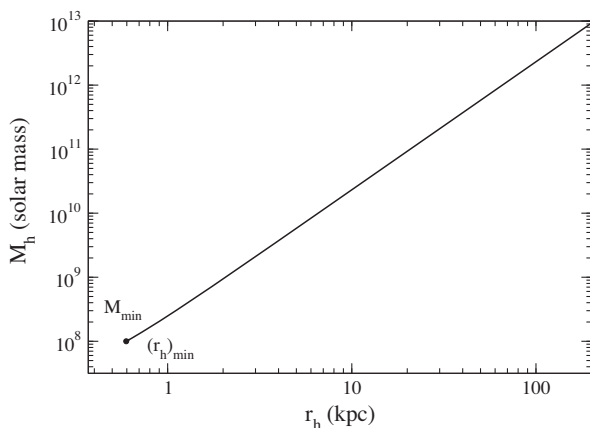


FIG. 27. Mass-radius relation of fermionic DM halos. In Model I, quantum mechanics (Pauli’s exclusion principle) is important only close to the ground state (bullet) where the halos have the form of a fermion ball surrounded by a tenuous isothermal atmosphere. Larger DM halos are purely isothermal without a quantum core. Note that the halo mass-radius relation from Eq. (53) remains valid for large halos in Models II and III since the quantum core mass M_c is always much smaller than the halo mass M_h (see Sec. IV).

the core mass *decreases* as the halo mass increases so that large DM halos are essentially classical without quantum core.

This model leads to the mass-radius relation reported in Fig. 16 of [25] and reproduced in Fig. 27 (adapted to fermions). It coincides with the classical law from Eq. (53) except at small halo masses. Quantum mechanics just determines the ground state of DM halos at $(M_h)_{\min} = 10^8 M_\odot$ and $(r_h)_{\min} = 597$ pc.

This scenario does not account for the presence of a compact object, such as a SMBH, at the center of the galaxies. Of course, we can always add “by hand” a primordial SMBH at the center of a classical isothermal halo but this is almost assuming the result. In order to explain self-consistently the presence of a SMBH at the center of the galaxies, we can consider the following scenarios.

C. Model II: Core-halo solution with a large quantum bulge

Another possibility to solve the paradox of Sec. IX A and “save” the quantum core-halo solution from Sec. VI is to assume that the constraint from Eq. (52) should be replaced by

$$\Sigma_0 = \rho_c r_h = 141_{-52}^{+83} M_\odot/\text{pc}^2, \quad (123)$$

where ρ_c is not the true central density ρ_0 but rather an “apparent” central density. It corresponds to the density at the separation between the quantum core and the classical halo in configurations such as those from Fig. 17. Similarly, r_h is the radius at which ρ_c (instead of ρ_0) is divided by 4. The idea underlying this replacement is that observations may not be able to resolve the presence of a quantum bulge at the center of the galaxies. Therefore, we have to distinguish between the true central density ρ_0 (which is the central density of the quantum core) from the apparent central density ρ_c (which is the “central” density of the classical isothermal halo surrounding the quantum core). Similarly, we have to distinguish the halo radius r_h which typically corresponds to the distance where the apparent central density ρ_c is divided by 4 from the core radius R_c which is of the order of the distance where the core central density ρ_0 is divided by 4. The distinction between these quantities is explicitly shown in Fig. 17. It is clear that the radius of large DM halos is given by r_h not by the quantum core radius R_c . This leads to Model II of [25] in which the DM halos of large mass have a core-halo structure. More precisely:

- (i) At $(M_h)_{\min}$ the DM halo is completely degenerate (see Sec. V). The values of M_h and r_h for this minimum halo are consistent with the constraint from Eq. (52).
- (ii) Ultracompact DM halos with a mass $(M_h)_{\min} \leq M_h \leq (M_h)_{\text{CCP}}$ have a quantum core surrounded by

a tenuous isothermal atmosphere. The presence of a small isothermal halo allows us to satisfy the constraint from Eq. (52) as discussed in Sec. VI of [25] for BECDM halos. All the profiles constructed in Sec. VI of [25] satisfy the constraint from Eq. (52). The same results apply to fermionic DM halos.

- (iii) Small DM halos with a mass $(M_h)_{\text{CCP}} \leq M_h \leq (M_h)_{\text{MCP}}$ have a core-halo structure made of a large quantum bulge surrounded by a classical isothermal halo. The core mass M_c increases with the halo mass M_h according to Eq. (111). The constraint from Eq. (52) is satisfied provided that we replace the central density ρ_0 by the apparent central density ρ_c , i.e., provided that we use Eq. (123). From the outside (i.e., considering the external structure of the DM halo and ignoring the quantum bulge), the system looks like a classical isothermal sphere. This leads to the mass-radius relation from Eq. (53) which is consistent with the observations.
- (iv) For large DM halos with a mass $M_h \geq (M_h)_{\text{MCP}}$, the quantum bulge is replaced either by a small out-of-equilibrium quantum core or by a SMBH. In that case, the replacement of Eq. (52) by Eq. (123) is even more justified. What is relevant is not the central density of the compact object but rather the density of the classical halo at the contact with this object.⁴⁷

This model leads to the mass-radius relation from Fig. 27. It coincides with the classical law from Eq. (53) except at small halo masses. Quantum mechanics determines the ground state of DM halos at $(M_h)_{\text{min}} = 10^8 M_\odot$ and $(r_h)_{\text{min}} = 597$ pc. It also implies the existence of a large quantum bulge of mass M_c that increases with the halo mass M_h according to Eq. (111). For very large halos, the fermionic bulge is replaced by an out-of-equilibrium compact quantum core or by a SMBH.

These arguments may solve, or alleviate, the problem reported in Sec. IX A. The crucial point is to know if observations are able to detect a large quantum bulge of typical mass $M_c = 9.45 \times 10^9 M_\odot$ and size $R_c = 240$ pc at the center of the Milky Way that is predicted by our model. This possibility is discussed in the Remark of Sec. VII F.

D. Model III: Core-halo solution mimicking a SMBH

Finally, we note that the apparent paradox reported in Sec. IX A does not arise in the model of Argüelles *et al.* [60,62] where the fermion ball mimics a SMBH of negligible extent. Indeed, in that case, there is a clear separation between the quantum core and the classical

⁴⁷The same comment holds if the quantum bulge in scenario (iii) has led to the formation of a SMBH in the past by accretion of the gas (see Sec. VII C).

isothermal halo as depicted in Fig. 19. It is clear that the central density to consider in Eq. (52) is not the central density ρ_0 of the fermion ball but rather the density ρ_c of the plateau that connects the fermion ball to the classical isothermal halo. Similarly, the halo radius r_h is not the radius where the central density is divided by 4 (which would coincide with the radius of the quantum core R_c) but the radius where the density of the plateau is divided by 4.

In model III, the DM halo behaves from the outside as a classical isothermal halo but harbors a tiny massive fermion ball mimicking a SMBH. The halo mass-radius relation is similar to that reported in Fig. 27 except that it starts at a much smaller minimum halo mass $(M_h)_{\text{min}} = 1.30 M_\odot$ corresponding to $(r_h)_{\text{min}} = 0.0683$ pc. This may be a problem as discussed in Sec. VIII E.

X. THERMAL OR QUANTUM CORE?

In this paper, we have assumed that a fermionic DM halo reaches a statistical equilibrium state described by the Fermi-Dirac DF (see Sec. II). The same assumption was made by other authors [49,62,67,119,120]. However, this is a strong assumption and the establishment of a statistical equilibrium state for self-gravitating systems is far from trivial.

Let us first consider a collisionless system of classical self-gravitating particles. According to the statistical theory of Lynden-Bell [31], it should reach a Fermi-Dirac-like DF, reducing to the classical isothermal DF in the dilute limit. The corresponding density profile has a core due to effective thermal effects (in the sense of Lynden-Bell). However, this prediction is *not* consistent with numerical simulations of classical collisionless self-gravitating systems. Indeed, such simulations lead to NFW profiles [1] presenting a r^{-1} central cusp, not a core. This demonstrates that, for classical collisionless self-gravitating systems, the Lynden-Bell prediction does not work in the central part of the system.⁴⁸ Therefore, classical collisionless self-gravitating systems are not in a maximum entropy state. Since observations show that DM halos possess a core rather than a cusp, we conclude that DM halos are either quantum or collisional, two features that are not accounted for in NFW numerical simulations [1].

Let us now consider a collisionless system of quantum self-gravitating particles (fermions). If the fermion mass is small ($m \lesssim 1$ keV/ c^2), as assumed in Sec. VII, DM halos should harbor a large quantum bulge of radius $R_c \gtrsim 240$ pc (Model II) according to the Lynden-Bell prediction. In that case, the r^{-1} cusps are prevented by the Pauli exclusion principle which forbids high densities. As a result, the

⁴⁸It does not work well neither in the outer part of the system since it predicts a density profile decaying as r^{-2} instead of r^{-3} . However, we have previously argued that the difference is not very strong and that it can even be reduced if we take into account tidal effects (see Fig. 1) [33,34].

classical cusp is replaced by a large quantum bulge. It is possible that, for quantum systems with a small fermion mass $m \lesssim 1 \text{ keV}/c^2$, the Lynden-Bell prediction works well in the central part of the system. This is not in contradiction with NFW numerical simulations [1] since they do not take into account quantum mechanics. Quantum effects may facilitate the collisionless relaxation of the system towards a maximum entropy state. Therefore, when $m \lesssim 1 \text{ keV}/c^2$, quantum effects may solve the core-cusp problem.

By contrast, if the fermion mass is large ($m \gg 1 \text{ keV}/c^2$), as assumed in Sec. VIII, the quantum core predicted by the Lynden-Bell theory is very small ($R_c \leq 6 \times 10^{-4} \text{ pc}$). In the main part of the DM halo excluding the tiny fermion ball at the very center (i.e., for $r > R_c$) the system is essentially in the classical regime. In that case, we should recover the NFW profile which displays a r^{-1} cusp while Argüelles *et al.* [60] find a classical isothermal profile with a thermal core. This is because their model assumes that the Lynden-Bell DF is valid everywhere (even in the classical region) while we have just seen that the Lynden-Bell DF is not valid in a classical system. Therefore, when $m \gg 1 \text{ keV}/c^2$ (e.g., $m \sim 50 \text{ keV}/c^2$), quantum effects cannot solve the core-cusp problem if the system is collisionless.

One possibility to solve this problem and “save” the scenario of Argüelles *et al.* [60] is to assume that the fermions are self-interacting and that the evolution of DM halos is collisional.⁴⁹ In that case, the Fermi-Dirac DF is established through a collisional relaxation of nongravitational origin, not through a collisionless relaxation (see Secs. II and XI). In the classical (nonquantum) regime, collisions lead to an isothermal core of size r_h instead of a r^{-1} cusp. The classical core is due to thermal effects like in the SIDM model. This is not in contradiction with NFW numerical simulations [1] since they do not take into account self-interaction and collisions among the particles. In the quantum + collisional regime, we should both have a quantum core of size R_c and an isothermal core of size r_h . Therefore, quantum and/or thermal (collisional) effects may solve the core-cusp problem. In particular, collisions can establish a Maxwell-Boltzmann DF for classical particles and a Fermi-Dirac DF for fermions.

XI. INCOMPLETE RELAXATION SAVED BY SELF-INTERACTIONS?

We have seen that collisionless self-gravitating systems like DM halos can achieve a form of statistical equilibrium state on a coarse-grained scale through a process of violent relaxation. As we have explained, the Lynden-Bell theory

of violent relaxation [31] can provide a justification of the Fermi-Dirac DF for fermionic DM halos without the need of gravitational encounters [33,34]. However, when coupled to the Poisson equation, this DF has an infinite mass. Therefore, there is no statistical equilibrium state for self-gravitating systems in a strict sense. A way to cure this problem is to take into account tidal effects and the evaporation (loss) of particles when they reach sufficiently high energies. This leads to the fermionic King DF [71,72]

$$\bar{f} = \eta_0 \frac{1 - e^{\beta\eta_0(\epsilon - \epsilon_m)}}{1 + e^{\eta_0(\beta\epsilon + \alpha)}} \quad (\epsilon \leq \epsilon_m), \quad (124)$$

$$\bar{f} = 0 \quad (\epsilon \geq \epsilon_m), \quad (125)$$

instead of the Fermi-Dirac DF (7). This truncated DF takes into account the Pauli (or Lynden-Bell) exclusion principle as well as tidal effects. It leads to a relevant model of fermionic DM halos with a finite mass. The fermionic King model has been studied in [33,34]. It can be derived from a fermionic Kramers equation describing the process of collisionless relaxation [130] by looking for a stationary solution of this equation respecting the boundary condition $f = 0$ when $\epsilon \geq \epsilon_m$ [72,131].

There still remains the complicated problem of incomplete relaxation [31,82]. In practice, the violent fluctuations of the gravitational potential which are the engine of the collisionless relaxation die away before the system has reached a statistical equilibrium state in the sense of Lynden-Bell. Therefore, it may be necessary to take into account other processes of relaxation to guarantee that the system truly relaxes towards a DF of the form of Eq. (124).⁵⁰ This will be the case if the system is submitted to external stochastic perturbations (like a “cosmic noise”) from neighboring galaxies or if the fermions are self-interacting. In this latter case, the kinetic evolution of the system is governed by the Boltzmann equation adapted to the case of fermions. Although this equation is more complicated than the fermionic Kramers equation, its study could explain the rapid collisional relaxation of the system towards a DF similar to Eq. (124). Probably the two processes (violent collisionless relaxation and strong collisions due to self-interactions) are responsible for the relaxation of the system towards the truncated Fermi-Dirac DF (124). However, collisions due to self-interactions continue to drive a secular evolution of the system on a long timescale after the violent fluctuations of the gravitational potential have died away. Therefore, self-interacting DM halos may evolve secularly along the series of equilibria characterized by the truncated Fermi-Dirac DF (124), and possibly undergo a gravothermal catastrophe like

⁴⁹In this respect, Yunis *et al.* [129] have taken into account self-interaction in fermionic DM halos with $m = 48 \text{ keV}/c^2$ and shown that the extended hydrostatic equilibrium equations for tidally-truncated systems (which account for such interactions) do not spoil the rotation curve fittings for typical cross sections.

⁵⁰In the absence of such processes, the system may reach a DF which is a stable stationary solution of the Vlasov equation different from the Lynden-Bell or fermionic King DF. However, it is difficult to predict this DF from first principles (see, however, [132,133] for some proposals).

in the case of globular clusters. Self-interactions may therefore justify the assumptions made in our model. Interestingly, our model makes a connection between studies of fermionic DM halos with a core-halo structure based on the Fermi-Dirac DF and studies of SIDM halos with an isothermal DF evolving secularly with time, and experiencing a gravothermal catastrophe and a core collapse possibly resulting in the formation of a SMBH [98].

XII. SUMMARY AND CONCLUSIONS

In this paper, we have developed a predictive model of fermionic DM halos. We have considered different scenarios depending on the fermion mass m and on the DM halo mass M_h . We have discussed the case of a collisionless evolution and the case of a collisional evolution of non-gravitational origin possibly due to SIDM assuming that self-interactions do not dramatically alter the density profile of fermionic DM halos (see footnote 49 and Sec. XI). Below, we recall our basic assumptions, summarize our main results, present synthetic phase diagrams, and conclude.

A. Assumptions

We have used the following observational results:

- (i) The surface density of DM halos has a universal value $\Sigma_0 = 141 M_\odot/\text{pc}^2$ [83–85].⁵¹
- (ii) There exists a minimum halo of mass $(M_h)_{\min} \sim 10^8 M_\odot$ corresponding to dSphs like Fornax. Observations reveal that there is no DM halo below this typical mass.⁵²

We have made the following assumptions:

- (i) We assumed that DM is made of fermions and that DM halos are in a statistical equilibrium state of the self-gravitating Fermi gas (see Sec. III). This statistical equilibrium state may result from a process of collisionless violent relaxation in the sense of Lynden-Bell or, possibly, from a collisional relaxation of non-gravitational origin if the fermions are self-interacting (see Sec. II). Note that this is a strong assumption. It is possible that DM halos are in an out-of-equilibrium state (different from the Fermi-Dirac DF) in which case predictions become more complicated, or even impossible.
- (ii) We assumed that the minimum halo of mass $(M_h)_{\min} = 10^8 M_\odot$ (Fornax) is completely degenerate, i.e., it corresponds to the ground state of

the self-gravitating Fermi gas (see Sec. V). This automatically determines the fermion mass $m = 165 \text{ eV}/c^2$.⁵³ We then found that the radius of the minimum halo is determined by the constraint from Eq. (52) giving $(r_h)_{\min} = 597 \text{ pc}$ [see Eqs. (79) and (83)]. With this assumption, there is no free (undetermined) parameter in our model. In this sense, it is completely predictive.

- (iii) We assumed that the external structure of large DM halos [$M_h \gg (M_h)_{\min}$] is described by the classical isothermal distribution (see Sec. IV). This corresponds to the nondegenerate Fermi-Dirac DF, or to the approximate form of the Fermi-Dirac DF at sufficiently large distances where the density is low. This classical isothermal distribution is in agreement with the Burkert profile (see Sec. III C of [25]). Combining the properties of classical isothermal spheres with the constraint from Eq. (52) we obtained the mass-radius relation $M_h = 1.76 \Sigma_0 r_h^2$ [see Eq. (53)]. In principle, this relation is valid for $M \gg (M_h)_{\min}$. In practice, it is fulfilled as soon as M_h is slightly larger than $(M_h)_{\min}$ (see Fig. 27).
- (iv) We considered the possibility that large DM halos, in addition to their classical isothermal envelope of mass M_h and radius r_h , contain a quantum core (fermion ball) of mass M_c and radius R_c . In other words, we assumed that large DM halos may be partially degenerate (see Sec. VI).

B. Methodology

The structure of fermionic DM halos, and the mass M_c of the quantum core, are obtained by maximizing the Fermi-Dirac entropy at fixed mass and energy (microcanonical ensemble). To solve this problem, we proceeded as follows. We considered the thermodynamics of a gas of self-gravitating fermions in a box of radius $R = r_h$ containing a mass $M = M_h$ (see Sec. III). The caloric curve depends on a unique parameter μ which is a measure of the mass M_h of the DM halo [see Eq. (98)]. We then used the fact that the DM halos are virialized so that the dimensionless inverse temperature $\eta = \beta G M m / R$ is of order unity. The intersection between the line $\eta_v = 1$ and the caloric curve $\eta(\Lambda)$ determines the possible equilibrium states of the system consistent with the virial condition. For $M_h < (M_h)_{\text{CCP}}$ there is only one solution. However, for $M_h > (M_h)_{\text{CCP}}$ we found two relevant solutions:

⁵¹If this observational result were not (exactly) valid, our model could be generalized but it would depend on more parameters.

⁵²We have taken this value in order to be consistent with our previous papers. It is possible that this mass is overestimated. Some authors [49–54] (see also Refs. [34,95]) argue that the minimum halo mass is $(M_h)_{\min} = 0.39 \times 10^6 M_\odot$, corresponding to Willman I. Numerical applications have also been given in that case for a comparison.

⁵³This prediction could be refined by adopting a possibly more relevant value of the minimum halo mass but the order of magnitude of m should be correct up to a factor 10. For example, if we take $(M_h)_{\min} = 0.39 \times 10^6 M_\odot$ (Willman I) we get $m \sim 1 \text{ keV}/c^2$ and $(r_h)_{\min} = 33 \text{ pc}$ (see Sec. V C). A fermion mass in the keV scale (or slightly larger) is more consistent with the constraints coming from cosmological observations such as the Lyman α forest (see Sec. VII G).

- (i) A purely gaseous solution (G) without quantum core corresponding to the classical isothermal sphere [55]. Its density profile is consistent with the observational Burkert profile (see Sec. III C of [25]). This corresponds to Model I of Sec. IX B.
- (ii) A core-halo solution (CH) with a quantum core surrounded by a classical isothermal halo. The core is relatively large ($M_c = 9.45 \times 10^9 M_\odot$ and $R_c = 240$ pc for the Milky Way) so it can represent a quantum bulge. The core mass increases with the halo mass as $M_h^{3/8}$ [see Eq. (111)]. This corresponds to Model II of Sec. IX C.⁵⁴

The gaseous solution is always thermodynamically stable. The core-halo solution is thermodynamically stable for $M_h < (M_h)_{\text{MCP}}$ and unstable for $M_h > (M_h)_{\text{MCP}}$ (as explained before, we consider the thermodynamical stability in the microcanonical ensemble).

The formation of DM halos arises from a process of violent collisionless relaxation. The metaequilibrium state resulting from violent relaxation must be a maximum entropy state in the sense of Lynden-Bell. It turns out that the Lynden-Bell DF coincides with the Fermi-Dirac DF. For $M_h < (M_h)_{\text{MCP}}$, the gaseous solution and the core-halo solution are both entropy maxima in the sense of Lynden-Bell. They could naturally arise from a process of violent relaxation. For $M_h > (M_h)_{\text{MCP}}$, only the gaseous solution is a maximum entropy state in the sense of Lynden-Bell. Therefore, violent relaxation should lead to the gaseous solution, not to the core-halo solution. Actually, there exist stable core-halo solutions (CH_*) close to the last turning point of energy that may be physically relevant. Violent relaxation may also lead to a dynamically (Vlasov) stable quasistationary state, resulting from incomplete relaxation, that is not a maximum entropy state.

If the DM halos are collisionless, they remain in the state resulting from violent relaxation. If the DM halos are collisional, they follow the series of equilibria determined by the caloric curve towards states of higher and higher central density. When $M_h < (M_h)_{\text{MCP}}$, the system can evolve from the gaseous solution to the core-halo solution. When $M_h > (M_h)_{\text{MCP}}$, the system can follow the series of equilibria from the gaseous solution up to the point of minimum energy E_c . At that point, it becomes thermodynamically unstable and undergoes a gravothermal catastrophe. If the DM halo is small enough ($M_h < M_{\text{OV}}$), the gravothermal catastrophe stops when the core becomes degenerate. In that case, gravitational collapse is prevented by quantum mechanics (Pauli's exclusion principle). The system achieves a core-halo configuration with a small quantum core. This state does not correspond to a state of

statistical equilibrium such as solution C' which would have a too extended halo [scenario (a)] but it could be an out-of-equilibrium structure CH_{out} [scenario (b)]. Alternatively, if the DM halo is large enough ($M_h > M_{\text{OV}}$), the gravothermal catastrophe can lead to the formation of a SMBH by the mechanism discussed in Secs. VII D, VII E, and VIII D [scenario (c)].

Remark: For small halos $M_h < (M_h)_{\text{MCP}}$, the core-halo solution is stable (see Fig. 12) and the scaling $M_c \propto M_h^{3/8}$ from Eq. (111) is reliable. However, for large DM halos $M_h > (M_h)_{\text{MCP}}$, this is no more the case because the core-halo solution is unstable and is replaced by an out-of-equilibrium core-halo solution (see Fig. 14). It is possible, in that case, that DM halos of the same mass M_h may contain cores of different masses M_c depending on their evolution. In particular, when $M_h > M_{\text{OV}}$, the core mass M_c may evolve from a small value M_c^* corresponding to the beginning of the condensed branch at Λ_* up to the value M_{OV} corresponding to the end of the condensed branch at Λ_c'' at which it becomes unstable and collapses towards a SMBH (see Fig. 16).

C. Results for $m = 165 \text{ eV}/c^2$

For a fermion mass $m = 165 \text{ eV}/c^2$, we obtained the following results:

- (i) There exists a minimum halo of mass $(M_h)_{\text{min}} = 10^8 M_\odot$ and radius $(r_h)_{\text{min}} = 597$ pc corresponding to the ground state ($T = 0$) of the self-gravitating Fermi gas. This DM halo is a purely quantum object (fermion ball) without atmosphere. It is completely degenerate. It is equivalent to a polytrope of index $n = 3/2$. It is fully stable. Quantum mechanics (Pauli's exclusion principle) determines the minimum mass and the minimum radius of fermionic DM halos.⁵⁵ This minimum halo can be assimilated with ultracompact dSphs like Fornax.
- (ii) For $(M_h)_{\text{min}} = 10^8 M_\odot < M_h < (M_h)_{\text{CCP}} = 6.73 \times 10^8 M_\odot$, the caloric curve is monotonic ($\mu < \mu_{\text{CCP}}$; see Fig. 11). There is only one solution with $\eta \sim 1$: A quantum object corresponding to a fermionic ball surrounded by a tenuous isothermal atmosphere. This equilibrium state is fully stable. This situation may describe dSphs. Even if collisions allow the system to evolve along the series of equilibria, no instability occurs.

⁵⁴de Vega and coworkers [49–54] only considered the gaseous (nondegenerate) solution. A merit of our study is to have evidenced a bifurcation above the canonical critical point μ_{CCP} yielding a new branch of solutions possessing a quantum core.

⁵⁵Actually, the mass and the size of the DM halos should be determined by a theory of structure formation. The first stage of this theory is the Jeans instability, leading to the formation of clumps in the linear regime. When the density of the clumps has grown significantly, we enter in the nonlinear regime of structure formation where the overdensity regions experience free fall, violent relaxation, nonlinear Landau damping, merging and accretion, leading to the DM halos that we observe today.

- (iii) For $(M_h)_{\text{CCP}} = 6.73 \times 10^8 M_\odot < M_h < (M_h)_{\text{MCP}} = 1.08 \times 10^{10} M_\odot$, the caloric curve has an N -shape structure ($\mu_{\text{CCP}} < \mu < \mu_{\text{MCP}}$; see Fig. 12). There are two physical solutions with $\eta \sim 1$: A gaseous solution corresponding to a purely classical isothermal halo without quantum core and a core-halo solution with a quantum core surrounded by a massive atmosphere. The fermion ball may mimic a large bulge but not a SMBH because it is too much extended (see Sec. VII F). The gaseous solution and the core-halo solution are both stable. If the system evolves adiabatically along the series of equilibria under the effect of collisions, it can pass from the gaseous solution to the core-halo solution without collapsing. The gravothermal catastrophe is prevented by quantum mechanics. This situation may describe small and medium spiral galaxies. They may have a core-halo structure made of a quantum core (representing a bulge) and an isothermal atmosphere. The bulge may provide a favorable environment to induce the formation of a SMBH on a long timescale by an accretion process (see Sec. VII C).
- (iv) For $M_h > (M_h)_{\text{MCP}} = 1.08 \times 10^{10} M_\odot$, the caloric curve has a Z -shape structure ($\mu > \mu_{\text{MCP}}$; see Fig. 14). There are two physical solutions for a given value of $\eta \sim 1$ as before. The gaseous solution is stable while the core-halo solution is unstable (we must also keep in mind the potentially relevant core-halo solution CH_*). In principle, only the gaseous solution may result from a process of violent collisionless relaxation because the core-halo solution is not a maximum entropy state in the sense of Lynden-Bell. If, starting from the gaseous phase, the system evolves adiabatically along the series of equilibria under the effect of collisions, it can undergo a gravothermal catastrophe at the point of minimum energy E_c . Then, there are two possibilities:
- For $(M_h)_{\text{MCP}} < M_h < M_{\text{OV}} = 2.30 \times 10^{13} M_\odot$ the gravothermal catastrophe is stopped by quantum degeneracy. This leads to a possibly out-of-equilibrium small quantum core (different from a large quantum bulge) surrounded by an envelope. In that case, the core mass—halo mass relation from Eq. (111) may not be valid anymore.
 - For $M_h > M_{\text{OV}} = 2.30 \times 10^{13} M_\odot$ a new turning point of energy occurs in the caloric curve [46,47] below which the condensed branch disappears and the core of the DM halo collapses towards a SMBH of mass M_{OV} (presumably). If $M_{\text{OV}} < M_h < M'_*$ the DM halo may either harbor a fermion ball or a SMBH. If $M_h > M'_*$ there is no condensed branch at all and the DM halo cannot harbor a fermion ball. It can just harbor a SMBH of mass M_{OV} .

This situation may apply to large spiral and elliptical galaxies. Therefore, large spiral and elliptical galaxies are

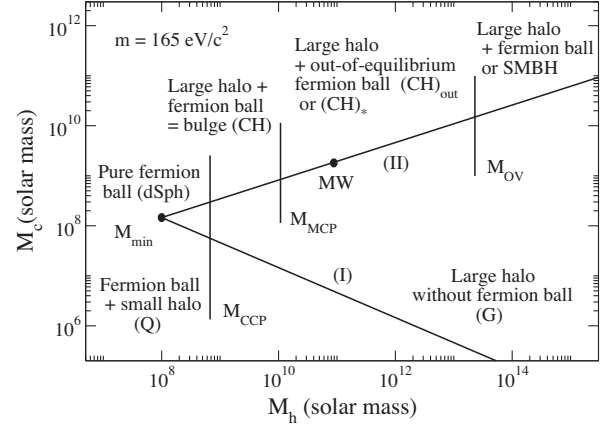


FIG. 28. Phase diagram for a fermion mass $m = 165 \text{ eV}/c^2$ summarizing our main results. It displays the minimum halo $(M_h)_{\text{min}} = 10^8 M_\odot$ (Fornax) where the DM halo is a pure fermion ball without isothermal atmosphere (ground state). It also displays the canonical critical point $(M_h)_{\text{CCP}} = 6.73 \times 10^8 M_\odot$ at which a bifurcation occurs between the gaseous branch (G) where the DM halos are purely isothermal without quantum core and the core-halo branch (CH) where the DM halos are made of a quantum core (bulge) surrounded by a classical isothermal halo. Finally, it displays the microcanonical critical point $(M_h)_{\text{MCP}} = 1.08 \times 10^{10} M_\odot$ above which the core-halo branch becomes unstable [there may be, however, potentially relevant core-halo solutions CH_*]. In that case, the DM halos may undergo a gravothermal catastrophe leading to the formation of an out-of-equilibrium fermion ball $(\text{CH})_{\text{out}}$ if $M_h < M_{\text{OV}}$, an out-of-equilibrium fermion ball or a central SMBH if $M_{\text{OV}} < M_h < M'_*$, or a SMBH if $M_h > M'_*$ (see Fig. 29 for a better illustration of these different cases when $m = 48 \text{ keV}/c^2$). We have located Fornax (dSph) and the Milky Way for reference.

expected to contain a small quantum core or a SMBH resulting from the gravothermal catastrophe instead of a large quantum bulge.⁵⁶ During the gravothermal catastrophe, their envelope is left undisturbed and should correspond to a marginal King profile (if we take into account tidal effects) which is in good agreement with the Burkert profile (see Refs. [33,34] and Fig. 1).

The main results of our study for $m = 165 \text{ eV}/c^2$ are summarized in the phase diagram of Fig. 28. The bullet corresponds to the minimum halo of mass $(M_h)_{\text{min}} = 10^8 M_\odot$. For $(M_h)_{\text{min}} = 10^8 M_\odot < M_h < (M_h)_{\text{CCP}} = 6.73 \times 10^8 M_\odot$, there is only one solution, the quantum solution. The canonical critical point $(M_h)_{\text{CCP}} = 6.73 \times 10^8 M_\odot$ determines a bifurcation between the branch of purely gaseous

⁵⁶We have argued that the Milky Way may contain a large quantum bulge in agreement with certain observations despite the fact that $M_h > (M_h)_{\text{MCP}}$. This is because its mass $M_h = 10^{11} M_\odot$ is close to the microcanonical critical point $(M_h)_{\text{MCP}} = 1.08 \times 10^{10} M_\odot$, especially if the fermion mass is larger (recall that $(M_h)_{\text{MCP}} = 4.21 \times 10^7 M_\odot$ for $m \sim 1 \text{ keV}/c^2$). Therefore, the large quantum bulge may be (marginally) stable.

solutions and the branch of core-halo solutions where the core represents a large quantum bulge. This bifurcation is associated with the occurrence of a region of negative specific heat in the caloric curve. The microcanonical critical point $(M_h)_{\text{MCP}} = 1.08 \times 10^{10} M_\odot$ determines the moment at which the DM halo can experience a gravothermal catastrophe. For $(M_h)_{\text{MCP}} < M_h < M_{\text{OV}}$ the gravothermal catastrophe is stopped by quantum mechanics and the DM halo harbors a possibly out-of-equilibrium small quantum core. Therefore, the microcanonical critical point $(M_h)_{\text{MCP}} = 1.08 \times 10^{10} M_\odot$ determines the transition between DM halos possessing a large quantum bulge and DM halos harboring a small quantum core CH_{out} (there are also potentially relevant CH_* solutions). This transition is associated with the instability of the large quantum bulge with respect to the gravothermal catastrophe. The mass $(M_h)_{\text{MCP}} = 1.08 \times 10^{10} M_\odot$ also determines the moment at which the behavior of the core mass—halo mass relation may change. On the other hand, the mass $M_{\text{OV}} = 2.30 \times 10^{13} M_\odot$ determines the moment at which the core of the DM halo may collapse towards a SMBH. For $M_{\text{OV}} < M_h < M'_*$ the DM halo may either harbor a fermion ball or a SMBH. For $M_h > M'_*$ the DM halo can only harbor a SMBH.

For $m = 165 \text{ eV}/c^2$, the value of $M_{\text{OV}} = 2.30 \times 10^{13} M_\odot$ is very large and may not be astrophysical relevant. The value of M_{OV} is reduced if the fermion mass is larger. For $m \sim 1 \text{ keV}/c^2$ we find $M_{\text{OV}} = 6.26 \times 10^{11} M_\odot$ but this value is still too large. It is comparable to the mass the whole Milky Way instead of being comparable to the mass of Sgr A*. Therefore, the fermionic DM model with a mass $m = 165 \text{ eV}/c^2$ or $m \sim 1 \text{ keV}/c^2$ cannot account for the presence of a supermassive compact object (either a SMBH or a fermion ball) of mass $M_c = 4.2 \times 10^6 M_\odot$ and radius $R_c < 6 \times 10^{-4} \text{ pc}$ at the center of the Milky Way. It rather predicts the existence of a large fermion ball (bulge) of mass $M_c = 9.45 \times 10^9 M_\odot$ and radius $R_c = 240 \text{ pc}$ (Model II), or no fermion ball at all (Model I). In that case, in order to account for the observation, we have to generalize the fermionic DM model by introducing “by hand” a primordial SMBH (Sgr A*) at the center of the Milky Way.

We note that the fermionic model developed in the present paper is based on the same ideas as those developed in Ref. [25] for bosonic DM halos. The general scenario is the same (the fermion ball replacing the soliton in the BEC model) but the $M_c(M_h)$ relation and the values of the characteristic masses and radii are different. Therefore, a detailed comparison between the two models may help determining whether DM is made of fermions or bosons.

D. Results for $m = 48 \text{ keV}/c^2$

We have also considered the possibility suggested by other authors [59,67] that the fermion ball may mimic a

SMBH at the center of the galaxies. This scenario requires a larger particle mass $m = 48 \text{ keV}/c^2$ (see footnote 44).

We have first considered the case of the usual Fermi-Dirac DF. We have shown that our simple semianalytical box model, leading to the relation from Eq. (111), reproduces the numerical results of Bilic *et al.* [67] and Ruffini *et al.* [59]. However, the size of the fermion ball is too large to satisfy the observational constraints corresponding to Sgr A*. On the other hand, in line with our previous claims [25,34,46], we showed that the core-halo solution in these models is thermodynamically unstable. Therefore, it cannot result from a process of violent relaxation.

We then mentioned the recent results of Argüelles *et al.* [60,62] based on the fermionic King model. In a first work, Argüelles *et al.* [60] obtained a density profile with a core-halo structure that satisfies the observational constraints of Sgr A*. In a second work, Argüelles *et al.* [62] showed that this solution is thermodynamically stable in the microcanonical ensemble so that it is likely to result from a process of violent relaxation. However, it is not clear if the process of violent relaxation can lead to a core-halo solution with such a high value of the central density because of the problem of incomplete relaxation [31,82].⁵⁷ The purely gaseous solution (without quantum core) whether stable or metastable may be reached more easily. This issue can be settled only with direct numerical simulations.

According to the work of Argüelles *et al.* [62], medium size galaxies like the Milky Way may harbor a fermion ball mimicking a SMBH of mass $M_c = 4.2 \times 10^6 M_\odot$ and radius $R_c = 6 \times 10^{-4} \text{ pc}$. This corresponds to a stable configuration CH_* located on the condensed branch of the caloric curve of the self-gravitating Fermi gas close to the last turning point of energy E_* (see Fig. 22). Using the results of Alberti and Chavanis [46], we have argued that larger galaxies cannot harbor a fermion ball because, above a critical mass $M_h > M'_*$, the condensed branch disappears completely (see Fig. 24) and the system forms a SMBH of mass $\sim M_{\text{OV}}$ (presumably). Therefore, if $m = 48 \text{ keV}/c^2$, very large galaxies are likely to contain a SMBH of mass $M_{\text{OV}} = 2.71 \times 10^8 M_\odot$ possibly accounting for AGNs. Medium size galaxies like the Milky Way may also follow the branch of condensed states up to the turning point of energy E'_c and undergo core collapse towards a SMBH. However the mass of the SMBH should be much smaller than $M_{\text{OV}} = 2.71 \times 10^8 M_\odot$ in order to account for the characteristics of Sgr A*. This may be achieved with a larger fermion mass. For a fermion mass $m = 386 \text{ keV}/c^2$ the disappearance of the condensed branch and the collapse of the core of the system towards a SMBH already occur in galaxies like the Milky Way and lead to a SMBH of mass $M_{\text{OV}} = 4.2 \times 10^6 \text{ keV}/c^2$ similar to Sgr A*.

⁵⁷We have mentioned that this problem could be alleviated if the fermions are self-interacting.

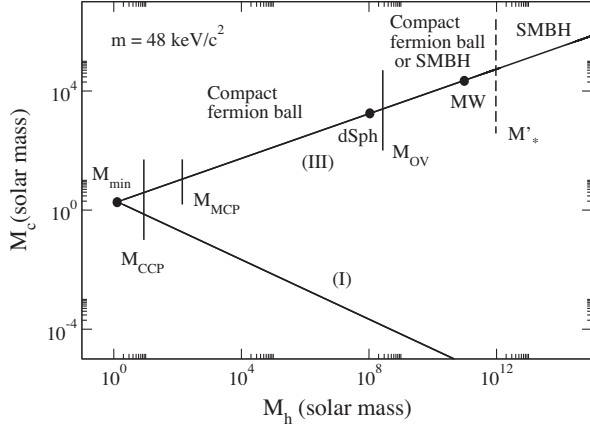


FIG. 29. Phase diagram for a fermion mass $m = 48 \text{ keV}/c^2$ summarizing our main results. The mass of the minimum halo (ground state) is considerably reduced to $(M_h)_{\min} = 1.30 M_\odot$ leading to potential problems (see Sec. VIII E). For $M_h < M_{\text{OV}} = 2.71 \times 10^8 M_\odot$, the DM halos should harbor a small fermion ball mimicking a SMBH. For $M_{\text{OV}} < M_h < M'_*$ they may harbor either a small fermion ball, mimicking a SMBH, or a true SMBH (for $m = 48 \text{ keV}/c^2$ an ultracompact fermion ball in the Milky Way is preferred over a SMBH which would have a too large mass, $M_{\text{OV}} = 2.71 \times 10^8 M_\odot$, larger than the mass of Sgr A*). For $M_h > M'_*$ they can harbor only a SMBH of mass $M_{\text{OV}} = 2.71 \times 10^8 M_\odot$ possibly accounting for AGNs. We have located Fornax (dSph) and the Milky Way for reference.

We also mentioned potential difficulties with the model of Argüelles *et al.* [62]. If the fermion mass is $m = 48 \text{ keV}/c^2$, the mass of the minimum halo (ground state) is $(M_h)_{\min} = 1.30 M_\odot$. Therefore, there should exist DM halos with a mass much below $10^8 M_\odot$, up to $1 M_\odot$. On the other hand, under the same conditions, DM halos of mass $M_h = 10^8 M_\odot$ such as dSphs like Fornax should have a core-halo structure (see Figs. 25 and 26). As far as we know, these two features are not observed (see, however, footnote 46): There are no DM halos with a mass much smaller than $10^8 M_\odot$ (Fornax) and the density profiles of dSphs have not a core-halo structure (they look like Figs. 7 and 8 instead of Figs. 25 and 26). More precisely, the fermionic DM model with a fermion mass $m = 48 \text{ keV}/c^2$ predicts that dSphs of mass $M_h = 10^8 M_\odot$ should contain a fermion ball of mass $M_c = 1.57 \times 10^4 M_\odot$ and radius $R_c = 5.42 \text{ mpc}$ possibly mimicking an intermediate mass BH (see Sec. VIII E). This is either a very important prediction (if confirmed by observations) or the evidence that this model is incorrect (if invalidated by observations). The main results of our study for $m = 48 \text{ keV}/c^2$ are summarized in the phase diagram of Fig. 29.

E. The importance of the DM particle mass

There is a strong structural difference between the core-halo density profile corresponding to a large fermion mass $m = 48 \text{ keV}/c^2$ or a small fermion mass $m = 165 \text{ eV}/c^2$

when the fermionic model is applied to a DM halo of mass $M_h = 10^{11} M_\odot$ (Milky Way). In the first case, the degeneracy parameter μ is very large ($\mu = 3.09 \times 10^{14}$) and the core-halo profile presents a strong separation between the quantum core and the classical halo (see Fig. 19). They are separated by an extended plateau. Furthermore, the fermion ball has a mass $M_c = 4.2 \times 10^6 M_\odot$ and a radius $R_c = 6 \times 10^{-4} \text{ pc}$, mimicking a small SMBH (Sgr A*). In the second case, μ is relatively small ($\mu = 4.31 \times 10^4$) and the separation between the core and the halo is mild with no clear plateau between them (see Fig. 17). Furthermore, the fermion ball has a mass $M_c = 9.45 \times 10^9 M_\odot$ and a radius $R_c = 240 \text{ pc}$ mimicking a large quantum bulge, not a small SMBH. Therefore, depending on the DM particle mass, the fermionic model predicts very different types of structures. Comparison with observations of the Milky Way should determine which type of structure (a large quantum bulge or a small quantum core mimicking a SMBH) is the most relevant in the fermionic model. In this respect, we note that the BECDM model also leads to core-halo configurations in which the fermion ball is replaced by a soliton. For the commonly adopted boson mass $m \sim 10^{-22} \text{ eV}/c^2$ the core-halo profiles obtained in direct numerical simulations [16–24] do not show a very pronounced separation between a core and a halo (there is no extended plateau) and look similar to Fig. 17 rather than Fig. 19. In addition, the soliton mimics a large quantum bulge rather than a SMBH. Such a large quantum bulge seems to be necessary to account for the dispersion velocity peak observed in the Milky Way [108]. This may be a strong observational evidence for the presence of a large quantum bulge (bosonic or fermionic) at the center of the galaxies. Therefore, the comparison of the fermionic and bosonic models tends to favor a fermion mass of the order of $m = 165 \text{ eV}/c^2$ (or $1 \text{ keV}/c^2$) instead of $m = 48 \text{ keV}/c^2$. It would be interesting to consider BECDM models with a boson mass much larger than $m \sim 10^{-22} \text{ eV}/c^2$ to see if they can lead to a soliton mimicking a SMBH like in the model of Argüelles *et al.* [60,62] for fermions. Considering a noninteracting boson for simplicity, we find that its mass should be $m = 1.84 \times 10^{-18} \text{ eV}/c^2$ (see Sec. VA of [40]). However, for such a large mass, BECDM is expected to behave like CDM and present a central cusp instead of a core as demonstrated by Mocz *et al.* [20] (see also the discussion in Sec. X). Similarly, for a large fermion mass $m \sim 50 \text{ keV}/c^2$ such as the one considered in the models of Argüelles *et al.* [60,62], DM should behave like CDM and may not be described by the Lynden-Bell DF as assumed by these authors. The Lynden-Bell DF may be valid only for a smaller fermion mass $m \sim 1 \text{ keV}/c^2$ where the cusps are prevented by the Pauli exclusion principle. However, these difficulties may disappear if DM is both quantum and self-interacting (see the discussion in Sec. X). In that case, the Fermi-Dirac DF may be justified by the self-interaction (collisions) of the fermions, not by a process of collisionless violent

relaxation. The same remarks apply to the bosonic model; one should consider a repulsive self-interaction like in Ref. [25].

The comparison between the bosonic and fermionic models that we have initiated in this paper and in [15,25,34,38,39] may help determining the DM particle mass and whether it is a fermion or a boson. We would like to close this paper by suggesting that DM may be made of different types of particles (fermions and bosons) with different characteristics (mass, scattering length...). Some family of particles may be responsible for creating a large quantum bulge (fermion ball or soliton) [16,17,25,34] at the center of the galaxies which could explain the dispersion velocity peak observed in the Milky Way [108] while other family of particles may be responsible for creating a very compact object (fermion ball or soliton) at the very center of the galaxies mimicking a SMBH [60,62,67], or even leading to the formation a true SMBH.⁵⁸ If this suggestion is correct, it would give interest to all kinds of research made on quantum (fermionic and bosonic) DM and SIDM. If not, some physically interesting theoretical models may be ruled out by the observations.

ACKNOWLEDGMENTS

I am grateful to C. Argüelles for a careful reading of my manuscript and for interesting comments.

APPENDIX A: APPROXIMATE EQUATIONS OF STATE

Instead of using the exact equation of state of an ideal Fermi gas at finite temperature determined by Eqs. (8) and (9), we can consider the approximate equation of state

$$P = \frac{1}{20} \left(\frac{3}{\pi} \right)^{2/3} \frac{\hbar^2}{m^{8/3}} \rho^{5/3} + \rho \frac{k_B T}{m}, \quad (\text{A1})$$

which is simply the sum of the polytropic equation of state (69) valid at high densities and the isothermal equation of state (43) valid at low densities.

Similarly, in the case of self-interacting BECDM halos in the TF limit, we have used in Ref. [25] an approximate equation of state of the form

$$P = \frac{2\pi a_s \hbar^2}{m^3} \rho^2 + \rho \frac{k_B T}{m}, \quad (\text{A2})$$

where a_s is the scattering length of the bosons.

Finally, in the case of noninteracting BECDM halos, we have used in Refs. [37,134] an approximate equation of state of the form

$$P = \left(\frac{2\pi G \hbar^2}{9m^2} \right)^{1/2} \rho^{3/2} + \rho \frac{k_B T}{m}, \quad (\text{A3})$$

where the first term mimics the quantum potential (see Appendix E of [38] for the justification of this equation of state).

These equations of state are of the generic form

$$P = K \rho^\gamma + \rho \frac{k_B T}{m} \quad (\gamma = 1 + 1/n). \quad (\text{A4})$$

They involve a polytropic equation of state of index n and an isothermal (linear) equation of state. In the models discussed above, the polytropic index is $n = 3/2$ for fermions, $n = 1$ for self-interacting bosons, and $n = 2$ for noninteracting bosons [38]. DM halos described by the mixed equation of state (A4) have been studied in [25]. They are governed by a generalized Lane-Emden equation introduced in Appendix E of [25].⁵⁹ These DM halos have a core-halo structure with a quantum core surrounded by an isothermal envelope. The quantum core corresponds to a fermion ball ($n = 3/2$), a self-interacting BEC ($n = 1$), or a soliton ($n = 2$). Their caloric curves present similar features. On the other hand, using a maximum entropy principle, we found in Ref. [38] that the generic core mass—halo mass relation is given by

$$\frac{M_c}{(M_h)_{\min}} \sim \left[\frac{M_h}{(M_h)_{\min}} \right]^{(3-n)/4} \propto M_v^{(3-n)/3}. \quad (\text{A5})$$

This relation is equivalent to the velocity dispersion tracing relation. For fermionic DM halos ($n = 3/2$), we get

$$\frac{M_c}{(M_h)_{\min}} \sim \left[\frac{M_h}{(M_h)_{\min}} \right]^{3/8} \propto M_v^{1/2}. \quad (\text{A6})$$

For self-interacting bosonic DM halos ($n = 1$), we get

$$\frac{M_c}{(M_h)_{\min}} \sim \left[\frac{M_h}{(M_h)_{\min}} \right]^{1/2} \propto M_v^{2/3}. \quad (\text{A7})$$

For noninteracting bosonic DM halos ($n = 2$), we get

$$\frac{M_c}{(M_h)_{\min}} \sim \left[\frac{M_h}{(M_h)_{\min}} \right]^{1/4} \propto M_v^{1/3}. \quad (\text{A8})$$

⁵⁸The compact object at the center of the Galaxy (Sgr A*) of mass $M = 4.2 \times 10^6 M_\odot$ could be a mixed structure made of a SMBH surrounded by a compact fermion or boson ball. In that case, the mass of the SMBH could be smaller than commonly thought ($M_{\text{BH}} \leq 4.2 \times 10^6 M_\odot$) since part of the mass of the compact object (Sgr A*) would be in the fermion or boson ball.

⁵⁹The mixed equation of state (A4) has also been introduced and studied in a cosmological context (in the framework of general relativity) in Refs. [135–137]. In that case, ρc^2 represents the energy density of the Universe.

Remark: BECDM halos are described by the GPP equations with a self-interaction potential that accounts for their equation of state. Because of the analogy between fermionic and bosonic DM halos, we could also try to describe fermionic DM halos by the GPP equations. This idea is developed in Appendix G of [29]. The generalized wave equation associated with the equation of state (A4) is

$$i\hbar \frac{\partial \psi}{\partial t} = -\frac{\hbar^2}{2m} \Delta \psi + k_B T \ln(|\psi|^2) \psi + \frac{K\gamma m}{\gamma-1} |\psi|^{2(\gamma-1)} \psi + m\Phi \psi - i\frac{\hbar}{2} \xi \left[\ln\left(\frac{\psi}{\psi^*}\right) - \left\langle \ln\left(\frac{\psi}{\psi^*}\right) \right\rangle \right] \psi. \quad (\text{A9})$$

It must be coupled to the Poisson equation

$$\Delta \Phi = 4\pi G |\psi|^2. \quad (\text{A10})$$

For self-interacting bosons [see Eq. (A2)], we get [29]

$$i\hbar \frac{\partial \psi}{\partial t} = -\frac{\hbar^2}{2m} \Delta \psi + k_B T \ln(|\psi|^2) \psi + \frac{4\pi a_s \hbar^2}{m^2} |\psi|^2 \psi + m\Phi \psi - i\frac{\hbar}{2} \xi \left[\ln\left(\frac{\psi}{\psi^*}\right) - \left\langle \ln\left(\frac{\psi}{\psi^*}\right) \right\rangle \right] \psi. \quad (\text{A11})$$

For fermions [see Eq. (A1)], we obtain [29]

$$i\hbar \frac{\partial \psi}{\partial t} = -\frac{\hbar^2}{2m} \Delta \psi + k_B T \ln(|\psi|^2) \psi + \frac{1}{8} \left(\frac{3}{\pi}\right)^{2/3} \frac{\hbar^2}{m^{5/3}} |\psi|^{4/3} \psi + m\Phi \psi - i\frac{\hbar}{2} \xi \left[\ln\left(\frac{\psi}{\psi^*}\right) - \left\langle \ln\left(\frac{\psi}{\psi^*}\right) \right\rangle \right] \psi. \quad (\text{A12})$$

When $\xi = T = 0$, we recover the standard GPP equations with a potential accounting for the self-interaction between the bosons [in Eq. (A11)] or taking into account the Pauli exclusion principle for fermions [in Eq. (A12)]. The kinetic term (or the quantum potential) is generally negligible for strongly self-interacting bosons and for fermions, justifying the Thomas-Fermi approximation, but it may nevertheless be relevant in order to regularize the dynamics at small scales when the system undergoes gravitational collapse. The wave equation (A12) could be used to describe the dynamics of self-gravitating fermions and the formation of fermionic DM halos similarly to the numerical simulations performed with bosons using Eq. (A11) [16–24]. It is usually acknowledged that the processes of violent relaxation and gravitational cooling produce an isothermal halo and a source of dissipation

(see the Introduction). Equations (A9)–(A12) with $\xi \neq 0$ and $T \neq 0$ may provide a relevant parametrization of these complicated processes (see Ref. [29] for a more detailed discussion).

APPENDIX B: ENTROPY

Using the Gibbs-Duhem formula (see Eqs. (40), (47), and (58) of [30]), the entropy of the nonrelativistic self-gravitating Fermi gas is given by⁶⁰

$$S = -\frac{\mu}{T} N + \frac{5E_{\text{kin}}}{3T} + \frac{2W}{T}. \quad (\text{B1})$$

Using the virial theorem from Eq. (32) and introducing the total energy $E = E_{\text{kin}} + W$, we obtain

$$\frac{S}{Nk_B} = -\frac{\mu}{k_B T} + \frac{7E}{3Nk_B T} - \frac{P_b V}{Nk_B T}. \quad (\text{B2})$$

Using

$$k = e^{-\beta\mu} e^{\beta m \Phi_0} \quad (\text{B3})$$

and

$$\begin{aligned} \psi(\alpha) &= \beta m (\Phi(R) - \Phi_0) \\ &= \beta m \left(-\frac{GM}{R} - \Phi_0 \right) = -\eta - \beta m \Phi_0 \end{aligned} \quad (\text{B4})$$

from Eq. (16), we get

$$\beta\mu = -\ln k - \eta - \psi(\alpha). \quad (\text{B5})$$

Substituting Eq. (B5) into Eq. (B2) and introducing the dimensionless variables defined in Sec. III, we finally obtain

$$\frac{S}{Nk_B} = \ln k + \eta + \psi_k(\alpha) - \frac{7}{3} \Lambda \eta - \frac{2\alpha^6}{9\tilde{\mu}^2} I_{3/2}(k e^{\psi_k(\alpha)}), \quad (\text{B6})$$

where $\tilde{\mu}$ denotes the degeneracy parameter from Eq. (29) (we use the notation $\tilde{\mu}$ here to distinguish it from the chemical potential μ). This returns in a more direct manner the result obtained in [41].

The entropy of the nonrelativistic self-gravitating Boltzmann gas is also given by Eq. (B1) (see footnote 60). Using Eq. (61) and introducing the total energy $E = E_{\text{kin}} + W$, we obtain

$$S = -\frac{\mu}{T} N + \frac{2E}{T} - \frac{1}{2} N k_B. \quad (\text{B7})$$

⁶⁰It is shown in [30] that this expression is valid for an arbitrary form of entropy.

On the other hand, applying Eq. (41) at $r = R$ and using Eqs. (57)–(59) and $\Phi(R) = -GM/R$, we find that

$$\beta\mu = 2 \ln(\alpha) + \frac{1}{2} \ln \eta - \psi(\alpha) - \eta - \ln \tilde{\mu} + \ln 2 - \frac{1}{2} \ln \pi. \quad (\text{B8})$$

Substituting Eq. (B8) into Eq. (B7), we finally obtain

$$\begin{aligned} \frac{S}{Nk_B} = & -\frac{1}{2} \ln \eta - 2 \ln(\alpha) + \psi(\alpha) + \eta - 2\Lambda\eta \\ & + \ln \tilde{\mu} + \frac{1}{2} \ln \pi - \ln 2 - \frac{1}{2}. \end{aligned} \quad (\text{B9})$$

APPENDIX C: BASIC EQUATIONS AND DEFINITIONS

For classical self-gravitating systems, or for quantum self-gravitating systems in the TF approximation (where the quantum potential can be neglected), the condition of hydrostatic equilibrium reads

$$\nabla P + \rho \nabla \Phi = \mathbf{0}. \quad (\text{C1})$$

Combined with the Poisson equation

$$\Delta \Phi = 4\pi G \rho, \quad (\text{C2})$$

we obtain the fundamental differential equation

$$\nabla \cdot \left(\frac{\nabla P}{\rho} \right) = -4\pi G \rho. \quad (\text{C3})$$

This equation determines the density profile $\rho(r)$ of a DM halo described by a barotropic equation of state $P(\rho)$.

The halo radius r_h is defined as the distance at which the central density ρ_0 is divided by 4:

$$\frac{\rho(r_h)}{\rho_0} = \frac{1}{4}. \quad (\text{C4})$$

The mass $M(r)$ contained within a sphere of radius r is given by

$$M(r) = \int_0^r \rho(r') 4\pi r'^2 dr'. \quad (\text{C5})$$

The halo mass is

$$M_h = M(r_h). \quad (\text{C6})$$

The circular velocity is defined by

$$v^2(r) = \frac{GM(r)}{r}. \quad (\text{C7})$$

The circular velocity at the halo radius is

$$v_h^2 = v^2(r_h) = \frac{GM_h}{r_h}. \quad (\text{C8})$$

We have the identity

$$\frac{v_h^2}{G\rho_0 r_h^2} = \frac{M_h}{\rho_0 r_h^3}. \quad (\text{C9})$$

APPENDIX D: ISOTHERMAL PROFILE

1. Emden equation

We consider a DM halo with an isothermal equation of state

$$P = \rho \frac{k_B T}{m}, \quad (\text{D1})$$

where T is the temperature [55]. The fundamental differential equation of hydrostatic equilibrium (C3) takes the form

$$\frac{k_B T}{m} \Delta \ln \rho = -4\pi G \rho. \quad (\text{D2})$$

Writing

$$\rho = \rho_0 e^{-\psi}, \quad (\text{D3})$$

where ρ_0 is the central density, introducing the normalized radial distance

$$\xi = r/r_0, \quad r_0 = \left(\frac{k_B T}{4\pi G \rho_0 m} \right)^{1/2}, \quad (\text{D4})$$

where r_0 is the thermal core radius, and assuming that the DM halo is spherically symmetric, we obtain the Emden equation [55]

$$\frac{1}{\xi^2} \frac{d}{d\xi} \left(\xi^2 \frac{d\psi}{d\xi} \right) = e^{-\psi} \quad (\text{D5})$$

with the boundary conditions

$$\psi(0) = \psi'(0) = 0. \quad (\text{D6})$$

The density profile has the self-similar (homology) form $\rho(r)/\rho_0 = e^{-\psi(r/r_0)}$. Using Eqs. (C5), (D3), (D4), and (D5), the mass contained within the sphere of radius r is given by

$$M(r) = 4\pi \rho_0 r_0^3 \xi^2 \psi'(\xi). \quad (\text{D7})$$

According to Eqs. (C7), (D4) and (D7), the circular velocity is

$$v^2(r) = 4\pi G\rho_0 r_0^2 \xi \psi'(\xi). \quad (\text{D8})$$

Using Eq. (D4), we find that the temperature satisfies the relation

$$\frac{k_B T}{m} = 4\pi G\rho_0 r_0^2. \quad (\text{D9})$$

Therefore, we can rewrite Eq. (D8) as

$$\frac{m v^2(r)}{k_B T} = \xi \psi'(\xi). \quad (\text{D10})$$

2. Halo mass and halo radius

The halo radius defined by Eq. (C4) is given by $r_h = \xi_h r_0$, where ξ_h is determined by the equation

$$e^{-\psi(\xi_h)} = \frac{1}{4}. \quad (\text{D11})$$

Solving the Emden equation (D5) numerically, we find

$$\xi_h = 3.63, \quad \psi'(\xi_h) = 0.507. \quad (\text{D12})$$

The normalized halo mass is

$$\frac{M_h}{\rho_0 r_h^3} = 4\pi \frac{\psi'(\xi_h)}{\xi_h} = 1.76. \quad (\text{D13})$$

The normalized circular velocity at the halo radius is

$$\frac{v_h^2}{4\pi G\rho_0 r_h^2} = \frac{\psi'(\xi_h)}{\xi_h} = 0.140. \quad (\text{D14})$$

The normalized temperature is

$$\frac{k_B T}{Gm\rho_0 r_h^2} = \frac{4\pi}{\xi_h^2} = 0.954. \quad (\text{D15})$$

The normalized inverse temperature of the halo is

$$\eta_v = \frac{\beta G M_h m}{r_h} = \xi_h \psi'_h = 1.84. \quad (\text{D16})$$

APPENDIX E: POLYTROPIC PROFILES

1. Lane-Emden equation

We consider a DM halo with a polytropic equation of state of the form

$$P = K\rho^\gamma, \quad (\text{E1})$$

where K is the polytropic constant and $\gamma = 1 + 1/n$ is the polytropic index [55]. The fundamental differential equation of hydrostatic equilibrium (C3) takes the form

$$K(n+1)\Delta\rho^{1/n} = -4\pi G\rho. \quad (\text{E2})$$

In the following, we restrict ourselves to spherically symmetric distributions. We also assume $K > 0$ and $6/5 < \gamma < +\infty$ (i.e., $0 \leq n < 5$) in order to have density profiles with a compact support (see below).

Writing

$$\rho = \rho_0 \theta^n, \quad (\text{E3})$$

where ρ_0 is the central density, introducing the normalized radial distance

$$\xi = r/r_0, \quad r_0 = \left[\frac{K(n+1)}{4\pi G\rho_0^{1-1/n}} \right]^{1/2}, \quad (\text{E4})$$

where r_0 is the polytropic core radius, and assuming that the DM halo is spherically symmetric, we obtain the Lane-Emden equation [55]

$$\frac{1}{\xi^2} \frac{d}{d\xi} \left(\xi^2 \frac{d\theta}{d\xi} \right) = -\theta^n \quad (\text{E5})$$

with the boundary conditions

$$\theta(0) = 1, \quad \theta'(0) = 0. \quad (\text{E6})$$

The density profile has the self-similar (homology) form $\rho(r)/\rho_0 = \theta^n(r/r_0)$. Using Eqs. (C5), (E3), (E4), and (E5), the mass contained within the sphere of radius r is given by

$$M(r) = -4\pi\rho_0 r_0^3 \xi^2 \theta'(\xi). \quad (\text{E7})$$

According to Eqs. (C7), (E4) and (E7), the circular velocity is

$$v^2(r) = -4\pi G\rho_0 r_0^2 \xi \theta'(\xi). \quad (\text{E8})$$

2. Mass and radius

When $n < 5$, the polytropes are self-confined (their density has a compact support) [55,138]. We denote by ξ_1 the normalized radius at which the density vanishes: $\theta_1 = \theta(\xi_1) = 0$. Their radius R and their total mass M are given by

$$R = \xi_1 r_0, \quad M = -4\pi\rho_0 r_0^3 \xi_1^2 \theta'_1, \quad (\text{E9})$$

or, more explicitly, by

$$R = \xi_1 \left[\frac{K(n+1)}{4\pi G} \right]^{1/2} \frac{1}{\rho_0^{(n-1)/2n}}, \quad (\text{E10})$$

$$M = -4\pi \frac{\theta'_1}{\xi_1} \rho_0 R^3. \quad (\text{E11})$$

Eliminating the central density between these two equations, we obtain the mass-radius relation [55]

$$M^{(n-1)/n} R^{(3-n)/n} = \frac{K(n+1)}{G(4\pi)^{1/n}} \omega_n^{(n-1)/n}, \quad (\text{E12})$$

where $\omega_n = -\xi_1^{(n+1)/(n-1)} \theta'_1$ is a constant determined by the Lane-Emden equation (E5). It can be shown that a polytrope of index n is dynamically stable with respect to the Euler-Poisson equations if $n < 3$ and linearly unstable if $n > 3$ [55]. On the other hand, the gravitational energy of a polytrope of index n is given by the Betti-Ritter formula [55]

$$W = -\frac{3}{5-n} \frac{GM^2}{R}. \quad (\text{E13})$$

For the polytrope $n = 3/2$, solving the Lane-Emden equation (E5) numerically, we find

$$\xi_1 = 3.65375, \quad \theta'_1 = -0.203302. \quad (\text{E14})$$

This polytrope represents a nonrelativistic fermion star at $T = 0$. This leads to Eqs. (72)–(74) quoted in the main text. The mass-radius relation may be written as

$$MR^3 = \frac{9\omega_{3/2}}{8192\pi^4} \frac{h^6}{G^3 m^8}, \quad (\text{E15})$$

where $\omega_{3/2} = 132.3843$.

3. Halo mass and halo radius

The halo radius defined by Eq. (C4) is given by $r_h = \xi_h r_0$, where ξ_h is determined by the equation

$$\theta(\xi_h)^n = \frac{1}{4}. \quad (\text{E16})$$

The value of ξ_h can be obtained by solving the Lane-Emden equation (E5) for a given value of n . The normalized halo mass is

$$\frac{M_h}{\rho_0 r_h^3} = -4\pi \frac{\theta'(\xi_h)}{\xi_h}. \quad (\text{E17})$$

The normalized circular velocity at the halo radius is

$$\frac{v_h^2}{4\pi G \rho_0 r_h^2} = -\frac{\theta'(\xi_h)}{\xi_h}. \quad (\text{E18})$$

The halo radius r_h and the halo mass may be written more explicitly as

$$r_h = \xi_h \left[\frac{K(n+1)}{4\pi G} \right]^{1/2} \frac{1}{\rho_0^{(n-1)/2n}}, \quad (\text{E19})$$

$$M_h = -4\pi \frac{\theta'(\xi_h)}{\xi_h} \rho_0 r_h^3. \quad (\text{E20})$$

Eliminating the central density between Eqs. (E19) and (E20), we obtain the halo mass-radius relation

$$M_h r_h^{(3-n)/(n-1)} = -4\pi \theta'(\xi_h) \xi_h^{(n+1)/(n-1)} \left[\frac{K(n+1)}{4\pi G} \right]^{n/(n-1)}. \quad (\text{E21})$$

Let us assume that the minimum halo corresponds to a polytrope of index n (this includes the case of fermions corresponding to $n = 3/2$, the case of noninteracting bosons corresponding to $n = 2$, and the case of self-interacting bosons corresponding to $n = 1$ [38]). Using Eqs. (E19) and (E20) and introducing the universal surface density of DM halos from Eq. (52) we find that the minimum halo radius, the minimum halo mass, and the maximum halo central density are given by

$$(r_h)_{\min} = \xi_h^{2n/(n+1)} \left[\frac{K(n+1)}{4\pi G} \right]^{n/(n+1)} \frac{1}{\Sigma_0^{(n-1)/(n+1)}}, \quad (\text{E22})$$

$$(M_h)_{\min} = -4\pi \theta'(\xi_h) \xi_h^{(3n-1)/(n+1)} \left[\frac{K(n+1)}{4\pi G} \right]^{2n/(n+1)} \times \Sigma_0^{(3-n)/(n+1)}, \quad (\text{E23})$$

$$(\rho_0)_{\max} = \frac{1}{\xi_h^{2n/(n+1)}} \left[\frac{4\pi G}{K(n+1)} \right]^{n/(n+1)} \Sigma_0^{2n/(n+1)}. \quad (\text{E24})$$

For the polytrope $n = 3/2$, solving the Lane-Emden equation (E5) numerically, we find

$$\xi_h = 2.27, \quad \theta'_h = -0.360. \quad (\text{E25})$$

If the minimum halo corresponds to a fermion ball at $T = 0$ (equivalent to a polytrope $n = 3/2$) we obtain Eqs. (75)–(82) quoted in the main text.

- [1] J. F. Navarro, C. S. Frenk, and S. D. M. White, *Astrophys. J.* **462**, 563 (1996).
- [2] A. Burkert, *Astrophys. J.* **447**, L25 (1995).
- [3] G. Kauffmann, S. D. M. White, and B. Guiderdoni, *Mon. Not. R. Astron. Soc.* **264**, 201 (1993).
- [4] A. Klypin, A. V. Kravtsov, and O. Valenzuela, *Astrophys. J.* **522**, 82 (1999).
- [5] M. Kamionkowski and A. R. Liddle, *Phys. Rev. Lett.* **84**, 4525 (2000).
- [6] M. Boylan-Kolchin, J. S. Bullock, and M. Kaplinghat, *Mon. Not. R. Astron. Soc.* **422**, 1203 (2012).
- [7] B. Moore, T. Quinn, F. Governato, J. Stadel, and G. Lake, *Mon. Not. R. Astron. Soc.* **310**, 1147 (1999).
- [8] M. Boylan-Kolchin, J. S. Bullock, and M. Kaplinghat, *Mon. Not. R. Astron. Soc.* **415**, L40 (2011).
- [9] J. S. Bullock and M. Boylan-Kolchin, *Annu. Rev. Astron. Astrophys.* **55**, 343 (2017).
- [10] E. Romano-Díaz, I. Shlosman, Y. Hoffman, and C. Heller, *Astrophys. J.* **685**, L105 (2008).
- [11] A. Pontzen and F. Governato, *Nature (London)* **506**, 171 (2014).
- [12] J. Oñorbe *et al.*, *Mon. Not. R. Astron. Soc.* **454**, 2092 (2015).
- [13] P. H. Chavanis, *Phys. Rev. D* **102**, 083531 (2020).
- [14] D. Marsh, *Phys. Rep.* **643**, 1 (2016).
- [15] P. H. Chavanis, *Phys. Rev. D* **84**, 043531 (2011).
- [16] H. Y. Schive, T. Chiueh, and T. Broadhurst, *Nat. Phys.* **10**, 496 (2014).
- [17] H. Y. Schive, M.-H. Liao, T.-P. Woo, S.-K. Wong, T. Chiueh, T. Broadhurst, and W.-Y. P. Hwang, *Phys. Rev. Lett.* **113**, 261302 (2014).
- [18] B. Schwabe, J. Niemeyer, and J. Engels, *Phys. Rev. D* **94**, 043513 (2016).
- [19] P. Mocz, M. Vogelsberger, V. H. Robles, J. Zavala, M. Boylan-Kolchin, A. Fialkov, and L. Hernquist, *Mon. Not. R. Astron. Soc.* **471**, 4559 (2017).
- [20] P. Mocz, L. Lancaster, A. Fialkov, F. Becerra, and P. H. Chavanis, *Phys. Rev. D* **97**, 083519 (2018).
- [21] J. Veltmaat, J. C. Niemeyer, and B. Schwabe, *Phys. Rev. D* **98**, 043509 (2018).
- [22] P. Mocz *et al.*, *Phys. Rev. Lett.* **123**, 141301 (2019).
- [23] P. Mocz *et al.*, *Mon. Not. R. Astron. Soc.* **494**, 2027 (2020).
- [24] J. Veltmaat, B. Schwabe, and J. C. Niemeyer, *Phys. Rev. D* **101**, 083518 (2020).
- [25] P. H. Chavanis, *Phys. Rev. D* **100**, 083022 (2019).
- [26] E. Seidel and W. M. Suen, *Phys. Rev. Lett.* **72**, 2516 (1994).
- [27] F. S. Guzmán and L. A. Ureña-López, *Phys. Rev. D* **69**, 124033 (2004).
- [28] F. S. Guzmán and L. A. Ureña-López, *Astrophys. J.* **645**, 814 (2006).
- [29] P. H. Chavanis, *Eur. Phys. J. B* **95**, 48 (2022).
- [30] P. H. Chavanis, *Eur. Phys. J. Plus* **135**, 290 (2020).
- [31] D. Lynden-Bell, *Mon. Not. R. Astron. Soc.* **136**, 101 (1967).
- [32] P. H. Chavanis and J. Sommeria, *Mon. Not. R. Astron. Soc.* **296**, 569 (1998).
- [33] P. H. Chavanis, M. Lemou, and F. Méhats, *Phys. Rev. D* **91**, 063531 (2015).
- [34] P. H. Chavanis, M. Lemou, and F. Méhats, *Phys. Rev. D* **92**, 123527 (2015).
- [35] A. Krut, C. R. Argüelles, P. H. Chavanis, J. A. Rueda, and R. Ruffini (to be published).
- [36] P. H. Chavanis, *Eur. Phys. J. Plus* **136**, 703 (2021).
- [37] P. H. Chavanis, *Eur. Phys. J. Plus* **132**, 248 (2017).
- [38] P. H. Chavanis, *Phys. Rev. D* **100**, 123506 (2019).
- [39] P. H. Chavanis, *Phys. Rev. D* **101**, 063532 (2020).
- [40] P. H. Chavanis, *Phys. Rev. D* **103**, 123551 (2021).
- [41] P. H. Chavanis, *Phys. Rev. E* **65**, 056123 (2002).
- [42] P. H. Chavanis, *Phys. Rev. E* **69**, 066126 (2004).
- [43] P. H. Chavanis, *Int. J. Mod. Phys. B* **20**, 3113 (2006).
- [44] P. H. Chavanis, M. Lemou, and F. Méhats, The Fermionic King model in *Proceedings of the session “Hommage à Michel Hénon” during the Conference GRAVASCO held at the Institut Henri Poincaré, Paris*, edited by J. M. Alimi, R. Mohayaee, and J. Pérez (Hermann Press, Paris, 2013).
- [45] M. Kirejczyk, G. Müller, and P. H. Chavanis, arXiv:2110.01044 (to be published).
- [46] G. Alberti and P. H. Chavanis, *Eur. Phys. J. B* **93**, 208 (2020).
- [47] P. H. Chavanis and G. Alberti, *Phys. Lett. B* **801**, 135155 (2020).
- [48] Z. Roupas and P. H. Chavanis, *Classical Quantum Gravity* **36**, 065001 (2019).
- [49] C. Destri, H. J. de Vega, and N. G. Sanchez, *New Astron.* **22**, 39 (2013).
- [50] C. Destri, H. J. de Vega, and N. G. Sanchez, *Astropart. Phys.* **46**, 14 (2013).
- [51] H. J. de Vega, P. Salucci, and N. G. Sanchez, *Mon. Not. R. Astron. Soc.* **442**, 2717 (2014).
- [52] H. J. de Vega and N. G. Sanchez, *Int. J. Mod. Phys. A* **31**, 1650073 (2016).
- [53] H. J. de Vega and N. G. Sanchez, *Eur. Phys. J. C* **77**, 81 (2017).
- [54] H. J. de Vega and N. G. Sanchez, *Universe* **8**, 154 (2022).
- [55] S. Chandrasekhar, *An Introduction to the Theory of Stellar Structure* (Dover, New York, 1942).
- [56] C. R. Argüelles and R. Ruffini, *Int. J. Mod. Phys. D* **23**, 1442020 (2014).
- [57] C. R. Argüelles, R. Ruffini, and B. M. O. Fraga, *J. Korean Phys. Soc.* **65**, 809 (2014).
- [58] I. Siutsou, C. R. Argüelles, and R. Ruffini, *Astronomy Reports* **59**, 656 (2015).
- [59] R. Ruffini, C. R. Argüelles, and J. A. Rueda, *Mon. Not. R. Astron. Soc.* **451**, 622 (2015).
- [60] C. R. Argüelles, A. Krut, J. A. Rueda, and R. Ruffini, *Phys. Dark Universe* **21**, 82 (2018).
- [61] C. R. Argüelles, A. Krut, J. A. Rueda, and R. Ruffini, *Phys. Dark Universe* **24**, 100278 (2019).
- [62] C. R. Argüelles, M. I. Díaz, A. Krut, and R. Yunis, *Mon. Not. R. Astron. Soc.* **502**, 4227 (2021).
- [63] N. Bilic and R. D. Viollier, *Phys. Lett. B* **408**, 75 (1997).
- [64] N. Bilic, F. Munyaneza, and R. D. Viollier, *Phys. Rev. D* **59**, 024003 (1998).
- [65] N. Bilic and R. D. Viollier, *Eur. Phys. J. C* **11**, 173 (1999).
- [66] N. Bilic, F. Munyaneza, G. B. Tupper, and R. D. Viollier, *Prog. Part. Nucl. Phys.* **48**, 291 (2002).

- [67] N. Bilic, G. B. Tupper, and R. D. Viollier, *Lect. Notes Phys.* **616**, 24 (2003).
- [68] P. H. Chavanis, The self-gravitating Fermi gas in Newtonian gravity and general relativity, *Proceedings of the Sixteenth Marcel Grossman Meeting* (2021), arXiv:2112.02654.
- [69] J. Binney and S. Tremaine, *Galactic Dynamics* (Princeton University Press, Princeton, NJ, 1987).
- [70] P. H. Chavanis, *Astron. Astrophys.* **556**, A93 (2013).
- [71] R. Ruffini and L. Stella, *Astron. Astrophys.* **119**, 35 (1983).
- [72] P. H. Chavanis, *Mon. Not. R. Astron. Soc.* **300**, 981 (1998).
- [73] T. Padmanabhan, *Phys. Rep.* **188**, 285 (1990).
- [74] A. Campa, T. Dauxois, D. Fanelli, and S. Ruffo, *Physics of Long-Range Interacting Systems* (Oxford University Press, New York, 2014).
- [75] S. W. Randall, M. Markevitch, D. Clowe, A. H. Gonzalez, and M. Bradac, *Astrophys. J.* **679**, 1173 (2008).
- [76] D. Lynden-Bell and R. Wood, *Mon. Not. R. Astron. Soc.* **138**, 495 (1968).
- [77] A. Campa and P. H. Chavanis, *J. Stat. Mech.* (2010) P06001.
- [78] H. Poincaré, *Acta Math.* **7**, 259 (1885).
- [79] J. Katz, *Mon. Not. R. Astron. Soc.* **183**, 765 (1978).
- [80] P. H. Chavanis, *Astron. Astrophys.* **432**, 117 (2005).
- [81] I. R. King, *Astron. J.* **70**, 376 (1965).
- [82] P. H. Chavanis, *Physica (Amsterdam)* **365A**, 102 (2006).
- [83] J. Kormendy, K. C. Freeman, in S. D. Ryder, and D. J. Pisano, *Proc. IAU Symp. 220, Dark Matter in Galaxies*, edited by M. A. Walker and K. C. Freeman (Astron. Soc. Pac., San Francisco, 2004), p. 377.
- [84] M. Spano, M. Marcelin, P. Amram, C. Carignan, B. Epinat, and O. Hernandez, *Mon. Not. R. Astron. Soc.* **383**, 297 (2008).
- [85] F. Donato, G. Gentile, P. Salucci, C. F. Martins, M. I. Wilkinson, G. Gilmore, E. K. Grebel, A. Koch, and R. Wyse, *Mon. Not. R. Astron. Soc.* **397**, 1169 (2009).
- [86] P. H. Chavanis, *Eur. Phys. J. Plus* **130**, 130 (2015).
- [87] P. H. Chavanis, *Phys. Lett. B* **758**, 59 (2016).
- [88] P. H. Chavanis and S. Kumar, *J. Cosmol. Astropart. Phys.* **05** (2017) 018.
- [89] P. H. Chavanis, *Phys. Dark Universe* **24**, 100271 (2019).
- [90] P. H. Chavanis, arXiv:2201.05908.
- [91] P. H. Chavanis, arXiv:2201.05903.
- [92] V. A. Antonov, *Vest. Leningr. Gos. Univ.* **7**, 135 (1962).
- [93] P. H. Chavanis, *Astron. Astrophys.* **381**, 340 (2002).
- [94] A. Suárez and P. H. Chavanis, *Phys. Rev. D* **95**, 063515 (2017).
- [95] A. Suárez and P. H. Chavanis, *Phys. Rev. D* **92**, 023510 (2015).
- [96] J. R. Oppenheimer and G. M. Volkoff, *Phys. Rev.* **55**, 374 (1939).
- [97] N. Bar, D. Blas, K. Blum, and S. Sibiryakov, *Phys. Rev. D* **98**, 083027 (2018).
- [98] S. Balberg, S. L. Shapiro, and S. Inagaki, *Astrophys. J.* **568**, 475 (2002).
- [99] Y. Pomeau, M. Le Berre, P. H. Chavanis, and B. Denet, *Eur. Phys. J. E* **37**, 26 (2014).
- [100] P. H. Chavanis, B. Denet, M. Le Berre, and Y. Pomeau, *Eur. Phys. J. B* **92**, 271 (2019).
- [101] P. H. Chavanis, B. Denet, M. Le Berre, and Y. Pomeau, *Eur. Phys. Lett.* **129**, 30003 (2020).
- [102] Ya. B. Zel'dovich and M. A. Podurets, *Sov. Astron.* **9**, 742 (1966).
- [103] D. Fackerell, J. Ipser, and K. Thorne, *Comments Astrophys. Space Phys.* **1**, 134 (1969).
- [104] S. L. Shapiro and S. A. Teukolsky, *Astrophys. J.* **298**, 58 (1985).
- [105] S. L. Shapiro and S. A. Teukolsky, *Astrophys. J.* **292**, L41 (1985).
- [106] S. L. Shapiro and S. A. Teukolsky, *Astrophys. J.* **307**, 575 (1986).
- [107] L. Ferrarese, *Astrophys. J.* **578**, 90 (2002).
- [108] I. De Martino, T. Broadhurst, S.-H. H. Tye, T. Chiueh, and H.-Y. Schive, *Phys. Dark Universe* **28**, 100503 (2020).
- [109] N. Bar, K. Blum, J. Eby, and R. Sato, *Phys. Rev. D* **99**, 103020 (2019).
- [110] A. Chatterjee, P. Dayal, T. R. Choudhury, and A. Hutter, *Mon. Not. R. Astron. Soc.* **487**, 3560 (2019).
- [111] M. Carena, N. M. Coyle, Y-Y Li, S. D. McDermott, and Y. Tsai, arXiv:2108.02785.
- [112] L. Hui, J. Ostriker, S. Tremaine, and E. Witten, *Phys. Rev. D* **95**, 043541 (2017).
- [113] S. Gillessen, F. Eisenhauer, T. K. Fritz, H. Bartko, K. Dodds-Eden, O. Pfuhl, T. Ott, and R. Genzel, *Astrophys. J.* **707**, L114 (2009).
- [114] R. Schödel *et al.*, *Nature (London)* **419**, 694 (2002).
- [115] M. J. Reid, *Int. J. Mod. Phys. D* **18**, 889 (2009).
- [116] R. Genzel, F. Eisenhauer, and S. Gillessen, *Rev. Mod. Phys.* **82**, 3121 (2010).
- [117] D. F. Torres, S. Capozziello, and G. Lambiase, *Phys. Rev. D* **62**, 104012 (2000).
- [118] F. S. Guzmán, *Phys. Rev. D* **73**, 021501 (2006).
- [119] V. Domcke and A. Urbano, *J. Cosmol. Astropart. Phys.* **01** (2015) 002.
- [120] L. Randall, J. Scholtz, and J. Unwin, *Mon. Not. R. Astron. Soc.* **467**, 1515 (2017).
- [121] N. Bar, D. Blas, K. Blum, and H. Kim, *Phys. Rev. D* **104**, 043021 (2021).
- [122] E. A. Becerra-Vergara, C. R. Argüelles, A. Krut, J. A. Rueda, and R. Ruffini, *Astron. Astrophys.* **641**, A34 (2020).
- [123] E. A. Becerra-Vergara, C. R. Argüelles, A. Krut, J. A. Rueda, and R. Ruffini, *Mon. Not. R. Astron. Soc.* **505**, L64 (2021).
- [124] C. P. Ahn *et al.*, *Astrophys. J.* **839**, 72 (2017).
- [125] C. P. Ahn *et al.*, *Astrophys. J.* **858**, 102 (2018).
- [126] D. D. Nguyen *et al.*, *Astrophys. J.* **872**, 104 (2019).
- [127] H. Deng, M. P. Hertzberg, M. H. Namjoo, and A. Masoumi, *Phys. Rev. D* **98**, 023513 (2018).
- [128] A. Burkert, *Astrophys. J.* **904**, 161 (2020).
- [129] R. Yunis, C. R. Argüelles, N. E. Mavromatos, A. Moliné, A. Krut, M. Carinci, J. A. Rueda, and R. Ruffini, *Phys. Dark Universe* **30**, 100699 (2020).
- [130] P. H. Chavanis, arXiv:2112.13664.
- [131] P. H. Chavanis, *Physica (Amsterdam)* **332A**, 89 (2004).

-
- [132] M. Stiavelli and G. Bertin, *Mon. Not. R. Astron. Soc.* **229**, 61 (1987).
- [133] J. Hjorth and J. Madsen, *Mon. Not. R. Astron. Soc.* **253**, 703 (1991).
- [134] P. H. Chavanis, *Phys. Dark Universe* **22**, 80 (2018).
- [135] P. H. Chavanis, *Eur. Phys. J. Plus* **129**, 38 (2014).
- [136] P. H. Chavanis, *Eur. Phys. J. Plus* **129**, 222 (2014).
- [137] P. H. Chavanis, [arXiv:1208.1185](https://arxiv.org/abs/1208.1185).
- [138] R. Emden, *Gaskugeln* (Teubner Verlag, Leipzig, 1907).